Elastodynamic Analysis of Vehicle Suspension Uprights

Harsh Mehta

Thesis submitted to the faculty of the Virginia Polytechnic Institute and State University in partial fulfillment of the requirements for the degree of

Master of Science

In

Mechanical Engineering

Robert L. West Jr., Chair

John Ferris

Steve Southward

May 15, 2018

Blacksburg, Virginia

Keywords: Finite Element Analysis, Suspension Design, Formula SAE, Vehicle Dynamics, Abaqus

Elastodynamic Analysis of Vehicle Suspension Uprights

Harsh Mehta

Abstract

The ability of a Formula SAE sports car to negotiate a turn in a race is influenced by many parameters which include car's overall geometry, its shape, weight distribution, type of suspension used, spring and shock absorber characteristics that are used in the tire properties, static and dynamic loading. "Steady-state cornering" implies that the forces acting on the vehicle are unchanging for a given time. The suspension uprights form a connection between the wheel assembly and the suspension linkages. The criticality of the upright is that it is considered an un-suspended body, but in fact, it is subjected to very high stresses. The dynamic load imposed on the vehicle from various road conditions, cornering, braking and suspension assembly constraints generate stress on the upright body.

The equations of motion generally govern vehicle dynamics. For a kinematic and rigid body dynamics analysis, a multibody dynamics (MBD) approach is popular. The results of the dynamics analysis yield internal loads which are used to analyze suspension components for structural stiffness and strength. Automotive companies with relatively lower structural loads have made the MBD approach popular because it is supposed to be computationally less expensive. Elastodynamics is an alternative approach to solving dynamics equations while considering the components to be elastic. This approach can capture the inertial and elastic responses of the components and the load path with varying positions of the components in a mechanism.

In this research, a quarter-car suspension is modeled in a finite element code (Abaqus®), focusing on the vehicle upright but still modeling the connections and interactions of the quarter-car suspension system of a FSAE vehicle. The BEAM element modeling used for the suspension members captures the bending response. The overall model is created by making computationally conscious decisions, debugging and refining the interactions and connections to be representative. The modeling technique to create elastodynamic models is explored and established with a versatile set of suspension components and interactions providing good experience with finite element modeling. The models are created with incremental steps and early steps are verified with hand calculations. A further vehicle verification and validation plan is the next immediate priority to gain confidence in the model for accurate simulations which can be used to predict accurate structural and dynamic results. With extending the model capabilities and computational capabilities, a quarter-car suspension model is powerful enough to run the entire track simulations for formula races and even durability load cases for commercial vehicles. Fatigue loading and abusive test cases would be the load cases to investigate possible failure modes.

The quarter-car suspension model is a framework with different interactions, connections, components, boundary conditions and loads that are representative for different suspension configurations in different vehicles. The best practices of this modeling exercise are established and scalability to defeature or add details while preserving the connection behavior is achieved.

Elastodynamic Analysis of Vehicle Suspension Uprights

Harsh Mehta

General Audience Abstract

Automotive suspension analysis includes analysis the design of suspension components. In automotive parlance, suspension includes the wheel subassembly, brakes, tires, shock absorbers, subframes and the steering system. A quarter-car model is incorporated in this research to analyse a Formula SAE suspension. The quarter-car model is representative of relevant vehicle dynamics within the scope of this research. The suspension of the vehicle governs the "attitude" of the vehicle; it is a foundation on which the behavior of the car is built when it responds to operator wishes and terrain. Necessary but not sufficient for a great car is addressing multiple issues around strength and stiffness of the components during vehicle maneuvers. These issues are pulled against cost and packaging issues as jelly sets for engineering design with only a small number of physical iterations.

Finite element analysis employs its powerful solving capabilities to run an elastodynamic simulation. The representation of the component's elasticity yields elastic responses that can be observed and evaluated virtually for engineering design. Current state-of-the-art methods rely on rigid body analysis to develop dynamic simulations which do not show elastic response or response due to complex interactions between the components.

The elastodynamic model built for this research is scalable to include detail or defeatured components without losing their interactions and connection behaviors – examples include – rod end joints, bearing interference fits and bell crank connections for a pull rod suspension.

Several finite element modeling practices are established as part of this research to build a popular problem in the automotive industry – quarter-car suspension model.

The elastodynamic model is verified along the journey by building simpler building-block models. Further validation of the elastodynamic model is required for complete confidence – the path to which is covered in this thesis.

Acknowledgements

I would like to express my heartfelt gratitude to my advisor, Dr. Bob West, for guiding me from the first day of graduate school, for having faith in me, and for giving me the opportunity to work on this project. He has been more than accommodating with my personal and academic requirements and has a huge contribution to my growth as a researcher, a student, a professional and as a human being.

I want to thank the vehicle dynamics experts on my defense committee, Dr. Steve Southward, Dr. Jan Helge Bohn and Dr. John Ferris, for their review and their support for my research. I would also like to thank Dr. Pablo Tarazaga and Dr. Clay Gabler and all the faculty for inspiring me to work in Vehicle Dynamics, Crash Analysis and Automotive Engineering.

I would like to extend my special thanks to Arcimoto Inc. for being flexible to let me work on my thesis after recruiting me as a full time mechanical engineer. Jove Lachman-Curl, Mechanical Engineering Manager, and Mark Frohnmayer, CEO at Arcimoto, have been extremely supportive and understanding of my situation (since my very first interview) and I appreciate their confidence in me.

I would also like to thank my fellow researchers, my homies and roommates in Blacksburg who helped me with research and countless other things to make my grad school experience to be beautiful. I made some beautiful memories and learnt a great deal from the relationships I built at Virginia Tech.

Being away from my family back in Mumbai, I thank my family away from home – my friends in USA, for sharing my struggles and your joys, for partying and studying with me, for being there, be it to help me with research and coursework or play football, for being the best homies I could have asked for.

Further, I thank my parents, grandparents and my sister, for believing in me more than I ever have, and driving me to reach such heights with their constant encouragement. I am grateful to my mother, Dr. Mamta Mehta for her confidence in me and my father, Dr. Nimish Mehta for his encouragement and constant inspiration.

This journey at Virginia Tech was everything and nothing I had imagined to be, and I am forever grateful to this university, the Graduate School and the Mechanical Engineering department for giving me this wonderful opportunity.

Harsh Mehta

Table of Contents

List of Figures

List of Tables

1. Introduction

1.1. Needs Statement and Overview of the project

The Finite Element Method (FEM) is primarily used to give a mathematical description of the elastic and, where applicable, plastic characteristics of mechanical systems, in which mass and elasticity are distributed continuously throughout the body. The model consists of many finite elements of simple geometry (discretized) whose principal deformation fields are constrained by the governing vector field equations and the elementary functions used within the element. The FEM is widely used to examine the effect of external forces on the deformation and stress distribution of a body. The mathematical formulation of FEM leads to algebraic equations representing partial differential equations [1]. The number of algebraic equations depend on the number of degrees of freedom of a single body or multi body analysis.

As suspension geometry, loading and boundary conditions become more complex, the equations of statics and dynamics become more complicated and it may become difficult to account for all phenomena to simulate a real-time scenario. The finite element method has been used for decades to assist engineering in analyzing structures and components. The commercial finite element code Abaqus® employs different modeling techniques and solver configurations for a dynamic analysis, Currently, the method to develop loading scenarios hinges on multibody dynamics (MBD) equations which consider the members as rigid. Typically, the external load conditions for component analysis are developed from “vehicle dynamics” equations assuming the components are rigid bodies and then applied to the elastic structures. These multibody dynamics equations have underlying assumptions, contrary to actual loading scenarios, as well as over-simplified interactions, which miss critical details. Since the upright is a bending and torsion elastic member, the assumption of a rigid suspension upright component is not representative.

There are empirical rules with underlying assumptions which justify that the relative static stiffness of the upright can be equated to the rigidity of upright in dynamic loading studies. These rules of thumb are not proven case-by-case but are based on engineering experience. For example, while studying the tie rod in a geometry where the lateral loading is perfectly horizontal, it is found that

the critical buckling load is 42 kN – hence, the tie rod is rigid (since only the buckling mode is considered) since a FSAE steering system will not see loads, even abusive, which are that high. This doesn't allow the researcher to study the bending and torsion loads on the tie rod since it is considered rigid.

The challenge with multibody dynamics approaches for loads analysis is that typical vehicle suspensions involve closed-chain loops which require expensive differential-algebraic equation (DAE) integration techniques. Another serious drawback is the error drift that arises during the integration of the multibody dynamics equations of motion. The error drift is a numerical error that occurs when the solution does not stay on the manifold of constraints at the position or velocity levels. This error drift is usually handled within a DAE solver and error correction algorithms to manage the constraint error over time, adding additional computational cost and error in accuracy for the dynamics solution [2].

MBD commercial codes like Adams®, CarSim® and SuspensionSim® can simulate vehicle maneuvers. These MBD simulation codes are built on the same multibody dynamics concepts and assumptions found in vehicle dynamics equations.

Physical testing of existing vehicles to record loads for different maneuvers is another method. Requirements for physical testing:

1. Sensor equipment, installation and calibration
2. Signal conditioning equipment – enough channels for all sensors
3. Data acquisition code – to run pre and post processing on the data acquired
4. Time to refine test methods and achieve repetitive and accurate loads
5. Processing the data to achieve load curves

Along with having the capability of modeling detailed interactions and elastic components in finite element models, finite element solvers are also computationally expensive. Vehicle MBD equations are useful for evaluating suspension performance but only when the component is proven to be stiff enough to be considered rigid.

Virtual testing or simulation (after the model is verified and validated to be truly representative) is easier to gain information and iterate repeatedly to refine the design and suspension geometry. Borg [3] concludes from his thesis – "when considering suspension member load, bending should be

taken into account". Hellman [4] simulates vehicle dynamics on multibody dynamics (Adams) and on finite element analysis (Abaqus) environments and concludes vehicle maneuvers are well represented using finite elements.

This research focuses to create a proof-of-concept model that is scalable and representative to solve the problems of vehicle dynamics while incorporating inertia and elasticity. This proof-of-concept will incorporate elastodynamic methods for vehicle dynamics analysis for a Formula SAE quarter-car suspension.

1.2. Hypothesis Statement – Concept for the thesis

Automotive design engineers often find it difficult to predict system performance until very late in the design process. Mechanical, electrical, and other subsystems are validated against their specific requirements within the systems engineering process, but full vehicle physical testing and verification (VT&V) comes late. Consequently, this leads to rework and design changes that are riskier and costlier than those made much earlier [5].

Borg [3] and Angelini [6] performed early finite element modeling work on suspension members and composite chassis focusing on different components, different design concepts and different types of analyses collaborating with the VT Motorsports team. Their contributions to the Formula SAE team at Virginia Tech provides insights towards the development of design, analysis and optimization.

Vehicle maneuvers can be tested virtually with simulations generated by finite element codes like Abaqus. This thesis focuses on developing an approach to model the suspension assembly as an elastic structure and the various connections and interactions. The detail of each connection and interaction in the assembly is carefully modeled and verified independently with hand calculations or smaller representative "building-block" models. The model is used to simulate a dynamic load case scenario with time dependent loads which tries to emulate real time testing. FEM can contribute purposefully towards studying and applying durability in our designs using dynamic (time dependent) loading.

The focus of this thesis is the development of a representative finite element model for a Formula SAE vehicle suspension system focusing on the upright suspension component. The upright

suspension component is the non-rotating portion of the suspension on which the wheel bearings are installed. Loads are transferred from the top hat (wheel hub), through the wheel bearings, to the spindle on the upright. The upright is the component-in-question and the analysis is to evaluate the loads on the upright bodies.

That being said, the model is developed within a framework that includes various interactions, connections and modeling techniques developed to model the suspension as an elastic system with precise geometry and joints.

Hypothesis Statement: A study involving elastodynamics for nonlinear dynamics problems provides a better assessment of how loads vary throughout the full range of motion and operating environments. This research also develops a framework based on the "building block" approach to modeling. A linear elastodynamics study will not be able to model interfaces or contacts, geometric nonlinearities as well as material nonlinearities.

The features of this framework are:

1. The beam elements allow bending in the suspension members.
2. The shell elements allow elastic response for the sheet metal bodies without modeling 3D Stress "brick" elements
3. The connector elements allow and constraint the degrees of freedom as needed
4. Surface contact allows us to study the interference fit between the bearing and bearing housing
5. Unique modeling techniques developed while refining, developing, iterating and debugging the model which can preserve the connection behavior while not representing the components accurately
6. The model is scalable – components can be allowed to be defeatured or add more detail depending on the focus and the problem one is trying to solve
7. The connections modeled can be relevant best practices in modeling suspensions with different configurations and different purposes (heavy equipment vs. passenger cars vs. student racecars)

The resultant deformation, stresses and strains recorded in the elastic suspension members and components leads us to understand the durability issues of the design. The results of the simulation

will be interpreted as guidelines for the suspension designer to make compliance provisions. They will also help the designer understand the behavior or "attitude" of the vehicle in different scenarios. The finite element model will begin a framework to model different iterations using a verified modeling technique.

This framework and lessons learned while modeling, currently helps the author of this thesis with his work at Arcimoto. Arcimoto is an electric vehicle manufacturer in Eugene, Oregon. The team at Arcimoto is driven to produce fast, efficient and fun to drive daily commuter vehicles at an affordable cost.

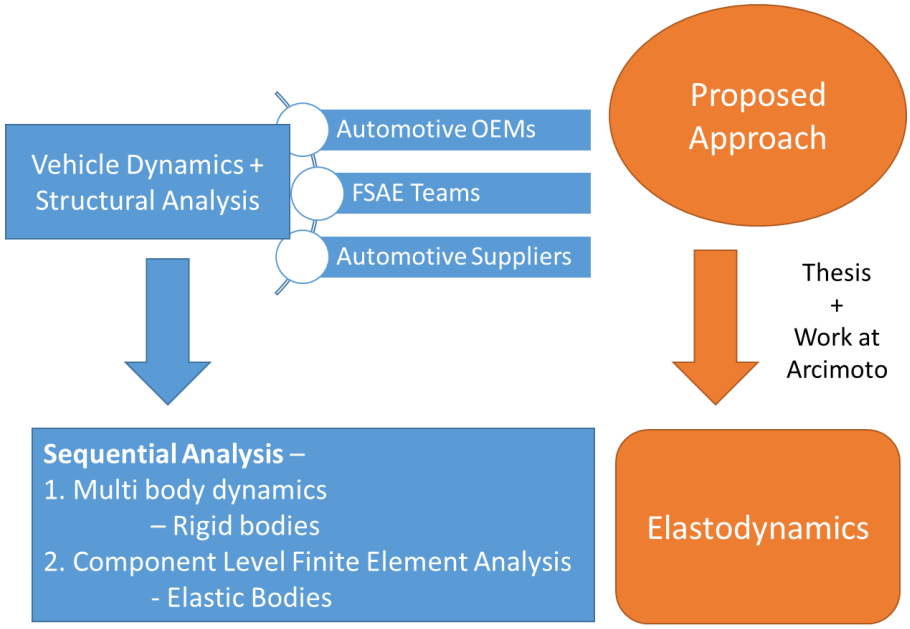

Figure 1.1: Comparison of Approaches to Suspension System Analysis in the Automotive Industry.

1.3. Objectives and Organization of the Thesis

Ford, Toyota and Daimler Chrysler have repeatedly realized the valued of finite element analysis for product development, design, vehicle dynamics and even for niche analyses like buzz, squeak and rattle (BSR) in automotive mechanisms [7, 8].

The thesis research was born from an idea to create a proof of concept finite element model that will represent the various behaviors of the suspension by applying elastodynamics. Elastodynamics can be defined as modeling components in dynamics problems to be elastic; an elastodynamic analysis extracts the elastic response, state of stress and strain, elastic compliance and internal

loads for component focused static analysis. The relevant interactions and connections are modeled to be less expensive computationally and still preserve their dynamic behaviors and the overall load path changes.

The organization of the thesis is compliant with the process of modeling – pre-processing, solving, post-processing – and then interpreting the results. The modeling scope of the suspension analysis is limited to a Formula SAE quarter-car suspension model. The details of the modeling scope will be discussed in Section 2.4.

1. One of the objectives of this research is to develop simulations of simple vehicle maneuvers using elastic structures in a quarter-car suspension assembly. *These simulations test the rigidity assumptions and develop more accurate internal loads which can be used in the future to optimally model the uprights and the suspension assembly. The models grow from stick beam elements to shell elements and then brick elements. The progression shows which modeling or meshing technique works for the purpose and problem.*
    - The load case scenarios incorporated in the model are:
        - Straight line driving,
        - Steady state cornering+braking
        - 5g bump loads.
    - Indication of computational requirements for a multibody elastodynamic analysis.
2. This thesis focuses on improving the preprocessing and solver representations for vehicle dynamics simulations. *The finite element model must be comprised of parts and joints that are established to be representative of the real physics.*
3. Starting with a simplified representation of the suspension assembly as a four bar 2D mechanism (Crank Rocker Mechanism), the goal is to establish a modeling technique for simple dynamics problems using the commercial finite element analysis code, Abaqus. *Hand calculations and four bar mechanisms help with the initial approach to solving the problem.*
4. One of the interactions taking place in the upright is the interference fit between the wheel bearings and the bearing housing. Establishing a simple model provides a better understanding of contact interactions associated with the interference fit of pressing bearings into the housing. *A convergence study is performed to further understand how meshing techniques affect the solution to a surface contact problem.*
5. The complete suspension assembly including constraints, connections and material properties is modeled using data from the Virginia Tech Formula SAE team. Appropriate

boundary conditions and loads obtained from the "Suspension Calculator" developed by Borg [3] are applied to the suspension finite element model. *The results from a quasi-static analysis will help understand the dominant mechanics, critical loading areas, the effects of internal bending moments on each component (suspension members and lever arms of the upright) as well as suspension articulation (large displacements) and compliance of the suspension will be determined.*

6. A recommendation for future work towards studying durability and directing suspension designers will be made. The framework for the established model will be shared with the VT Motorsports Formula SAE team.

A quasi-static simulation and a dynamic (implicit) simulation to represent cornering of the vehicle is performed. The solution and results presented in this thesis establish a framework for straight line and curvilinear dynamics. *The objective is to obtain the stresses and strains, loading trends, modeling shortcomings and performance metrics to assess durability of the design.*

1.4. Scope

Verifying each incremental step toward building the model was achieved by comparison of hand calculations with simple finite element models as proof of concepts. The simple models were used to develop the modeling techniques. The larger finite element model was built incorporating the modeling techniques developed.

There was no physical data available at the time of this research on the elastic response of the upright suspension component or the vehicle maneuver testing. The finite element simulations will be evaluated only on the overall response- energy balance, loads and stresses generated and deformation response. The model timeline can be broken down to different static analyses, but the inertial forces, dynamic modes, dynamic force transition and the respective responses would be lost. This research is focused only on developing a framework to analyze the suspension components elastodynamic response based on expected in-service developed loads, which can later be used for incremental design changes in the suspension and chassis components. The goal of this research is to demonstrate a framework for finite element modeling for vehicle dynamics models and not present a detailed validated design of the assembly.

Borg [3] presented his thesis to evaluate the assumption to consider suspension members as elastic members by using truss and beam elements. This thesis models the suspension geometry members as beam elements to include any bending/transverse shear-flexible deformation. The quarter-car model uses the front-right corner to investigate load changes with steering angle.

Suspension designers and race engineers can devote entire careers to developing knowledge of suspension systems; therefore, the scope of this thesis must be limited to a reasonable scale. The most necessary information to verify in this research includes

- Determining if the rigidity assumption of MBD is justified,
- Investigating a more accurate representation of the linkage dynamics, interference fits, kinematic connections and boundary conditions, and,
- Articulating the suspension appropriately for loading scenarios that require large displacement- small strain formulations.

The hand calculations for various aspects of building the finite element model are prepared initially. The more refined analysis, in this case, finite element analysis, is then developed. The hand calculations are considered as reference in the comparison. The hand calculations establish simpler models, the results of which can be verified, and the lessons learned in improving the modeling technique can be applied towards the more comprehensive model.

The intention of this work is also to provide a foundation for future graduate work that studies the effects and additional factors in more detail as well as validate the response experimentally.

Continuum and conventional shell elements are used for majority for analyses involving the upright and incremental FEM models. 3D stress “Brick” elements have also been used in the later stages to verify the computational results.

1.5. State of the Art in Vehicle Dynamics

Vehicle dynamics problems are solved in different industries including but not limited to automotive cars and trucks, automotive motorsports, agriculture and heavy construction vehicles, commercial vehicles as well as aerospace, rail, space and other vehicles. . The magnitude of static, dynamic and fatigue loads from a higher level between these industries is vastly different. Some suspensions are designed for low speed and smaller loads- for these conditions, the rigidity

assumption is applied with confidence. The passenger vehicle industry popularly uses multibody dynamics codes for solving vehicle dynamics problems. The commercial code, Adams is an example of a large-scale, 3-D multibody dynamics code used to compute and iterate different suspension parameters and geometry configurations. It answers questions for dynamics and is able to extract internal loading conditions from the reaction forces and moments on assembly components. Adams is also able to exhibit mechanism articulation for steer, bump, roll and pitch scenarios. Adams also has the capability to partially model simple elastic components but it does not allow user change control for mesh refinement or editing the meshing strategy.

Another popular computational simulation code used by vehicle dynamics groups in passenger vehicle industry as well as the heavy equipment automobile industry is CarSim®. CarSim features a full vehicle model that can be setup and iterated based on common vehicle parameters. CarSim is built on multibody dynamics (rigid body analysis) foundations but it answers higher level questions like:

1. Can the vehicle climb up the hill?
2. What is the braking distance in simulation?
3. What is the braking time in simulation?
4. Does the vehicle understeer on this track corner?

CarSim is also able to simulate the suspension articulation, inertial load transfers and powertrain simulations (gear shifting, engine RPM, etc.)

Automotive competitions like Formula SAE and BAJA have made the use of these codes widespread and popular among collegiate competition teams. The industry and professional competitive teams have developed sophisticated and complex models on these codes. These commercial codes are created and developed using the concepts of multibody dynamics and differential equations for rigid body dynamics analysis.

Some groups in the automotive industry have started adopting finite element solvers for solving dynamic scenario problems and concurrently solve for elastic response. Some of these groups are from the heavy machinery industry which experience higher loads.

2. Literature Review

2.1. Nature of Finite Element Solution

In an exact solution every differential element of material is in equilibrium, compatibility conditions are satisfied everywhere in the body and all boundary conditions on stress and displacement are met. A solution by finite element analysis (FEA) is approximate- it does not satisfy these requirements in every way. The extent to which the requirements are met in static FEA when elements are based on displacement fields is based on:

- Compatibility prevails at nodes and is satisfied within elements
- Compatibility may or may not be satisfied across interelement boundaries,
- Equilibrium of nodal forces and moments is satisfied in an average sense within an element,
- Equilibrium is usually not satisfied at or across interelement boundaries [9].

The nature of the solution and finite element analysis basics can be found in "Concepts and Applications of Finite Element Analysis" by Cook, Malkus, Plesha and Witt [9].

2.2. Nonlinearity in Structural Mechanics

Linearity and nonlinearity are defined as:

Linear: $L(au + b) = aL(u) + b$

Non-Linear: $L(au + b) \neq aL(U) + b$

where L is a mathematical operator for example: $\frac{d}{dx}$ differentiation

Assumptions for Linear Elastic Simulation:

- Small displacements and small strains
- Linear elastic material behavior
- No change in boundary conditions
- Loading (magnitude, direction and point of application of load) is constant with respect to time

Linear solutions are unique, scalable and can be superpositioned. Nonlinear solutions are non-unique, non-scalable and cannot use superposition. The three most common types of structural nonlinearity are geometric nonlinearity, nonlinear material properties and boundary/contact type of problems.

2.3. Handling Characteristics

Tuning suspension assembly on your car has more effect on handling than any other vehicle subsystem. By suspension assembly, it includes the tire, which is the only component in direct contact with the ground, the brake rotors and calipers, wheel hub, drive shaft coupling, upright, spring-damper assembly and the suspension members. To simplify how the suspension works, we can limit the analysis to input-output characteristics. This type of analysis is called "black box" analysis because we do not concern ourselves with what is going on inside the "box," or the suspension design in this case [10].

Vertical load – The input of suspension performance is the vertical load on the tire. The dynamics of the car in the vertical motion case has a load vector which varies continuously. By tuning the suspension, it is possible to adjust how the vertical loading on the chassis will change and by knowing how the tire will respond to the change in loading, the suspension behavior can be predicted [10].

The need for finite element analysis for designing suspension and handling mechanisms arises from demands for advanced functionality, reduced development time and increasing competition. Experiments on real prototypes will retain its position in the development process but simulations will be able to fulfill legal requirements, achieve close to performance targets and validate iterations. Comparison and correlation with carefully selected experiments will increase accuracy of simulation results as well as serve as a performance reference.

The tire performance curve- traction vs vertical load- is a non-linear curve which determines cornering efficiency. It is remarkable that the interactions between chassis, suspension, and powertrain have become more important with ride comfort analyses than with the established handling and system development investigations [11]. The system development investigations refer to the process of defining and designing the suspension system and its characteristic parameters- what the system is built to do and what is feasible.

2.4. Modeling Scope- Why quarter-car for this research?

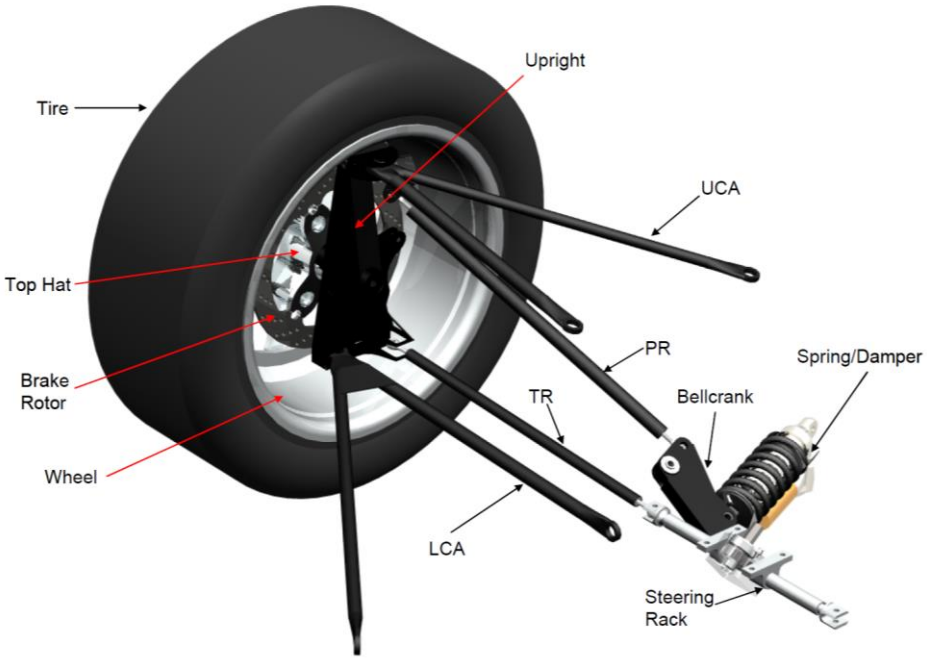

Figure 2.1: Quarter-Car Components - Suspension and Wheel Assembly- Image taken from [3]. Used under Fair Use, 2017. Acronyms: UCA- Upper Control Arm, LCA- Lower Control Arm, PR- Pull Rod, TR- Tie Rod.

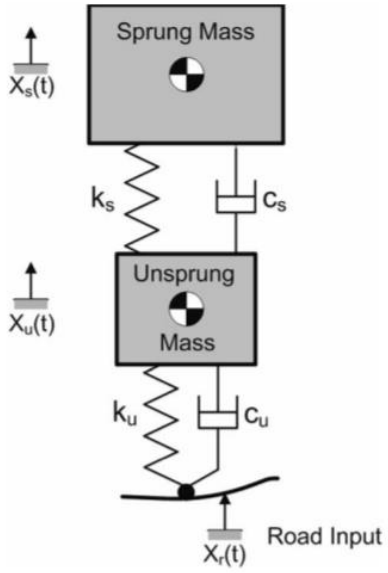

Figure 2.2: Quarter-Car Mathematical Model. Image taken from [12]. Used under Fair Use, 2017.

The assumptions of this quarter-car modeling in Figure 2.1 and Figure 2.2 are as follows:

1. The tire is modeled as a linear spring without damping with definite or indefinite constant stiffness
2. There is no rotational motion in wheel and body,

3. The behavior of the spring and damper are linear,
4. The tire is always in contact with the road surface,
5. Effect of friction is neglected so that the residual structural damping is not considered into vehicle modeling [13].

Conflicting views are found in the literature on the accuracy of the linear quarter-car model. Despite its widespread use, little dedicated research was found on the validity of the relatively simple model in predicting the movement of complex suspension systems [12]. A popular view among authors is that the linear quarter-car model is used due to its simplicity and that the information it provides in the initial stages of design outweighs the inaccuracy [12]. Elmadany and Abduljabbar [14] stated that the quarter-car model captures the most basic features of the real vehicle suspension corner problem. They followed this by saying that when a detailed model of vehicle motion is required, more elaborate models (two or three-dimensional models) must be used which take into account the features omitted from the quarter-car model. An important property of the quarter-car model is that it properly represents the problem of controlling wheel load variations and contains suspension system forces which are properly applied between unsprung and sprung masses. This fact has given rise to the widespread use of quarter-car models in the development of active and semi-active suspension control strategies.

The scope of modeling the quarter-car suspension assembly is limited to the upright, suspension control arms, tie rod (steering rod), pull rod, rocker and spring-damper system. This is to focus on the upright loads analysis and representing interactions and connections associated with it. The upright is subjected to large bending stresses from the suspension members and wheel bearing loads, while also needing to handle the braking forces created by the brake caliper which is mounted to the upright. This thesis does not focus on braking forces from calipers but longitudinal forces from braking is considered.

2.5. Static General Step Solver

A static analysis is sufficient if the interest is to investigate the long-term response of a structure to applied load where the inertial forces can be neglected. The equation of equilibrium governing static linear problems is:

$$[K]\{U\} = \{F\} \tag{1}$$

where K is the global assembled stiffness matrix, F is the external load vector and U is the global displacement field. The convention is upper case letters are for global coordinate system.

The problem can be either linear or nonlinear. Nonlinearities can arise from large displacement effects, material nonlinearity, and/or boundary nonlinearities such as contact and friction. If the problem is nonlinear a form of the Newton-Raphson, Quasi-Newton or Conjugate Gradient methods will be required to solve the incremental form of the system equations.

The static general step solver uses an incremental solving algorithm – with variable or fixed time increments. For some increments it makes multiple attempts to reach convergence in results (equilibrium conditions satisfied).

$$[dK]\{dU\} = \{F_{ext}\} - \{F_{int}\} \tag{2}$$

where the solver solves for {dU} with the increment:

$$\{U_{k+1}\} = \{U_k\} + \{dU\} \tag{3}$$

2.6. Dynamic Step Solvers

2.6.1. Response History: Direct Integration Methods

Direct Integration refers to calculation of response history using step by step integration in time, without first changing the form of dynamic equations, as is necessary in model methods. Response is evaluated at instants separated by time increments Δt. At the n^{th} time step, the equation of motion is

$$[M]\{\ddot{D}\}_n + [C]\{\dot{D}\}_n + [K]\{D\}_n = \{F^{ext}\}_n \tag{4}$$

Note: Generally, since the dimensions and material properties are constant throughout time, [K] does not change from one-time step to the next in linear problems.

In this discussion we assume that [M] is positive definite, but that [K] need only be positive semidefinite. This assumes that the system of matrix equations (ordinary differential equations) are linear and self-adjoint. Thus, the structure can have rigid body motion as part of its response. If there is a mechanism associated with element instability, it may produce such large non-physical displacements that results are unsatisfactory.

Methods of direct integration at time step $(n + 1)$ from the equation of motion, yields a difference expression, and known conditions at one or more preceding time steps. Algorithms can be classified as either explicit or implicit. In practical application, important differences between explicit and implicit methods are related to stability and economy [9].

2.6.2. Implicit Dynamics Solver Stability

The general direct-integration method provided in Abaqus Standard, called the Hilber-Hughes-Taylor operator; it is an extension of the trapezoidal rule. In this method the integration operator matrix must be inverted, and a **set of simultaneous nonlinear dynamic equilibrium equations must be solved at each time increment**. The implicit dynamic solution is performed iteratively using Newton's method [15].

This nonlinear equation solving process is expensive; and if the equations are very nonlinear, it may be difficult to obtain a solution. However, nonlinearities are usually accounted for more simply in

dynamic solutions than in static situations because the inertia terms provide additional force terms capable of providing mathematical stability to the system. Thus, the method is successful in all but the most extreme cases. Unfortunately, obtaining a solution does not guarantee a representative solution to the system being studied.

To control the accuracy in the solution, the method of half-step residual is used. The half-step residual method is based on calculating the equilibrium residual error (out-of-balance forces) halfway through a time increment. If the half-step residual is small enough the calculation will continue [12]. A big advantage of a step-by-step solution scheme based on this integration is that it can be used for solving both static and dynamic problems, whereas the central difference method solution could not be used if mass and damping effects are neglected. This is primarily a choice to use a difference approach to discretizing the response in time. It is a choice of formulation, not a limit on solution.

2.6.3. Explicit Dynamics Stability: Estimation of Δt_{cr}

If Δt is too large, explicit integration fails. If Δt is unnecessarily small, the calculations to cover the time interval are too expensive. Therefore, it is necessary to determine ω_{max}, or accurately bound it for use in evaluating conditional stability- calculations may "blow up" unless

$$\Delta t \leq \frac{2}{\omega_{max}} = \Delta t_{cr} \tag{5}$$

where frequency ω_{max} and its period T_{min} correspond to the highest natural frequency of $([K] - \omega^2[M])\{D\} = \{0\}$. The critical time step is independent of damping.

An analyst may wish to avoid calculating the exact ω_{max} because [K] must be assembled and an eigenvalue problem solved.

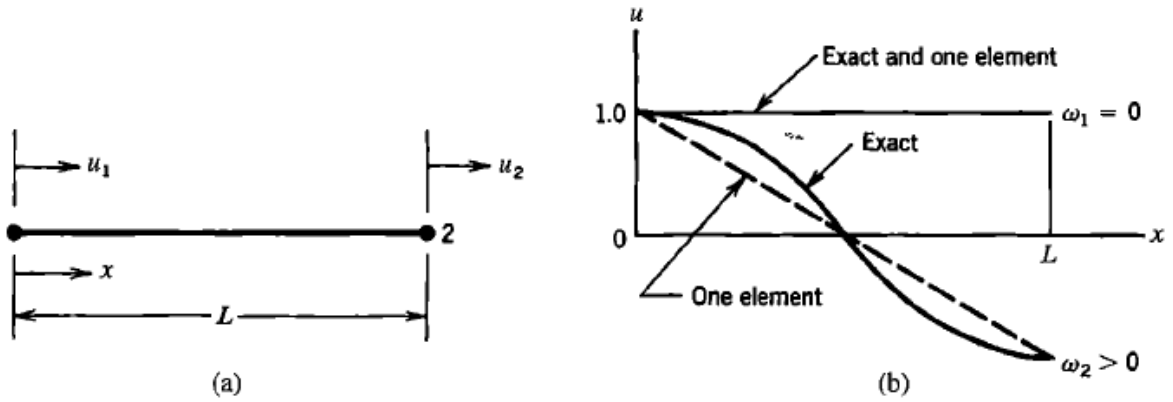

Figure 2.3: (a) Unsupported two d.o.f. uniform bar. (b) Modes for $\omega_1 = 0$ (rigid body translation) and $\omega_2 > 0$ (axial vibration mode) [9].Reprinted from Concepts and Applications of Finite Element Analysis by Cook, Malkus, Plesha, Witt– Copyright 2002.

One way to bound ω_{max} of the FE mesh is to note that is must be less than the largest ω_{max} of any unassembled and unsupported element of the mesh. The latter frequency can be obtained by hand calculation. In the case of an unsupported two- d.o.f. uniform bar as in Figure 2.3 - the highest frequency is calculated by

$$\omega_{max} = 2\sqrt{\frac{AE}{mL}} \tag{6}$$

$$\text{where } m = \rho AL \quad \text{hence } \omega_{max} = \frac{2}{L}\sqrt{\frac{E}{\rho}} = \frac{2c}{L} \tag{7}$$

where $c = \sqrt{E/\rho}$ is the speed of sound in that material.

Using this estimate, the critical time step $2/\omega_{max}$ for an undamped material is

$$\Delta t_{cr} \leq \frac{L}{c} \tag{8}$$

which is called the CFL condition after Courant, Friedrichs and Lewy. The physical interpretation is that Δt must be small enough that a signal entering on end of the elements doesn't propagate more than the distance between adjacent nodes during a single time step [9].

2.6.4. Comparison between Direct Integration Methods for Response History

Table 2.1: Differences between Explicit and Implicit Dynamics Methods in FEA.

Explicit Direct Integration: Dynamics	**Implicit Direct Integration: Dynamics**
• Conditionally stable There is a critical time step Δt_{cr} that must not be exceeded if the numerical process is not to "blow up" by becoming unstable.	• Unconditionally stable Calculations remain stable regardless of how large Δt becomes
• Large number of steps Since Δt_{cr} is quite small, great many time steps are needed	• Accuracy suffers with larger Δt
• Computational cost per time step is lower $\{D\}_{n+1}$ can be made diagonal in explicit method cheaply because of smaller time steps	• Computational cost per time step is greater
• Explicit methods do not check for equilibrium directly for each time step. Hence, they are conditionally stable	• Implicit methods attempt for internal equilibrium convergence for each increment

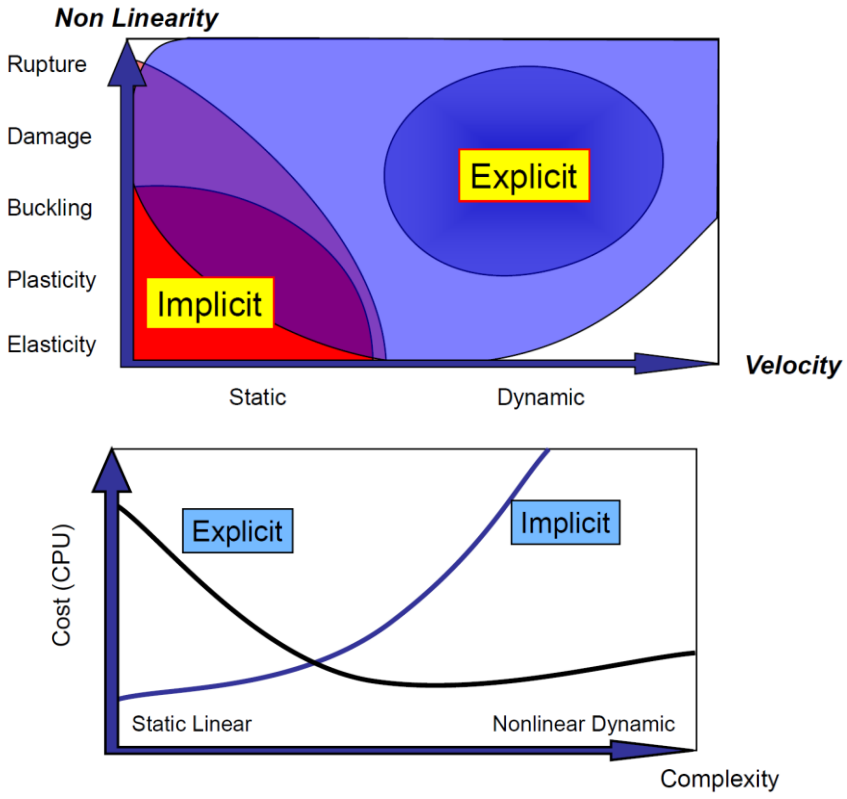

Figure 2.4: Qualitative Graphs representing suitability of different dynamics methods of FEA.

2.7. Modeling Interactions

2.7.1. Surface to Surface Contact

Surface-to-surface contact interactions describe contact between two deformable surfaces or between a deformable surface and a rigid surface. Self-contact interactions describe contact between different areas on a single part/component surface.

A contact simulation using contact pairs or general contact is defined by specifying:

- surface definitions for the bodies that could potentially be in contact;
- the surfaces that interact with one another (the contact interactions);
- any nondefault surface properties to be considered in the contact interactions;
- the mechanical and thermal contact property models, such as the pressure-overclosure relationship, the friction coefficient, or the contact conduction coefficient;
- any nondefault aspects of the contact formulation; and
- any algorithmic contact controls for the analysis [15].

2.7.2. Constraints

Tie

The *TIE command writes multi-point constraint equations between the displacement d.o.f. (degrees of freedom) of nodes of two separate surfaces that effectively ties the surfaces together such that there is no relative motion between the nodes of the two surfaces. It allows to fuse together two regions even though the meshes created on the surfaces of the regions may be incompatible. A tie constraint can be defined between edges of a wire or between faces of a solid or shell.

A surface-based tie constraint:

- ties two surfaces together for the duration of a simulation,
- can be used only with surface-based constraint definitions,
- will take the initial thickness and offset of shell elements underlying the surface into account by default, and
- eliminates the degrees of freedom of the slave surface nodes that are constrained, where possible [15].

Coupling

A coupling constraint, also a multipoint constraint, is used to constrain the motion of a surface to the motion of one or more points. It can be created by specifying one or more control points, a constraint region, and an influence radius that defines the points in the constraint region to include in the constraint. There are 2 types of coupling constraints - kinematic or distributing couplings.

Kinematic coupling constraints:

- limit the motion of a group of nodes to the rigid body motion defined by a reference node;
- can be applied only to specific user-specified degrees of freedom at the constrained nodes;
- can be specified with respect to local coordinate systems at the constrained nodes; and
- can be used in geometrically linear or nonlinear analysis [15].

Multi Point Constraints

Multi-point constraints (MPCs):

- allow constraints to be imposed between different degrees of freedom of the model; and
- can be quite general (nonlinear and nonhomogeneous) [15].

Using MPC type LINK

MPC type LINK provides a pinned rigid link between two nodes to keep the distance between the nodes constant. The displacements of the first node are modified to enforce this constraint. The rotations at the nodes, if they exist, are not involved in this constraint [15].

2.7.3. Connector Elements

There are different ways to model kinematic relationships between nodes in Abaqus [6]:

1. Multi-point constraints (MPCs)
2. Springs/dampers
3. Connector elements

MPCs and springs/dampers are generally used to specify basic relationships which have no other flexibilities. The advantage of using connector elements is that unlike MPCs they do not delete nodal degrees of freedom from the solution and they allow for complex relationships relative to a local coordinate system that moves with the model. This complexity implies MPCs tend to be more computationally efficient than connector elements, but the utility of connector elements lies in the complex relationship between kinematic degrees of freedom of specific joints that can be modeled and included in a finite element model.

Connector elements define degrees of freedom that can have relative motion between two nodes relative to the coordinate system. These relative degrees of freedom can be given properties like elastic stiffness, damping, friction, allowable range of motion, etc. For example, a damper could be modeled as a connector element where the relative degrees of freedom would be the 1-direction in a coordinate system where the 1-axis is the line connecting the two nodes. A definition of an axial connector element is shown in Figure 2.5 where nodes ‘a’ and’ b’ represent the two ends of a Macpherson strut shock.

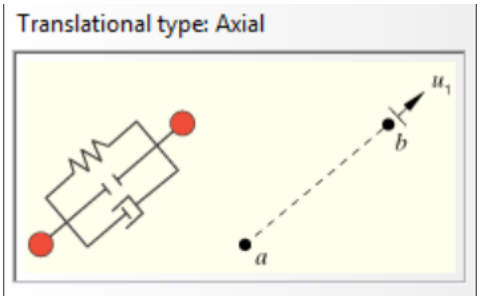

Figure 2.5: AXIAL connection representation. Image taken from [15]. Used under Fair Use.

2.8. Small Strain - Large Displacement Model

Changes in the internal loads due to member compliance is observed by representing the suspension members as elastic structural components in a kinematic linkage. There is a need for a FE code capable of large displacement-small strain analysis. Each finite element and node will move by large displacements (translational and rotational) which is relative to small deformations on the members. The suspension members are subjected to small strain, if elastic, relative to the movement of the quarter-car. Large displacements as any deflection or movement of element is not accounted for in first-order engineering static structure analysis. Since the suspension is a kinematic linkage as well, the FE code should have the capability to represent the movement of elements from factors other than internal load. Abaqus is known to be a good FE solver for the above needs. [3]

ADAMS (and Adams/Car) is a multi-body dynamics (MBD) program that is often used in suspension analysis. The ADAMS program allows the user to enter suspension points into a user defined or pre-existing template and run kinematic simulations on the suspension design. Common outputs include camber gain, toe change, and camber gain versus degrees of body roll. This data is of great interest to the suspension designer in determining the best kinematic design for the suspension.

The primary purpose of this research is to study the structural behavior of the suspension members. This includes the internal forces and moments resulting in stress and strain within the members as well as the compliance these loads cause under load. While Adams can calculate the member loads for various conditions, the program does not handle the actual stress and strain of the members as each member is modeled as a rigid part. Informational material by the company MSC suggests taking the loads calculated in Adams and using them as a loading condition in a

proper FE program such as Nastran (or in the case of this research Abaqus). Since one of the goals of this research is to develop a model that can be used for structural analysis of future teams, it is desirable to have a program that is fundamentally FE-based and capable of modeling compliances in addition to kinematic movements [3].

2.9. Formula SAE Suspension Design

The Virginia Tech Formula SAE team – VT Motorsports would like a thorough structural analysis of the internal upright loads due to the expected design loads. In the world of formula racing, the pinnacle of technology exists in the Formula 1 racing series. These cars are capable of cornering at nearly 5g's and reach speeds as high as 230 MPH (~375 km/h). Formula 1 teams will spend millions of dollars for fractions of a second in reduced lap times. Part of reducing lap times of any racing vehicle is to optimize the suspension. The suspension controls the "attitude" of the tire to the road surface through the design of the suspension linkage kinematics. The suspension also reacts to the loads created by the tire. The loads will force the suspension to elastically deform. This compliance will change the orientation of the tire to the road. To control and predict this compliance, race engineers will thoroughly analyze the suspension members for deflection, stresses, and strains [3].

Depending on the racing series, a simplified method of load calculation can be used to minimize the time and effort required to determine the suspension loads. One simplified method often used assumes that the suspension can be represented by a truss structure consisting of six independent members. A space truss eliminates several of the structural responses that could be present in the suspension; the most prominent of which is any bending moments. It is also assumed that a space truss is constrained such that there is no large elastic displacement of the structure. A suspension will have a great deal of displacement, a small amount due to the internal strain in the members in the form of compliance, as well as the large displacement caused by the wheel movement relative to the chassis [3].

The other typical analysis method seen in the automotive industry is creating all suspension parts in an FE model and loading the entire assembly with the expected tire loads or road inputs. This method is often used to determine stress and strain, including stress concentrations in the

individual parts, beyond determining loads within each member. The reason for looking at stress concentrations in addition to member loads is due to the nature of production vehicle suspension designed to meet certain fatigue and cost criteria [3].

2.10. Formula SAE Suspension Analysis

Fundamentally Formula SAE is a design competition, with on-track dynamic completion events being “proof of concept” exercises.

Most FSAE teams use some variation of statics methodology presented by Milliken [16] and Gillespie [17] to design and analyze their suspension systems. The physics behind Ride and Roll Rates, Suspension Kinematic Geometry, Lateral Load Transfer and Multibody Dynamics is applied to analyze the static and rigid body dynamics of the suspension and wheel assembly.

Gillespie further discusses elasticity and non-uniform dynamic behavior in wheel assemblies in another book [18]. Computing solutions for elastodynamics for accurate dynamic behavior simulations have not been introduced widely among FSAE teams. The automotive industry has access to supercomputers to solve computationally expensive problems using finite element analysis but they rarely publish their proprietary internal work.

Harris [19] was one of the few people early on who started exploring vehicle dynamics using multibody dynamics concepts and applying them to Adams/Car. More recently, Angelini [6] has been working on simulating dynamic vehicle maneuvers for elastic members of an integrated composite chassis structure. Angelini [6] also presents how the torsional stiffness of the chassis affects the overall system stiffness and how it affects the vehicle dynamics. Borg [3] has employed finite element methods to validate suspension member loads using elastic “beam” elements. Borg also presents looking at the handling characteristics of the suspension assembly while studying the loads. Though he reports member loads, he does not model the wheel assembly or the upright and does not perform dynamic simulations. In most of the other literature, suspension members are modeled as truss elements because the assumption is that they are two0force members. Borg [3] showed when considering suspension member loads bending should be considered.

At the time of this writing there does not appear to be published literature of teams using loading scenarios to design their chassis, such analysis is likely being done. The current state of these loading scenarios, like some of the Virginia Tech load cases, are most likely based on vehicle dynamics models assuming rigid components or pure experimental test data. Teams like Texas A&M are doing full vehicle models in software like Adams, while other teams are simulating vehicle dynamics with other methods based on rigid-body dynamics. Extracting resultant loads from the tire contact patch is not only extremely difficult but can be unreliable. This is because elastic tires have numerous degrees of freedom and incorporating force transducers on the wheel is not always feasible.

Though not an FSAE system, Hellman [4] begins to simulate vehicle dynamics in finite elements as well as in Adams. His work in Abaqus begins to show how to incorporate the suspension components into finite element software and begin to simulate vehicle maneuvers. Hellman found a good correlation between Abaqus and Adams spring force/displacement results in straight-line dynamics and bump analysis. Due to lack of tire models, he did not consider turning maneuvers. Hellman's goal was to show that vehicle maneuvers could be simulated using a finite element code for consolidation of simulation software for small companies. While Hellman uses elastic components in his models, his primary goal and future goals center on using Abaqus as an Adams alternative. Abaqus, using rigid bodies, can effectively represent Adams simulations. The power of using Abaqus would be the ability to evaluate the elastodynamic response of the components during the simulations [6].

2.11. Incremental Approach towards FE Suspension Model Development – Modeling Technique

Calculating suspension member loads or displacement can be performed using different methods:

1. Kinematics – Analytical or Graphical Methods
2. Multibody Dynamics
3. Finite Element Method

The kinematics approach to calculating displacement in a mechanism or constrained structure assumes the linkages are rigid and does not consider external forces or internal body weights of the linkages. A multibody dynamics approach based on the geometry of the assembly also typically

assumes that the components are rigid, that there is no elastic deformation of the assembly. The finite element method is a flexible model of the problem based on the modeler's scope and given data. We can choose to consider a component rigid or elastic (or plastic) as well as obtain accurate results based on the finite element used and the mesh characteristics.

The underlying assumptions and a precise modeling technique must be established to proceed with a full assembly finite element model. The modeling technique is established in incremental steps. Finite element modeling, like other model classes, is dependent on representation. An inquiry driven approach was followed to explore the different representations of the assembly. An awareness towards machine elements and insight into solid mechanics provides reasoning in our simulations and these models can be further established for testing different loading scenarios and studying durability and dynamic behavior.

A flexible body dynamic solution developed to study vehicle dynamics problems is not typically used in early stages of design/analysis in the automotive industry. High fidelity system-level simulation requires a broad range of analysis functions such as nonlinear material behavior, contact interactions, and mechanisms with complex kinematic constraints [20]. The incremental steps discussed in this chapter complete the suspension assembly for a quarter-car within the scope of this work.

Once the finite element model is created for a static general analysis (quasi-static) in Abaqus, the solver capabilities are extended to include implicit dynamics problems and allowing the study of loads and behavior of the upright with time-depending loading scenarios.

2.12. Drawbacks of Elastodynamic Modeling Approach

1. Run Time

Finite element models have long run times. In a dynamics model, the solver reaches convergence of results for each time increment which leads to longer run times. Modeling complexity and computational expense is a major reason for finite element analysis not being adopted widespread for dynamics analysis. The run time for getting the simulations for this research were long as well and required the resources of Advanced Research Computing.

The run time can be much longer if the model is too detailed. Since the focus of this research is to evaluate the stress and strain on the upright, other suspension components have not been modeled with great detail. Their elastic properties and the joint connections have been preserved with this efficient method of modeling. The upright model also consists of conventional and continuum shell elements and not 3D brick elements so that the model is made more computationally efficient.

2. Mesh sensitivity

Finite element modeling has been notionally not used for modeling extremely complex systems because of a varying reasons. One of the important reasons is that the simulations are mesh-sensitive and with a different mesh density, the simulation behavior could change drastically.

To address this issue, in this research, steps were taken to prevent discrepancies with different mesh densities. A convergence study was performed and followed for further modeling. The convergence study was based on interference fit surface contact phenomenon, arguably most relevant towards mesh sensitivity.

Another step to prevent incorrect representation was to create simpler "building-block" models which were tested and verified from their isolated behavior in a simulation. For example, a simpler rocker model with connector elements and linkages was created to test the effectivity and modeling representation.

The model cannot be extended directly for use with universal suspension analysis but a good direction plan for another commercial code based on concepts of finite elements and elastodynamics can be initiated. The best practices for modeling and the proof of concept of the popular double wishbone quarter-car model will give valuable insights into building a code for suspension analysis.

3. Assumptions beneath the modeling approach

- The model has assumptions for rigid wheel assembly – tire, hub, disc rotors, etc.
- The elastic properties of tubing and sheet metal is considered to be the same. In reality, tubing, if cold drawn or drawn over mandrel will have different elastoplastic properties because of cold working.
- The model assumes the inboard chassis points are pure pinned joints (all translational degrees of freedom constrained) as well as the load curve inputs applied on the wheel center.

3. Four Bar Mechanism

The purpose of this study is to compare the kinematics and kinetics solution with the elastodynamic solution and get experience with the Abaqus dynamic solvers and decide on the preprocessor setup.

The suspension assembly of a vehicle is a 3D structure with six links that restrict/constrain the six degrees of freedom of the wheel. A simplified representation of the control arms and upright can be solved as a 2D four-bar mechanism. A preliminary dynamics analysis is the first incremental step towards establishing a finite element modeling technique which can be verified with the existing analytical solution.

3.1. Hand calculations- Excel file

A simple 2D four-bar mechanism dynamics analysis can be modeled using hand calculations. The hand solution consists of a study of mechanism kinematics and developing dynamics equations for each link using D'Alembert's principle. The equations obtained are solved using a matrix method. This solution is only valid for the particular instant of time when the angular velocity is applied on the crank. Incrementally, this solution technique can be extended to longer time periods. Solving for each time step using a computational engine will be the next step. A matrix approach is chosen to establish a mathematical framework towards a computational model.

Problem Statement:

The four mechanism is driven at O_2 at a constant angular velocity of 500 rad/s. From the data given, make a complete dynamic analysis including a kinematic analysis, inertia force determinations and a force analysis.

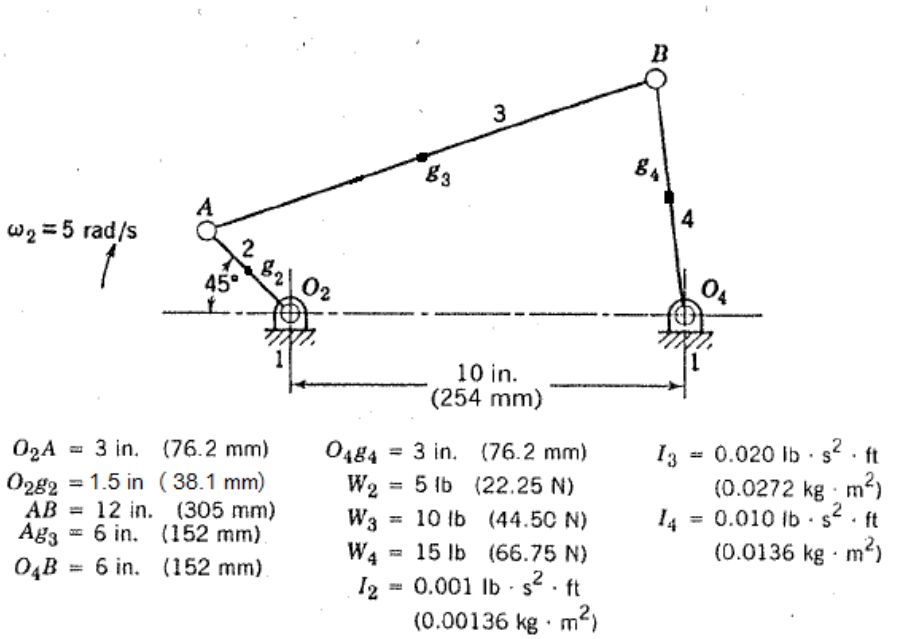

Figure 3.1: Four Bar Mechanism Example Problem – Image taken from Dr. West class notes. Used under Fair Use.

The detailed calculations, results and an MS-Excel Calculator Spreadsheet have been covered in Appendix A.

3.2. Four Bar Mechanism FE Model

The aim of this thesis is to explore the analysis of loads and elastodynamic behavior of the suspension system. The hand calculations for the dynamic analysis of a simplified four-bar mechanism which represents the control arms and upright 2-D assembly was performed for a single time step. Another model is created in Abaqus to employ the quasi-static solver and correlate the results. This exercise is a step towards establishing the modeling technique using finite element analysis for elastodynamics problems. The four-bar problem is a small strain, large displacement problem.

The four-bar mechanism has a crank-rocker configuration. A boundary condition is applied on the crank for a uniform angular velocity of 5 rad/s. The hand calculations assume that the linkages do not have any nodal rotational degrees of freedom (bending). Hence, as the first step in the finite element model, it would be typical to model the crank, the connecting rod and the rocker rod to be TRUSS elements. But since the crank has a rotational boundary condition for uniform angular

velocity, the crank model requires nodal rotation and hence BEAM elements are chosen. The geometry is recreated on Abaqus using the problem data.

Material and Section Properties

The problem statement provides mass, length and rotational moment of inertia at the center of gravity of each solid circular rod. This data is used to define material and section properties.

Table 3.1: Material and Section Properties for Abaqus model for four bar mechanism dynamics.

Model Parameters	**Crank (O_2A)**	**Connecting Rod (AB)**	**Rocker (O_4)**
Weight	5 lbf	10 lbf	15 lbf
Moment of Inertia ($I_{transverse\ axis}$)	0.0011 lbf-s^2-ft	0.035 lbf-s^2-ft	0.0132 lbf-s^2-ft
Density (Calculated)	3.46 lb/in^3	1.71 lb/in^3	5.13 lb/in^3
Solid Circular Cross Section Radius	0.393 in	0.393 in	0.393 in
Elastic Modulus – Steel	3e7 psi	3e7 psi	3e7 psi

Interactions Module

To emulate the rotational joints between the three bars, we use the *COUPLING constraint with constrained translational degrees of freedom. The *COUPLING constraint type selected is KINEMATIC.

Step Solver Module

The Abaqus Standard- Dynamic Implicit (General) Step is to run for two (2) revolutions (2.512 seconds). A fixed step solver is chosen to solve at equal time interval step frames and notice the dynamic behavior.

Mesh Module

Each bar of the 4-bar linkage meshes as a single element. The element type assigned to each bar is BEAM– B22H. It is a 3-node quadratic beam in a 2D plane. The B22H elements are Timoshenko type beam elements based on a hybrid shear flexibility formulation. The hybrid element uses a combination of strain energy (displacement-based) and complementary strain energy (force-based). This analysis did not require the hybrid element formulation. B22 would have been a better choice but the hybrid element would not be wrong to choose.

Loads and Boundary Conditions Module

Table 3.2: Loads and Boundary Conditions Applied to the Four-Bar Dynamics Analysis Model.

Loads		None
Boundary Conditions	Pinned	Pinned Joints at O_2 and O_4
	Angular Velocity	Angular Velocity UR3= 5 rad/s (Instantaneous) for O_2A Crank

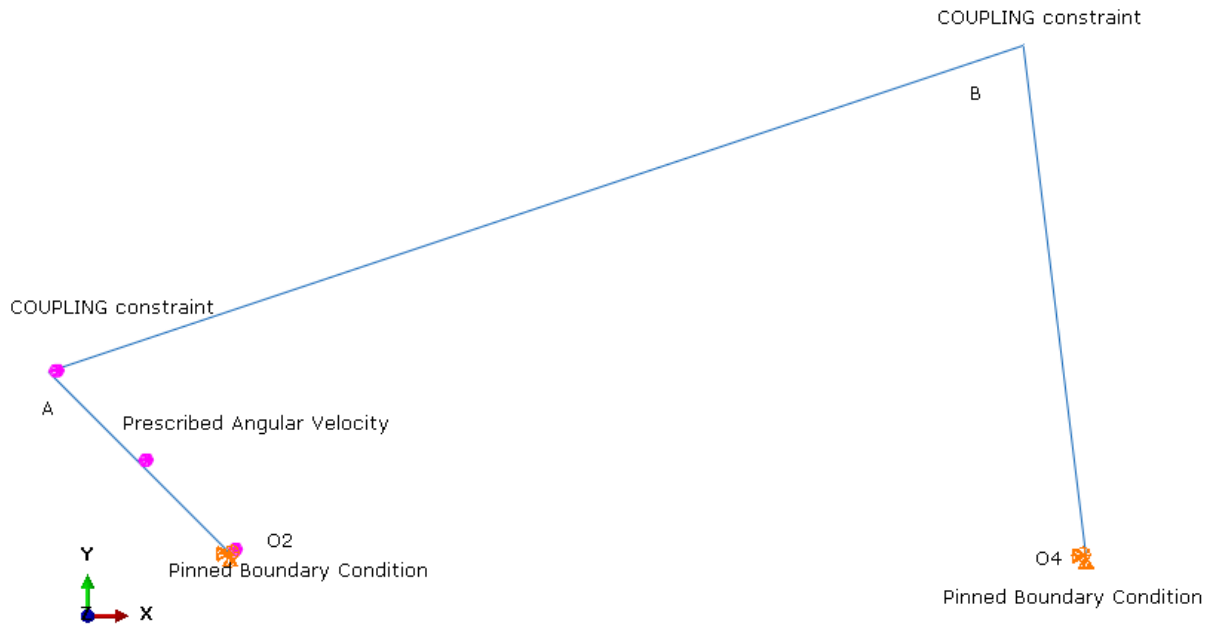

Figure 3.2: Loads Diagram for Four-Bar Dynamics Analysis Model

3.3. Comparison of Results

Developing and establishing the modeling technique depends on precise representation in the finite element model. Hand calculations are referred to for evaluating the model technique.

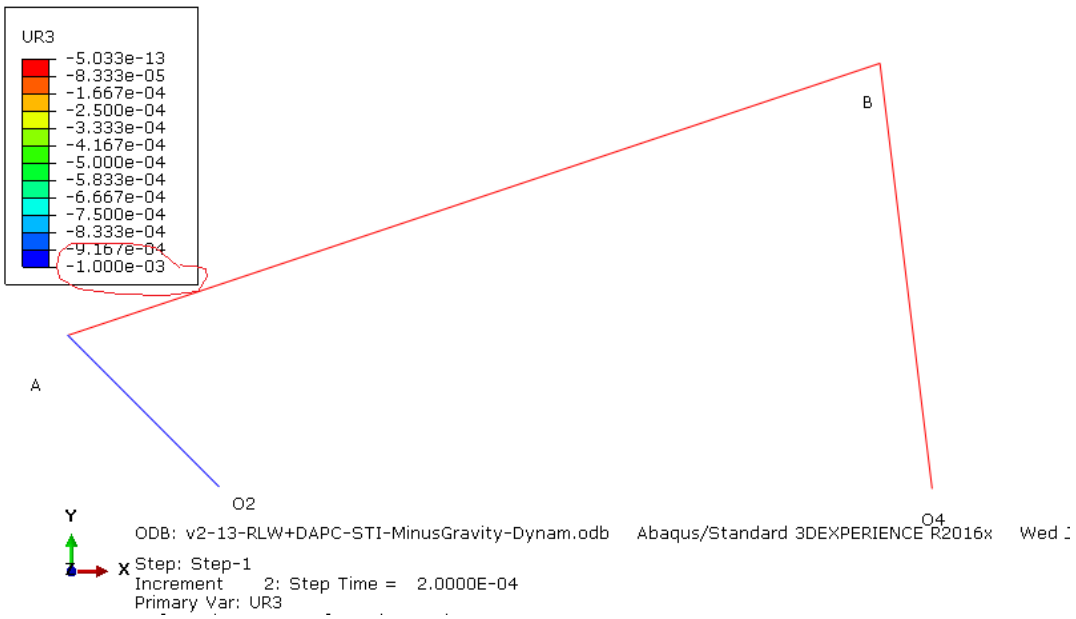

Figure 3.3: Rotation about Z-Axis Results for four bar mechanism at $2\ x\ 10^{-4}s$.

The time step at 2e-4 s has been chosen to compare the hand calculations of the dynamics problem which considers the first time instant of the problem. The crankshaft rotates 0.05 degrees in that time step. This means the reaction force results are calculated for close to zero displacement which is the assumption in the hand calculations.

With the time step chosen to evaluate and compare initial results, the reaction force and moment results are analyzed.

In the first "instant" of the time step 2e-4 s, a reaction force is developed to the point where the crank rod is connected to ground (4th bar of the mechanism). This reaction force was also calculated in the hand calculations. Hence, we compare the results for the point which is now the critical section of the mechanism for this time instant.

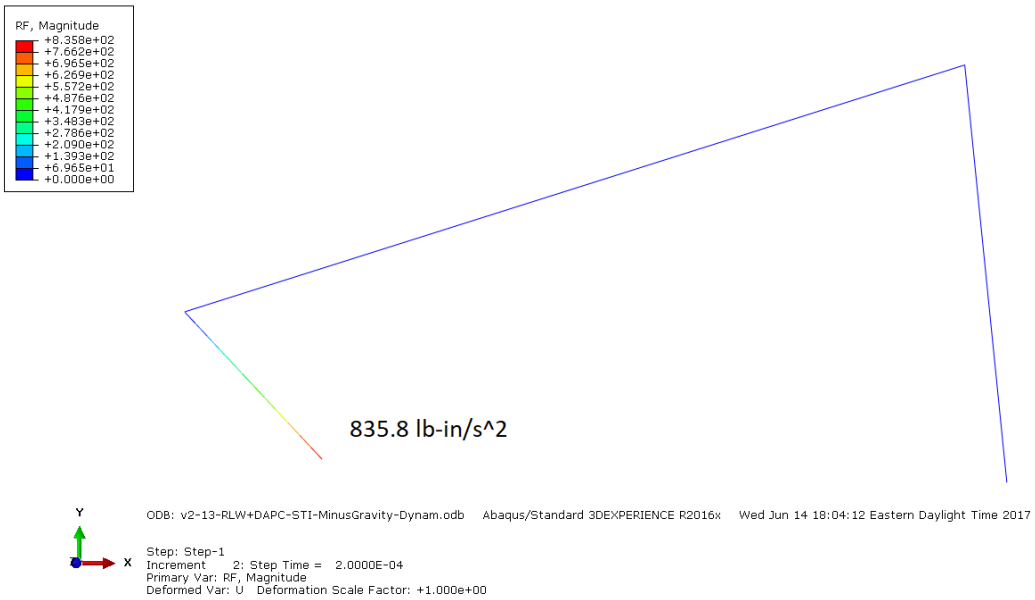

Figure 3.4: Reaction Force Contour Results for four bar mechanism at $2\ x\ 10^{-4} s$.

The reaction force, developed in the first instant of 2 e-4 seconds, does not significantly affect the connector bar (AB) or the rocker bar (O_4B). This can be because of a few possibilities:

- The large displacement small strain problem has not propagated enough until the said time step
- The strain energy is too low to propagate to the other links

These results will be again evaluated when we analyze the results after 2 revolutions of the crank bar.

This critical section, where the PINNED boundary condition is applied on the crank rod, is also expected to develop a reaction moment according to the dynamics hand calculations.

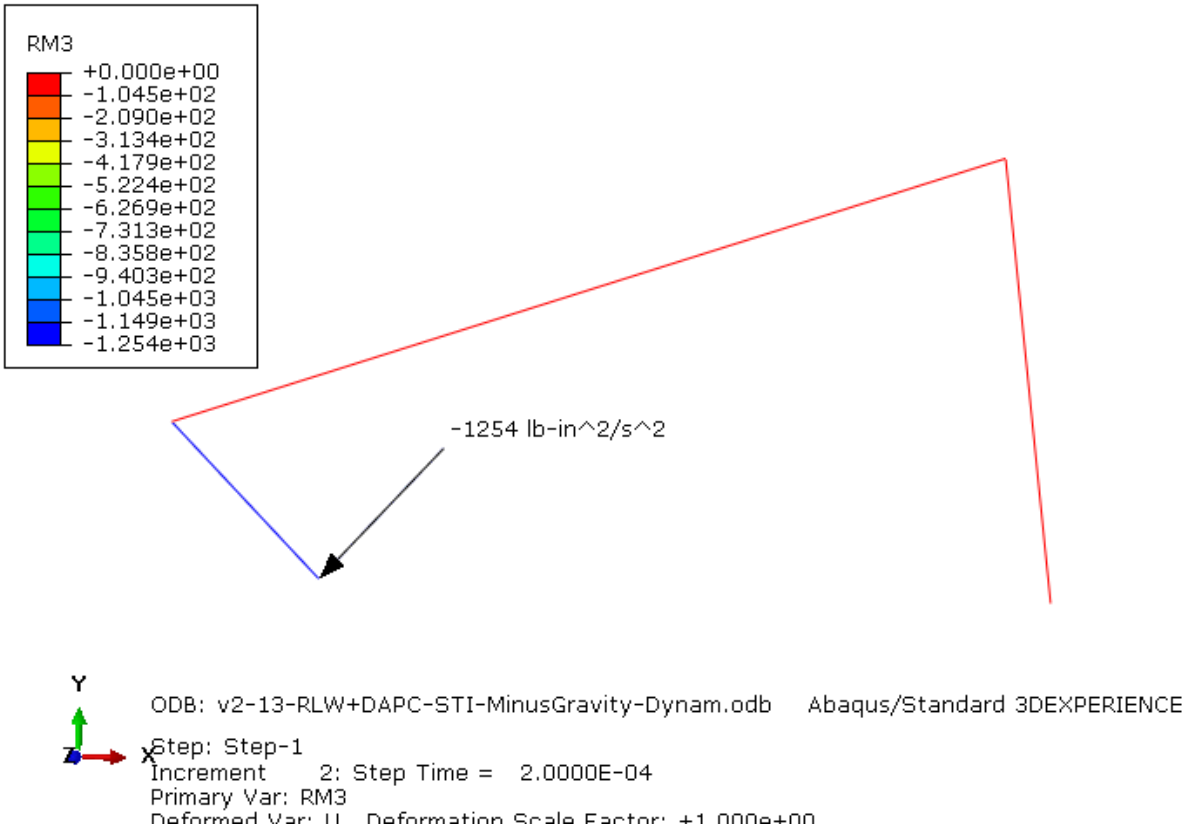

Figure 3.5: Reaction Moment about Z-axis Contour Results for four bar mechanism at $2\ x\ 10^{-4} s$.

Table 3.3: Reaction Loads at the Pinned Joint of the Crank Rod - Comparison of Abaqus Dynamics model and Hand Calculations.

At O_2	**Hand Calculations**	**Abaqus FE Model- Step Time= 2e-4 s**	**% Difference**
Reaction Force	$1.9596\ lbf$	$8.358e+02\ lb-in/s^2 = 2.163\ lbf$	+10.3%
Reaction Moment	$-2.6628\ lbf-in$	$-1253.71\ lb-in^2/s^2 = -3.244\ lbf-in$	+21.8%

On running a dynamic implicit solver simulation, results after 2 revolutions at uniform velocity of the crank for the same variables, reaction force and reaction moment, at O_2 are compared with the hand calculations.

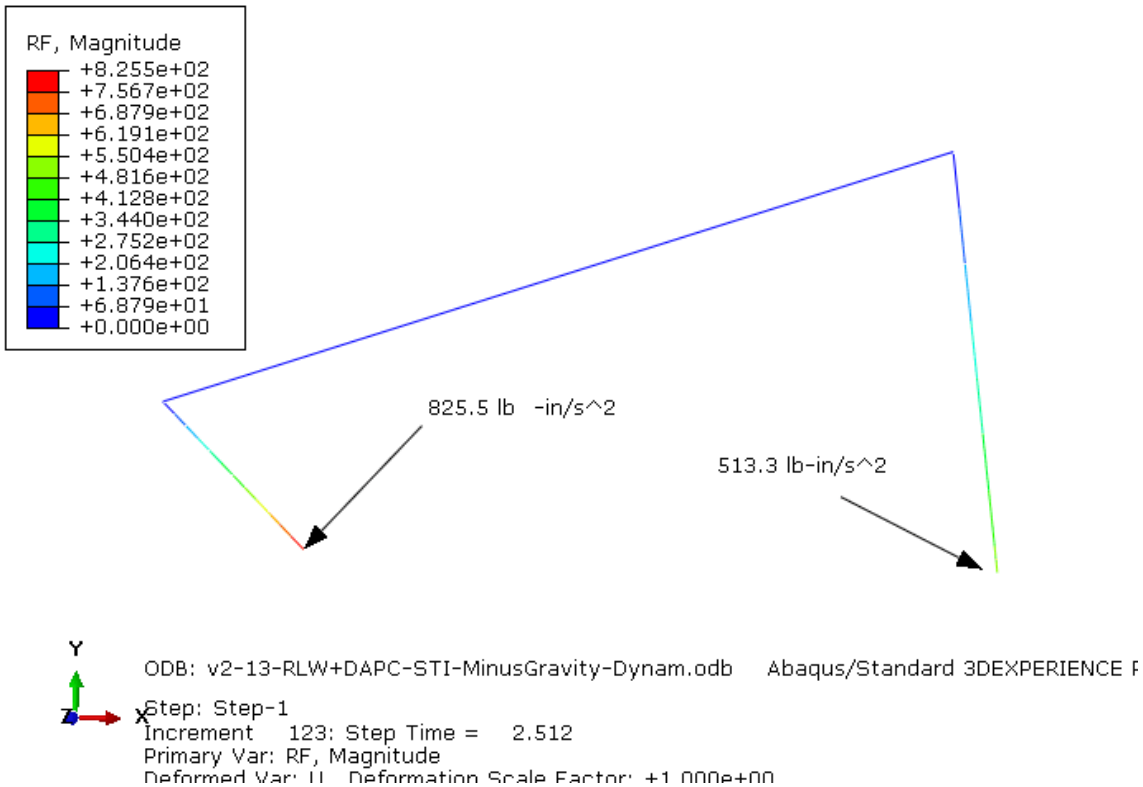

Figure 3.6: Reaction Force Contour Results for four-bar mechanism at 2.512 seconds i.e. 2 revolutions of crank at 5 rad/s.

As mentioned earlier, there is a reaction force developed at the PINNED end of the rocker bar O_4B. The tensile and bending stress and strain developed in each member will be explored as well.

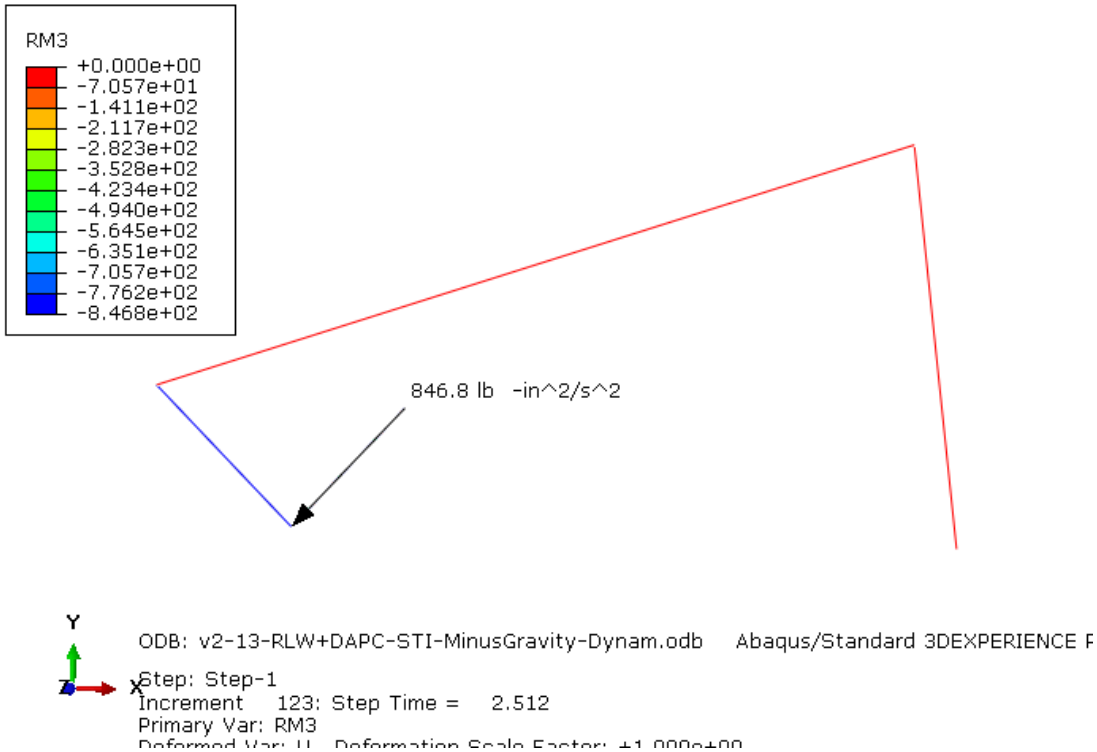

Figure 3.7: Reaction Moment Contour Results for four bar mechanism at $2.512\ s$ *i.e. 2 revolutions of crank at* $5\ rad/s$.

Table 3.4: Reaction Loads at the Pinned Joint of the Crank Rod - Comparison of Abaqus Dynamics model and Hand Calculations.

At O_2	**Hand Calculations**	**Abaqus FE Model- Step Time= 2.512 s**	**% Difference**
Reaction Force	$1.9596\ lbf$	$8.255e2\ lb - in/s^2 = 2.138\ lbf$	+9.1%
Reaction Moment	$-2.6628\ lbf - in$	$-8.468e2\ lb - in^2/s^2 = -2.193\ lbf - in$	-17.6%

A comparison and verification of the kinematics solution from the hand calculations and Abaqus results after 2 revolutions of the crank at uniform velocity of 5 rad/s is also presented.

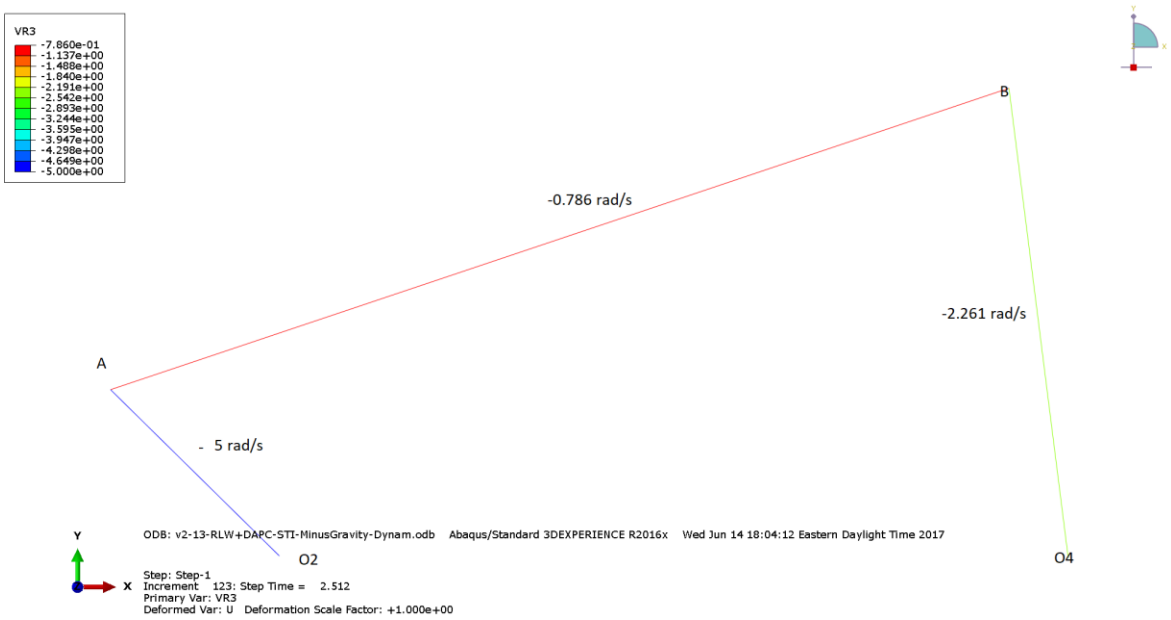

Figure 3.8: Angular Velocity Contour Results for four bar mechanism at 2.512 s.

Table 3.5: Angular Velocity – Kinematics Comparison of Abaqus Dynamics model and Hand Calculations.

	Hand Calculations	**Abaqus FE Model- Step Time= 2.512 s**	**% Difference**
Angular Velocity of AB	$-0.77\ rad/s$	$-0.786\ rad/s$	+2.07%
Angular Velocity of O_4B	$-2.29\ rad/s$	$-2.261\ rad/s$	-1.30%

Angular acceleration is recorded for the time instant before 2.512 s i.e. 2.492 s for accurate representation of the hand calculations. The instantaneous angular acceleration is computed at the iteration point with reference to the consequent time step. [15]

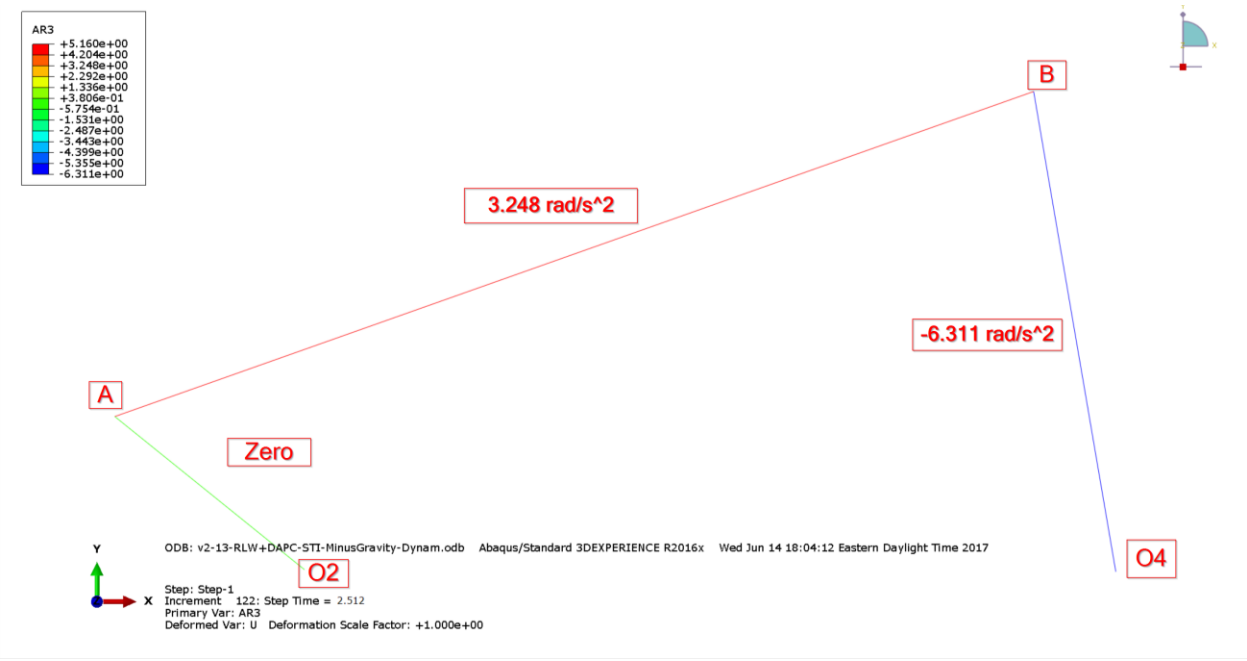

Figure 3.9: Angular Acceleration Contour Results for four bar mechanism at 2.512 s.

Table 3.6: Angular Acceleration – Kinematics Comparison of Abaqus Dynamics model and Hand Calculations.

	Hand Calculations	**Abaqus FE Model- Step Time= 2.492 s**	**% Difference**
Angular Acceleration of AB	$+2.42\ rad/s^2$	$+3.248\ rad/s^2$	+32.2%
Angular Acceleration of O_4B	$-6.311\ rad/s^2$	$-6.311\ rad/s^2$	+0.0%

Results to explore the elasticity/rigidity assumption for multibody dynamics approaches are also analyzed; these include stress and strain contours.

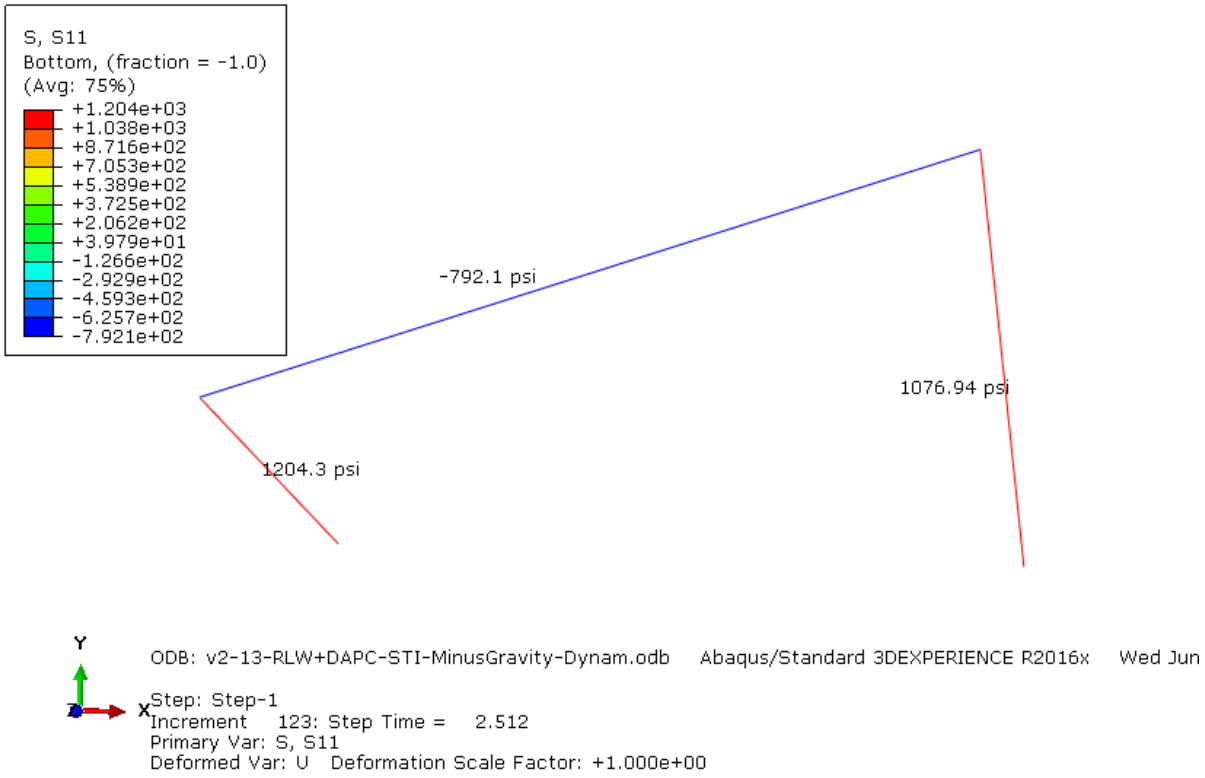

Figure 3.10: S11: Axial Stress Contour for the mechanism at 2.512 seconds.

The axial stress values oscillate from zero to ~4000 psi during the dynamics simulation. This means the strains generated are in the range of 10^{-4} to 10^{-5}.

The error percentage in the simulation results can be accounted for by the difference in solver approaches and the flexible nature of the linkages in the mechanism. The hand calculations use a matrix method for calculating the dynamic reaction forces instantaneously. The hand calculations also do not allow for any elastic strain energy generated because of the rigidity assumption. The Abaqus solver employs the direct integration implicit solver which also accounts for linkage elasticity and strain energy in equilibrium with potential and kinetic energy in a steady state condition for each time step. The mechanism linkages exhibit a small amount of tensile and bending behavior which might even bind the AB linkage. With mass scaling, the mass is likely to be different in the solution even though the density preserves the mass used in hand calculations. Mass scaling is an automated procedure whereby the code increases the time step by scaling up the density in the specific elements that are controlling the time step.

3.4. Summary of Four Bar Mechanism Modeling

1. Foundations with 2D model

The four bar mechanism model is the first step towards establishing a modeling technique for a simple dynamics problem. This problem can be conveniently worked out and compare against the FE model. The hand calculations have been documented in detail in Appendix A . The verification with hand calculations sets a precedent of making simple calculations by hand as an exercise before jumping to FE modeling.

2. Elastic BEAM elements

A typical kinematics or dynamics problem like the four bar mechanism is solved analytically using rigid body assumptions. Building the FE model with BEAM elements unravels how the linkages respond with elasticity and inertia involved. The difference in angular acceleration observed in link AB can be attributed to elastic compliance and inertial loads carrying over.

This elastic response acts in both tension as well as bending (BEAM elements). In fact instantaneous bending causes a major difference in response from the FE model.

3. Choice of solver

The Nonlinear Dynamic Implicit solver is chosen to solve this problem which checks for dynamic equilibrium at each time increment. Another solver choice explored is the Explicit Dynamic solver which does not check for equilibrium and takes less time to run.

4. Pinned Boundary Condition

In this 2D dynamics problem, the ground link is modeled by setting the pinned joints as PINNED boundary conditions. This enforces constrained translational degrees of freedom (U1, U2) and free rotational degrees of freedom (UR3). This is another step towards establishing best practices by exploring different combinations of modeling.

4. Interference fit between bearing housing and bearing

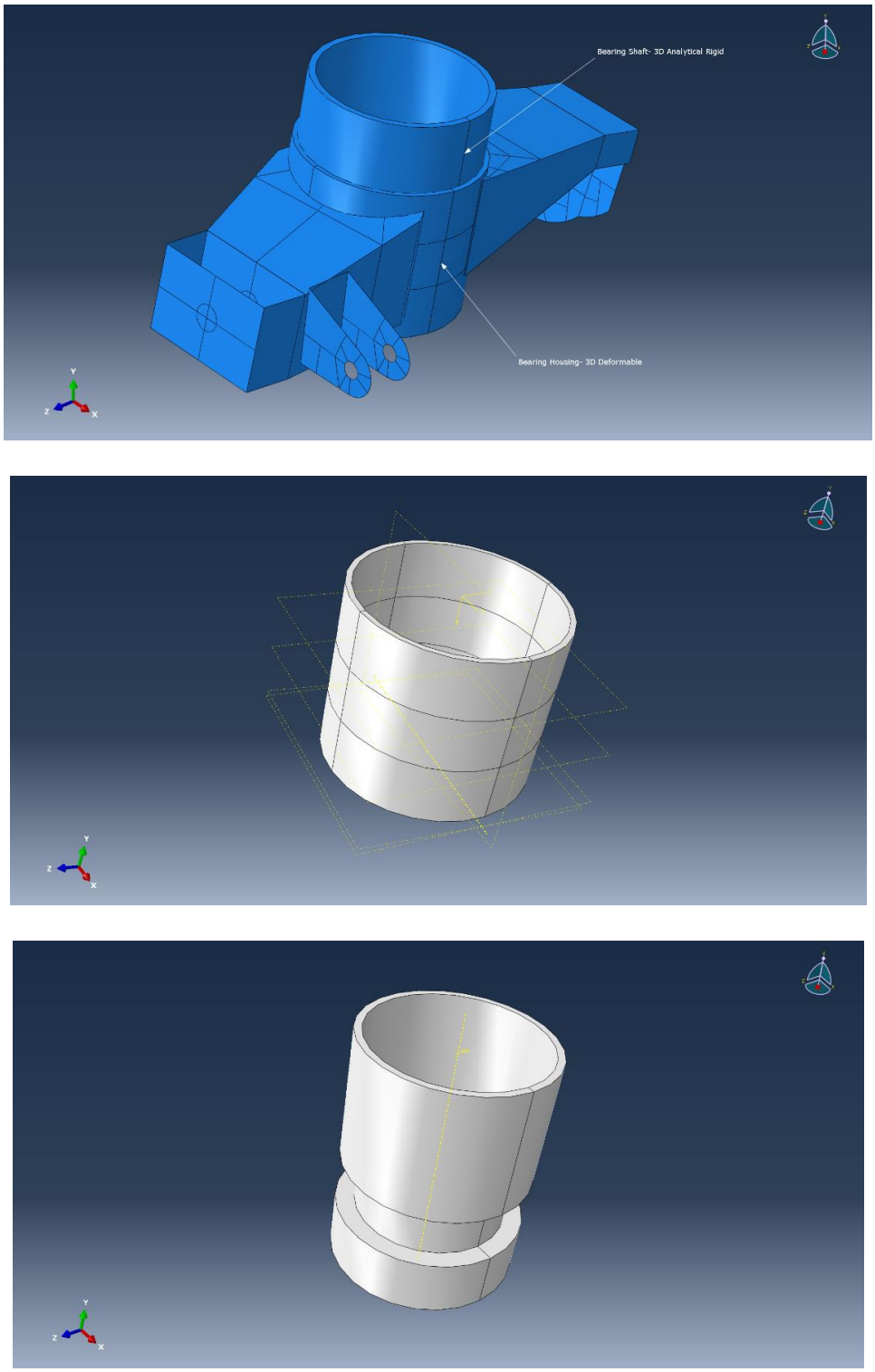

Figure 4.1: Top to Bottom: Defeatured Upright model on Abaqus, Bearing Housing component of Upright, Bearing- Rigid for 2 bearing races inside the Bearing Housing.

4.1. Hand calculations

Bearing and Bearing Housing Interference Fit Problem- Hand Solution

The hand calculations method is adopted from Shigley's Mechanical Engineering Design [21] and is explained in Appendix B.

Shaft and Hub Size Ranges:

An AISI 4130 upright bearing housing having a nominal hole diameter of 1.25 inch is to be shrink fitted to a carbon steel shaft using a Class H6-s5 interference fit (used for permanent and semi-permanent assemblies of steel and cast-iron parts.

Referring to [22], we select tolerances and fits.

Housing Inner (Hole) Radius: $1.25\ ^{+0.016\ mm}_{0}\ inches$ ⇒ 1.2506 in to 1.25 in

Bearing Outer (Shaft) Radius: $1.25\ ^{+0.054\ mm}_{+0.043\ mm}\ inches \Rightarrow 1.2521\ in\ to\ 1.2517\ in$

Radial Interference:

Table 4.1: Geometrical Dimensions and Tolerances for Interference Fit - Bearing Model.

	Loosest Fit	Tightest Fit
Housing Hole	1.2506	1.2500
Bearing Shaft	1.2517	1.2521
	-0.0011 in	-0.0021 in

Hence, the radial interferences are $\delta = 0.0011\ in$ for loosest fit and $\delta = 0.0021\ in$ for tightest fit

Interfacial Pressure

$$p = \frac{\left[\frac{1}{K_o + K_i}\right]\delta_{total}}{R}$$

$$r_o = 1.32\ in$$

$$r_i = 1.158\ in$$

$$R = 1.25\ in$$

Hence, for the housing,

$$\zeta_0 = \frac{r_o}{R} = \frac{1.32}{1.25} = 1.056$$

$$C_o = \frac{\zeta_o^2 + 1}{\zeta_o^2 - 1} = 18.371$$

$$K_o = \frac{1}{E_0}[C_o + v_o] = \frac{1}{30 \times 10^6\ psi}[18.371 + 0.293] = 6.2213\ \times 10^{-7}(\frac{1}{psi})$$

Similarly, for the bearing (shaft),

$$\zeta_i = \frac{R}{r_i} = \frac{1.25}{1.158} = 1.079$$

$$C_i = \frac{\zeta_i^2 + 1}{\zeta_i^2 - 1} = 13.177$$

$$K_i = \frac{1}{E_i}[C_i - v_i] = \frac{1}{\infty}[13.177 - 0.293] = 0(\frac{1}{psi})$$

Note: We model the bearing as a structurally and analytically rigid, we assume the bearing in our hand calculations to be of infinite modulus of elasticity (Zero Strain).

For the loosest fit case,

$$p_{loosest} = \frac{\left[\frac{1}{K_o + K_i}\right]\delta_{loosest}}{R}$$

$$= \left[\frac{1}{6.2213\ \times 10^{-7}}\right]\frac{0.0011}{1.25} = 1414.5\ psi$$

For the tightest fit case,

$$p_{tightest} = \frac{\left[\frac{1}{K_o + K_i}\right]\delta_{tightest}}{R}$$

$$= \left[\frac{1}{6.2213\ \times 10^{-7}}\right]\frac{0.0021}{1.25} = 2700.4\ psi$$

Radial and Tangential Stress Calculation for Bearing and Bearing Housing

We will only consider the tightest case since we would implement this setup in our subsequent finite element model.

Tightest fit $p = 1597.68\ psi$

Housing:

$$(\sigma_t)_{r=R} = p\left(\frac{r_o^2 + R^2}{r_o^2 - R^2}\right) = pC_o = 49609.1\ psi$$

$$(\sigma_r)_{r=R} = -p_i = -p = -2700.4\ psi$$

Bearing

$$(\sigma_t)_{r=R} = p\left(\frac{R^2 + r_i^2}{R^2 - r_i^2}\right) = -pC_i = 35583.2\ psi$$

$$(\sigma_r)_{r=R} = -p_i = -p = -2700.4\ psi$$

Note:

Since the individual bearing length in our case is lesser than the hub length, the design case violates one of the assumptions of interfacial pressure development. In this case, there would be an increase in the interfacial pressure at each end of the hub. This condition of increased interfacial pressure would typically be accounted for by applying a stress concentration factor, K_T, for stress calculated at points at the end of the hub such as,

$$\sigma_{t_{actual}} = K_{T_{tangential}}\sigma_t \tag{9}$$

$$\sigma_{r_{actual}} = K_{T_{radial}}\sigma_r \tag{10}$$

4.2. Interference fit FE model

Creating an Abaqus model on the interference fit was one of the significant modeling steps towards creating the entire model. In the actual bearing housing, there is provision made for two bearing races to support the stub axle (wheel hub).

The Abaqus FE model comprises of 2 parts –

1. "Bearing_Schematic" – which is one part that represents both the bearing races.
2. "BH_Cut" – which is the bearing housing.

The "Bearing_Schematic" is a 3D Analytical Rigid part because the scope of this research includes analyzing loads and behavior of the upright and not the bearing. As an analytical rigid part, it serves as a body to transfer loads and interaction properties – such as the interference fit.

"BH_Cut" is a 3D deformable part and the results of the model will be studied by looking at the stress and deformation results of the bearing housing.

Part Geometry

1. Bearing_Schematic

   Sketch for Solid of Revolution 3D Analytical Rigid part. A reference point is created at the corresponding coordinates of the wheel center. This reference point is by default tied to the surface of the rigid part. Hence it can be used for loading in subsequent models.

2. BH_Cut- Bearing Housing Part Model

   The Bearing Housing Hollow Cylinder is a 3D Deformable Solid Part and it has been partitioned longitudinally into quarters and transversely to align with the bearing races.

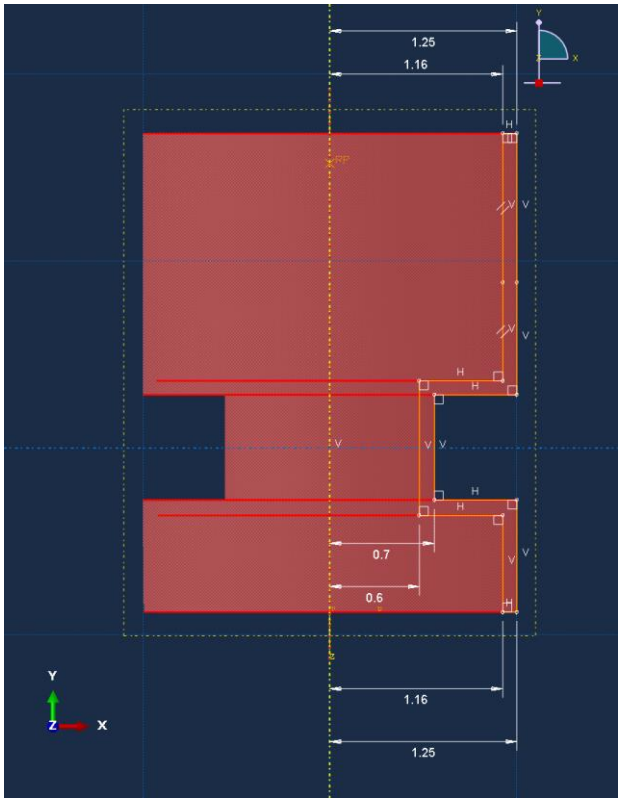

Figure 4.2: Axisymmetric Sketch Construction of Bearing Schematic for two Bearings.

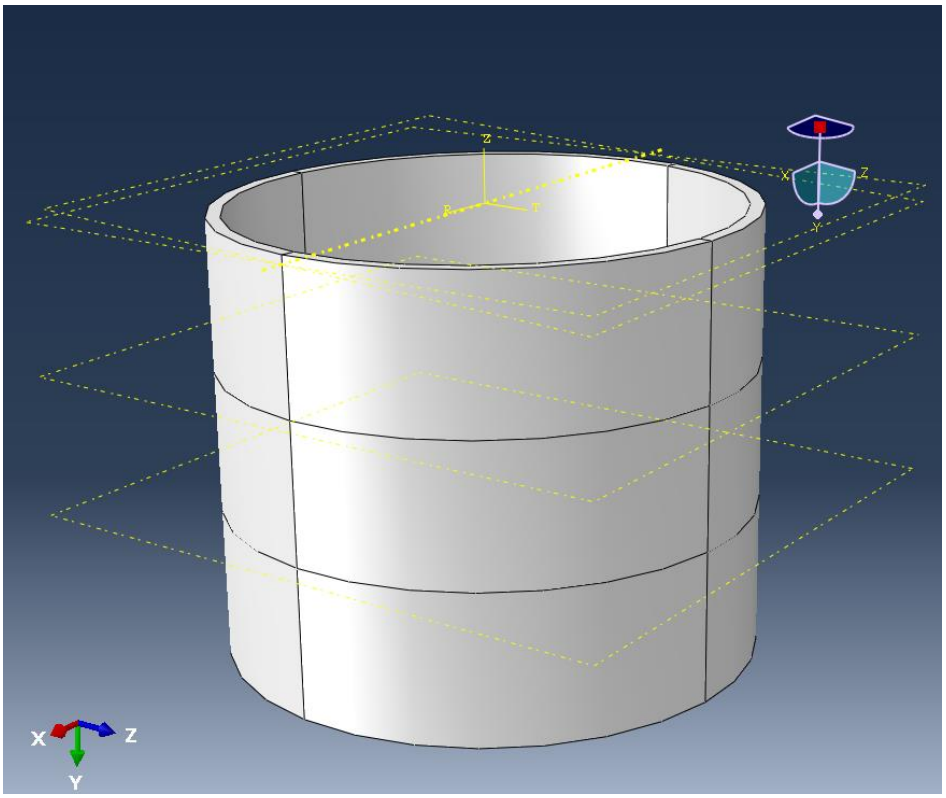

Figure 4.3: Bearing Housing Part Model.

Material Properties and Section Assignments Module

Table 4.2: Material and Section Property Specification Sheet for Interference Fit Model.

Bearing	Does not have material or section properties since it is analytically rigid- This is assumed because bearings are manufactured from materials that resist deformation from high loads.
Bearing Housing	**Material Properties:** Modulus of Elasticity = 3e7 psi Poisson's Ratio = 0.29 **Section Properties:** For 3D Stress "Brick" elements – Section assigned is Solid, Homogeneous For Shell elements – Section assigned is Continuum Shell, Homogeneous

Step Solver Module

Static General Step: used to compute the results for the interference fit interaction.
The interference fit step solver has NLGEOM turned on. If geometrically nonlinear behavior is expected in a step, the large-displacement formulation should be used. Deciding on increment size is done with repeated attempts and trial-and-error.

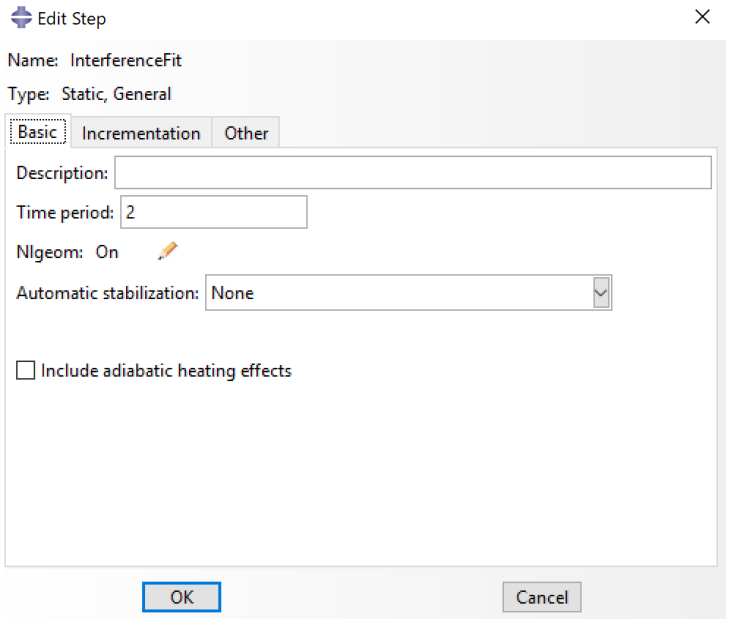

Figure 4.4: Step - General Parameters.

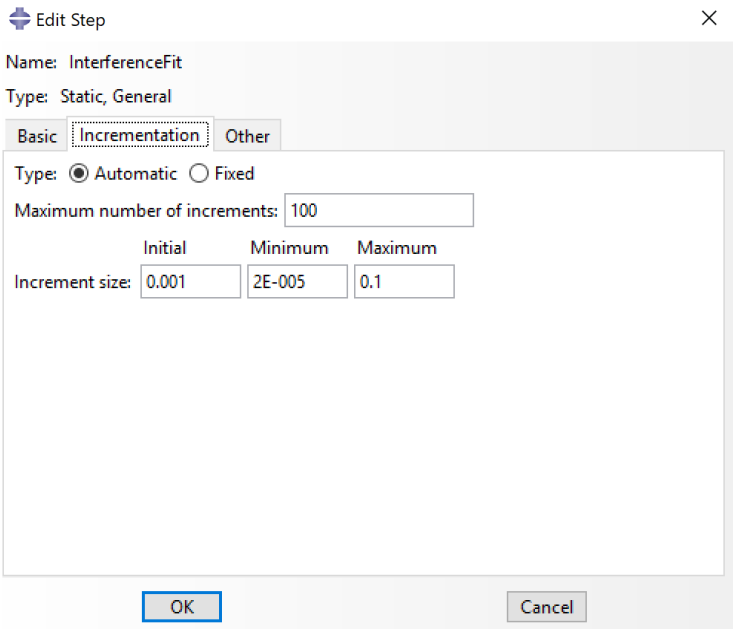

Figure 4.5: Step - Increment Parameters.

Assembly Module

An assembly cylindrical coordinate system is created. Each part also has a local datum cylindrical coordinate system with the R and θ coordinates on the circular face of the cylinder and Height (Z) coordinate set up so as the height of the cylinder is in the positive Z-direction. The local and assembly coordinate systems are made to coincide to mate the parts. The cylindrical coordinate system method also helps with applying boundary conditions.

Note: Part instances use a part dependent mesh.

Interactions Module

- Interaction Property: Contact
  - Tangential Behavior
    - Penalty Friction Formulation – Friction Coefficient = 0.16 [23]

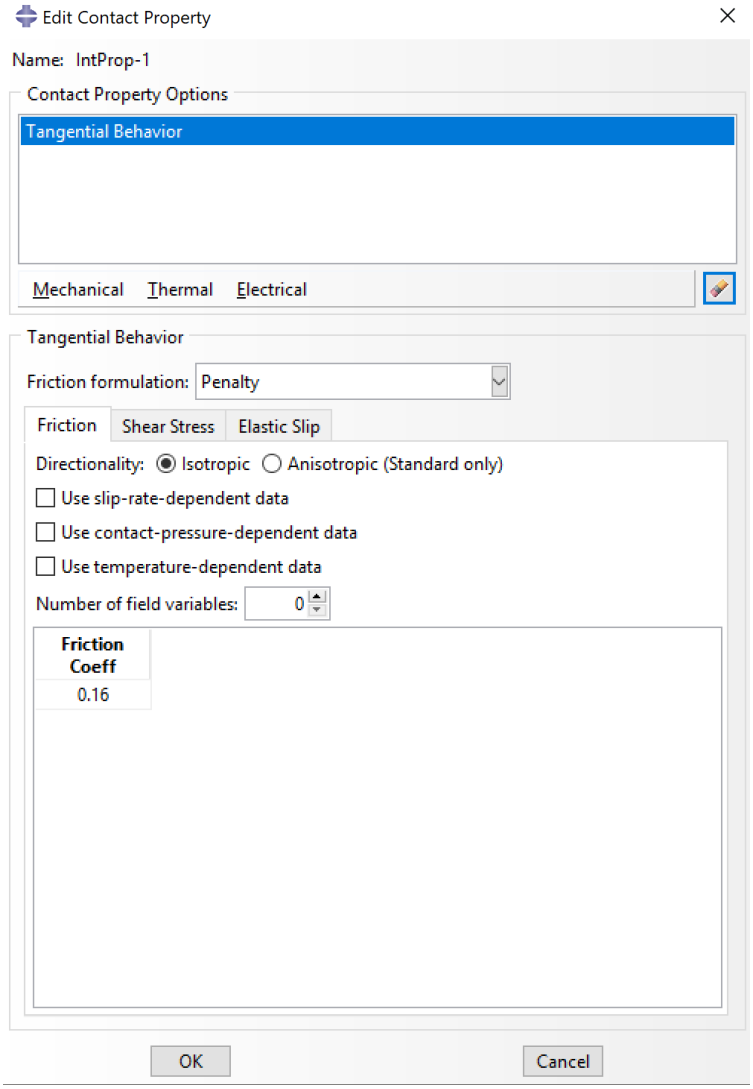

Figure 4.6: Interactions Property Dialog for Interference Fit Model.

- Interaction:
    - Surface to Surface Contact

    1. Contact direction is normal to the slave surface
    2. Works better with dissimilar mesh densities of slave and master – the solution can be computationally slower and/or expensive if the slave surface is coarser than the master surface.

    - Analytical Rigid Bearing is chosen as Master Surface

    1. General rule of thumb is to choose the stiffer part (in this case, the analytical rigid) to be master surface. Abaqus requires that the rigid part be the master surface.
    2. Since the load path is from the bearing to the housing, the bearing should be the master governing surface.

    - Bearing Housing Inner Surface is chosen as the Slave Surface

    1. Master and slave surface decisions have lesser impact on the solution with Surface to Surface (S2S) contact formulation than Node to Surface (N2S) contact formulation.
    2. Slave Surfaces are also supposed to be the smaller surface than the Master Surface.
    3. Slave surfaces must be meshed finer than the master to support the algorithm so that the slave nodes do not have initial penetrations on the master surface.

    - Sliding Formulation: Finite Sliding

    Finite Sliding allows for separation, sliding and rotation which is important as the upright model develops.

    - Discretization Method: Surface to Surface
    - No Slave Adjustment
    - Surface Smoothing- Automatic ON

    Even though surface smoothing is not needed for a S2S finite sliding formulation, surface smoothing is used in path based tracking algorithms which is applicable in this case.

    - Interference fit options – Interaction State in Static General Step:
        - Automatic Shrink Fit

    There is an entire section in the Abaqus Analysis User's Guide [15] on modeling contact interference fits.

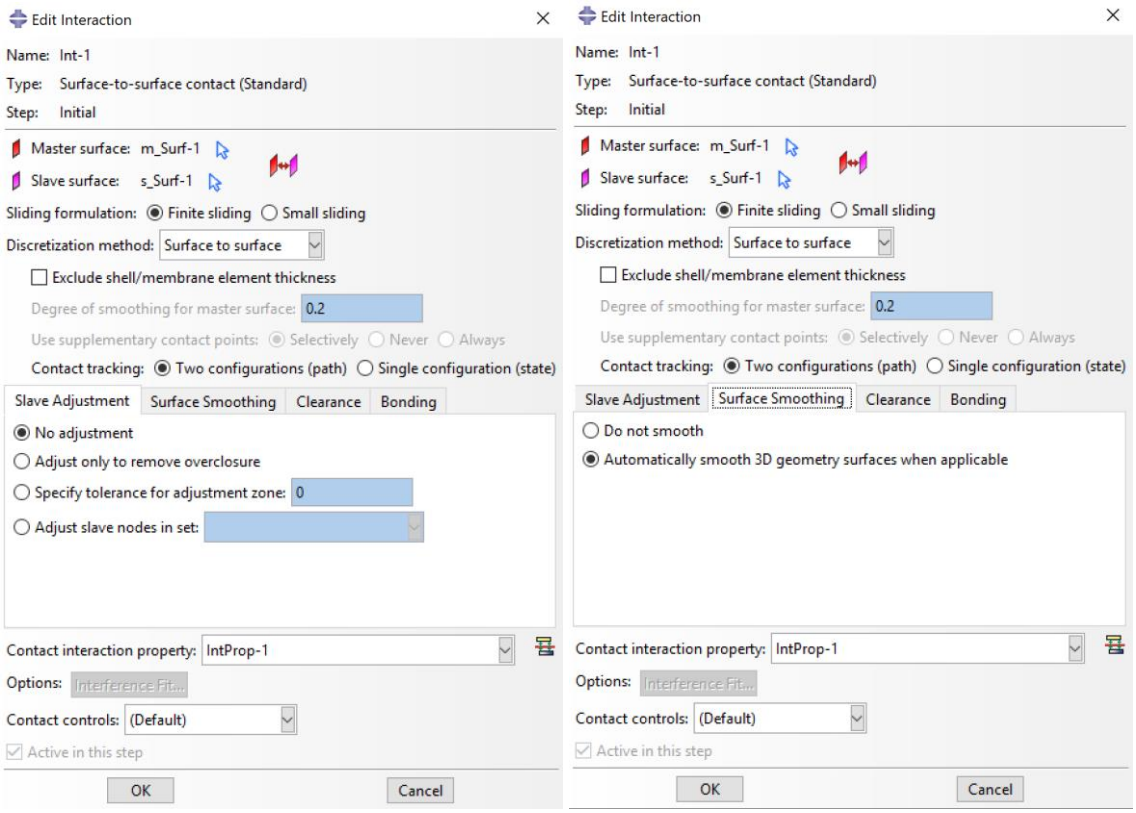

Figure 4.7: Interactions dialog for Initial Step.

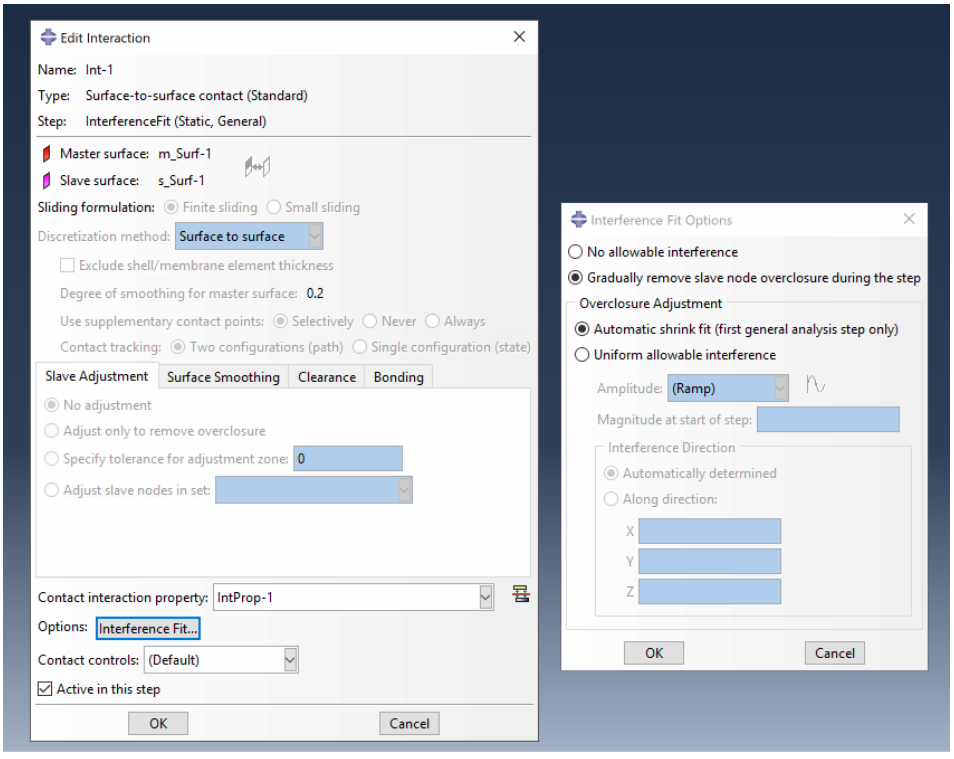

Figure 4.8: Interactions Dialog for Interference Fit Step.

Master Surface Assignment:

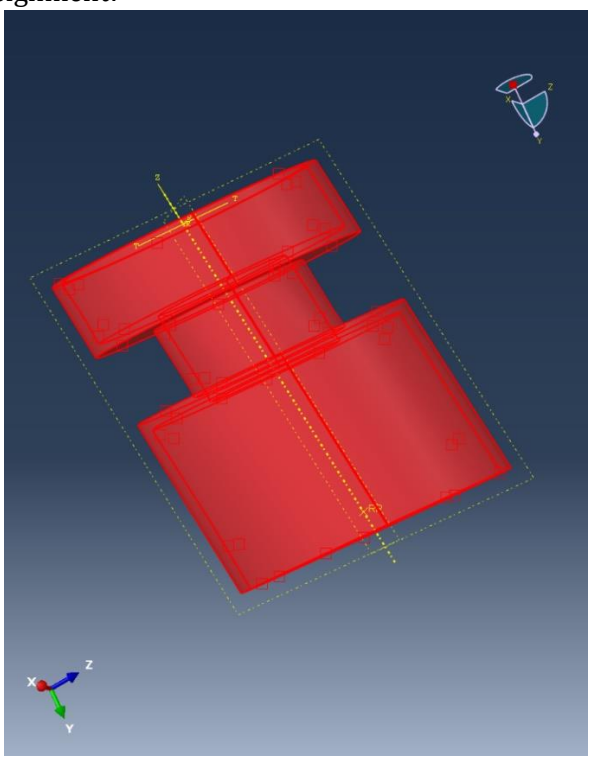

Figure 4.9: Master Surface Assigned to Bearing Schematic for Interaction Model.

Slave Surface Assignment:

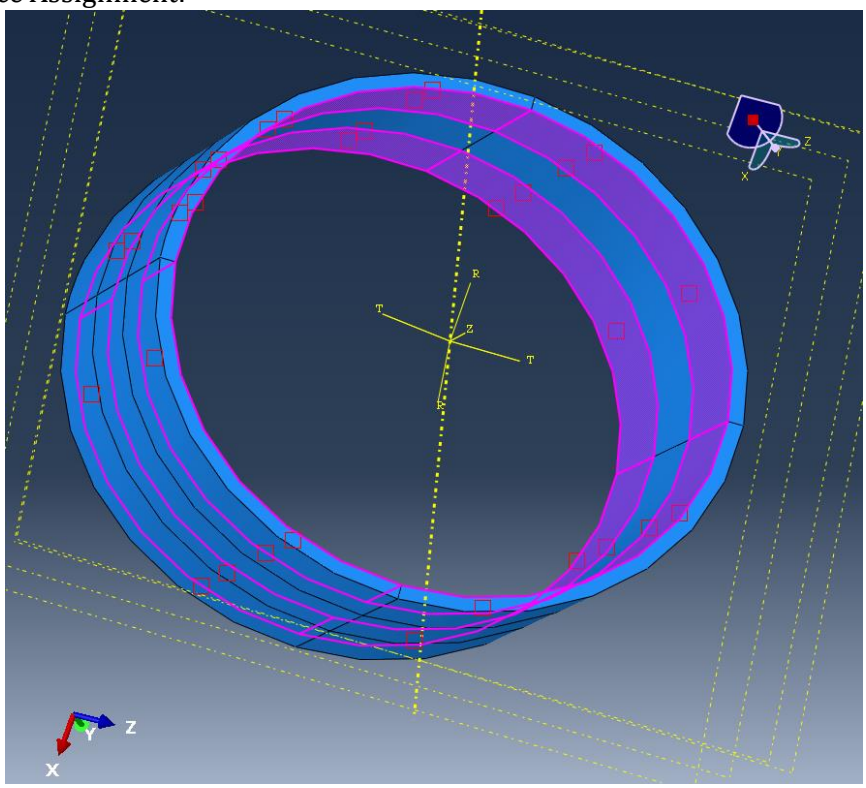

Figure 4.10: Slave Surface assigned to Inner Partitioned Curved Surface Area of Bearing Housing.

Loads and Boundary Conditions Module

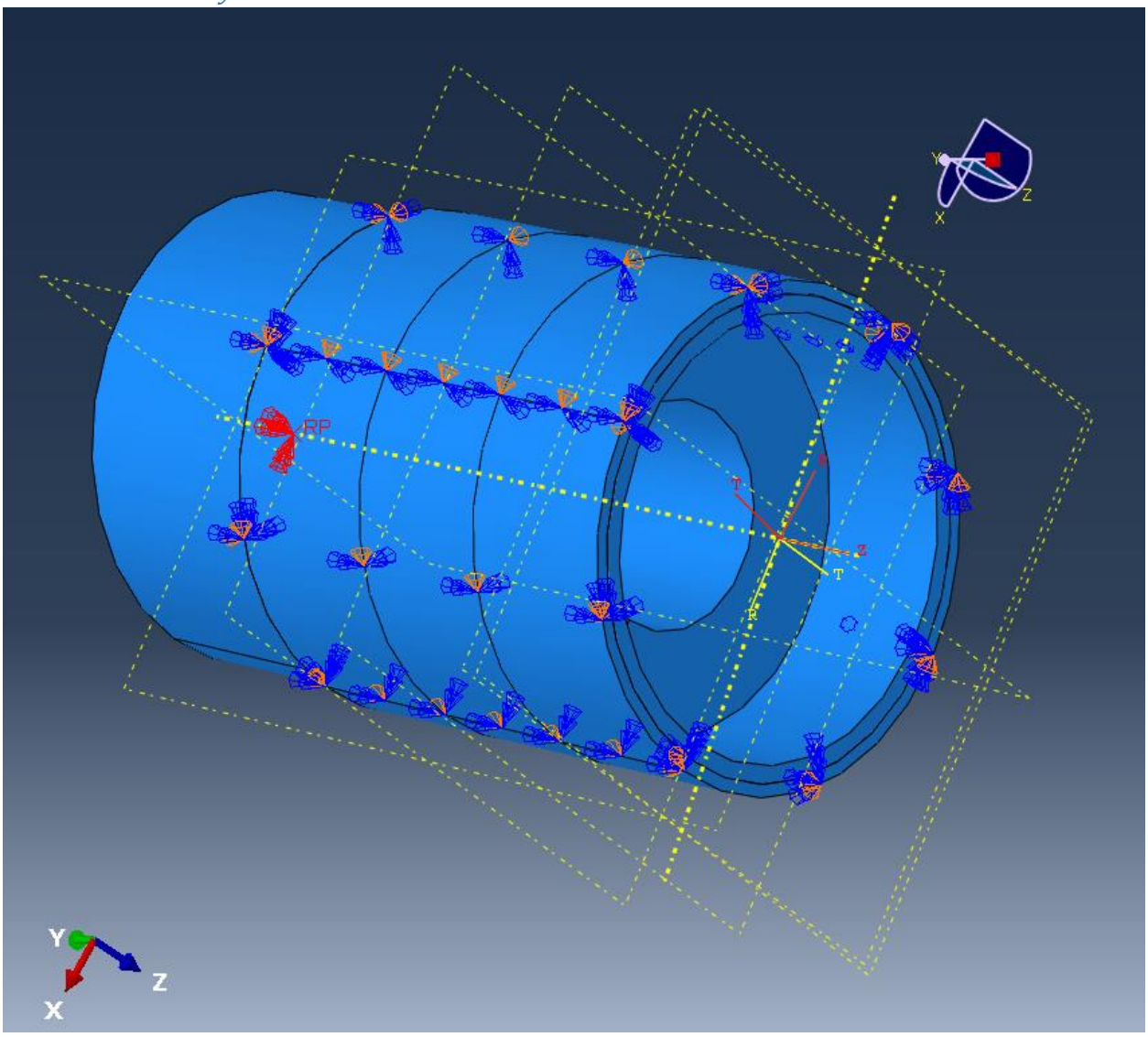

Figure 4.11: Load Diagram for Interference Fit Model.

Table 4.3: Loads and Boundary Conditions Specifications for Interference Fit Model – Preprocessing.

Load	None
Boundary Condition-ENCASTRE	Encastre(Fixed) on Bearing_Schematic Part – Part Reference Point
Boundary Condition-ZSYMM	Constraining Z-Direction Translation and Rotation normal to R-θ plane for Bearing Housing
Boundary Condition-YSYMM	Constraining Rotation in θ-direction and Tangential Translation for Bearing Housing.

Mesh Module

The Bearing Schematic Part is not meshed since it is an analytical rigid and hence there is no elasticity inherited in the model.

Bearing Housing:

The partitioning technique employed is to make sets in each cylindrical direction and govern the number of seeds/elements on each of those sets of edges.

Table 4.4: Abaqus Sets of Edges from a Partitioned Geometry of Bearing Housing. These sets help tune the mesh density is different dimensions.

1.	Circumferential Seed Edges	
2.	Radial Seed Edges	
3.	Z- direction Seed Edges	

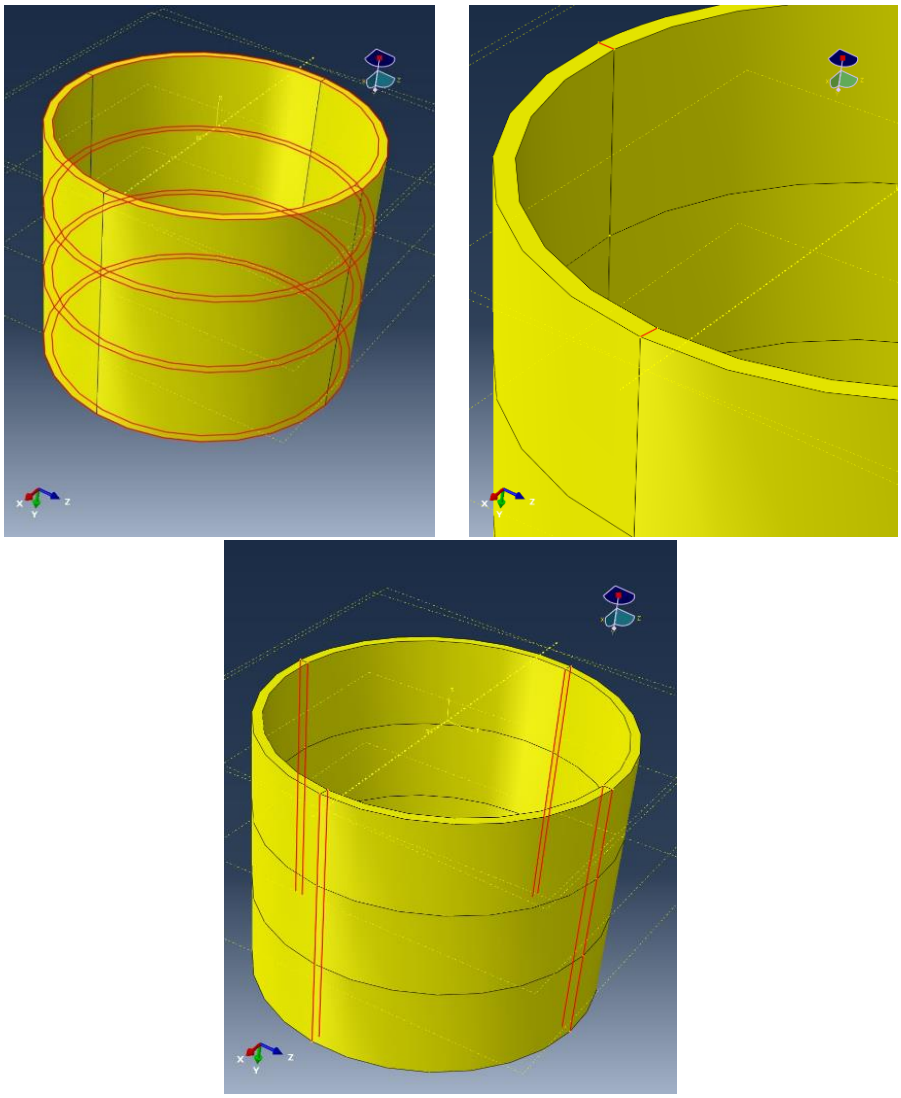

Figure 4.12: Bearing Housing Partitioned Part Diagram: Highlighted Edges are the part of a set defined to create circumferential seeds, radial seeds and Z-direction seeds respectively for a structured meshing technique.

These sets are used to tune the number of elements in a mesh refinement scheme while performing a convergence study.

Element Properties:

- Hex Elements – Sweep Technique – Radial Direction Sweep Path for each element
- 2 iterations- Continuum Shell Elements (SC8R) and 3D stress "Brick" Elements (C3D8R).
    - SC8R: An 8-node quadrilateral in-plane general-purpose continuum shell, reduced integration with hourglass control, finite membrane strains.
    - C3D8R: An 8-node linear brick, reduced integration, hourglass control.

Convergence Study Results:

Different combinations of meshing strategy using the seeding edges were used to study the progression of stress values on the probe points. Each point was then considered as an independent case to evaluate convergence.

As the mesh is refined, the FEM solution should approach the analytical solution of the mathematical model. This attribute is necessary to instill confidence in FEM results from the standpoint of mathematics.

Convergence requirements include approximation power, displacement continuity and stability. Stability includes excessive element distortion and initial penetrations in contact models. A model that gives consistent results along with stability can be defined to reach convergence. For interference fit modeling, the stresses at certain probe points on the Bearing Housing are recorded for different element densities and a valid number of elements is chosen as the system mesh density going forward. The validation is done by plotting stress vs number of elements and evaluating each defined probe point.

The meshing strategy of seeding 10 elements on the circumferential edge, 10 elements on the height (Z) edge and 3 elements on the radial edge was where the convergence curve (stress vs. no. of elements) became asymptotic. Hence this mesh was chosen as the strategy going forward to the upright model.

The convergence study results in detail and readings are attached in the Appendix B.

Example Mesh Diagram

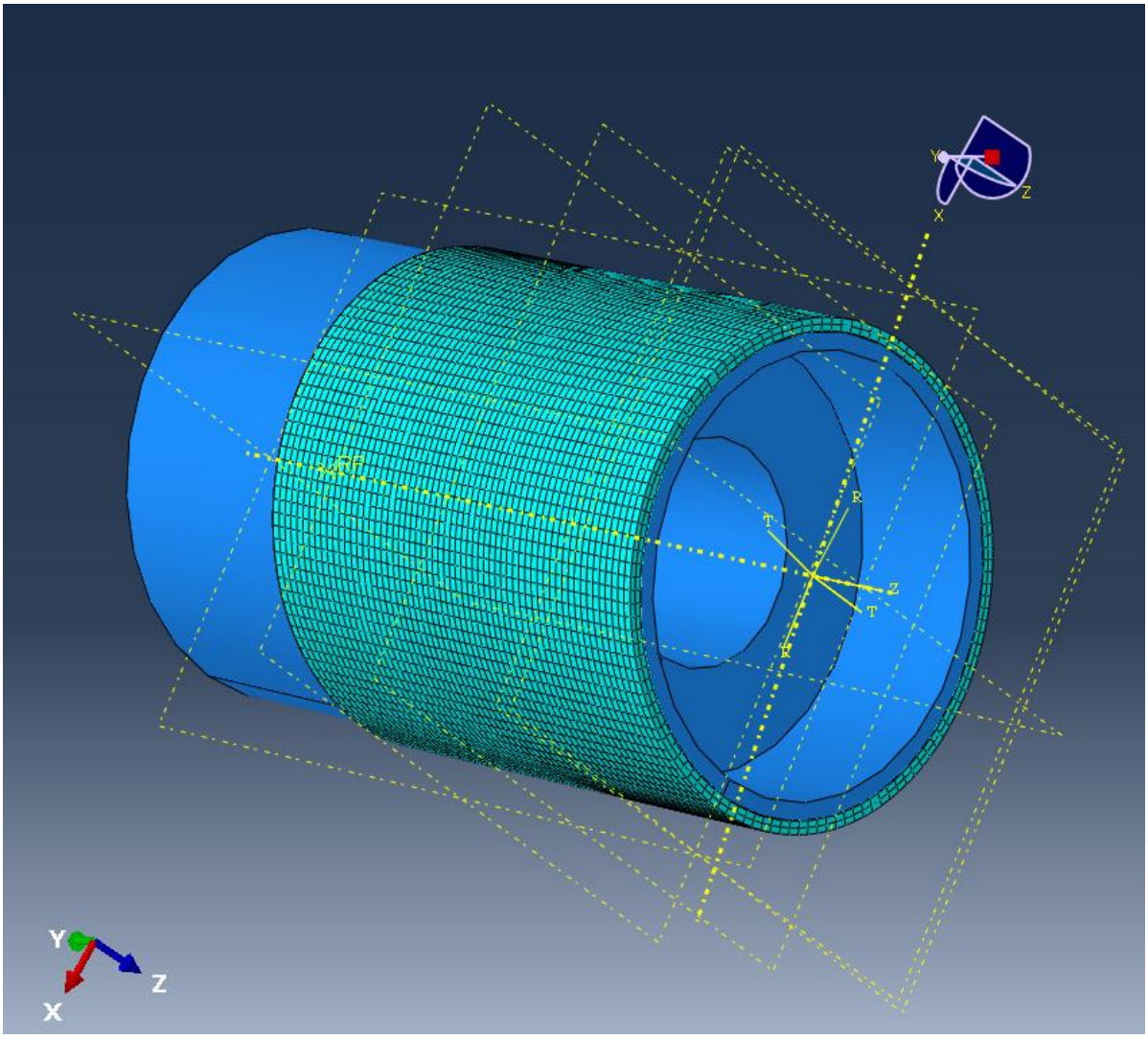

Figure 4.13: Mesh Diagram for Interference Fit Model.

No of Elements on the Bearing Housing after a convergence study = 216000.

Results

To verify the Abaqus FE model, inspection and evaluation of the finite element model results is required. The independent hand solution to the interference fit problem assumed that the shaft and the hole have equal widths and no stress concentration exists. The actual problem have two bearing races are inside the bearing housing, the influence of stress concentration is present. Yet, the midpoint of the bearing race width, which should have minimal stress concentration influence, is probed for results and a direct comparison is made to evaluate the finite element model.

Apart from just looking to verify the model, a closer look is taken at several probe points on the bearing housing to understand the mechanical behavior and interference fit response. A display group set of certain points on the bearing housing is created for this purpose; for the interference fit model, we choose 16 nodes as shown in Figure 4.14.

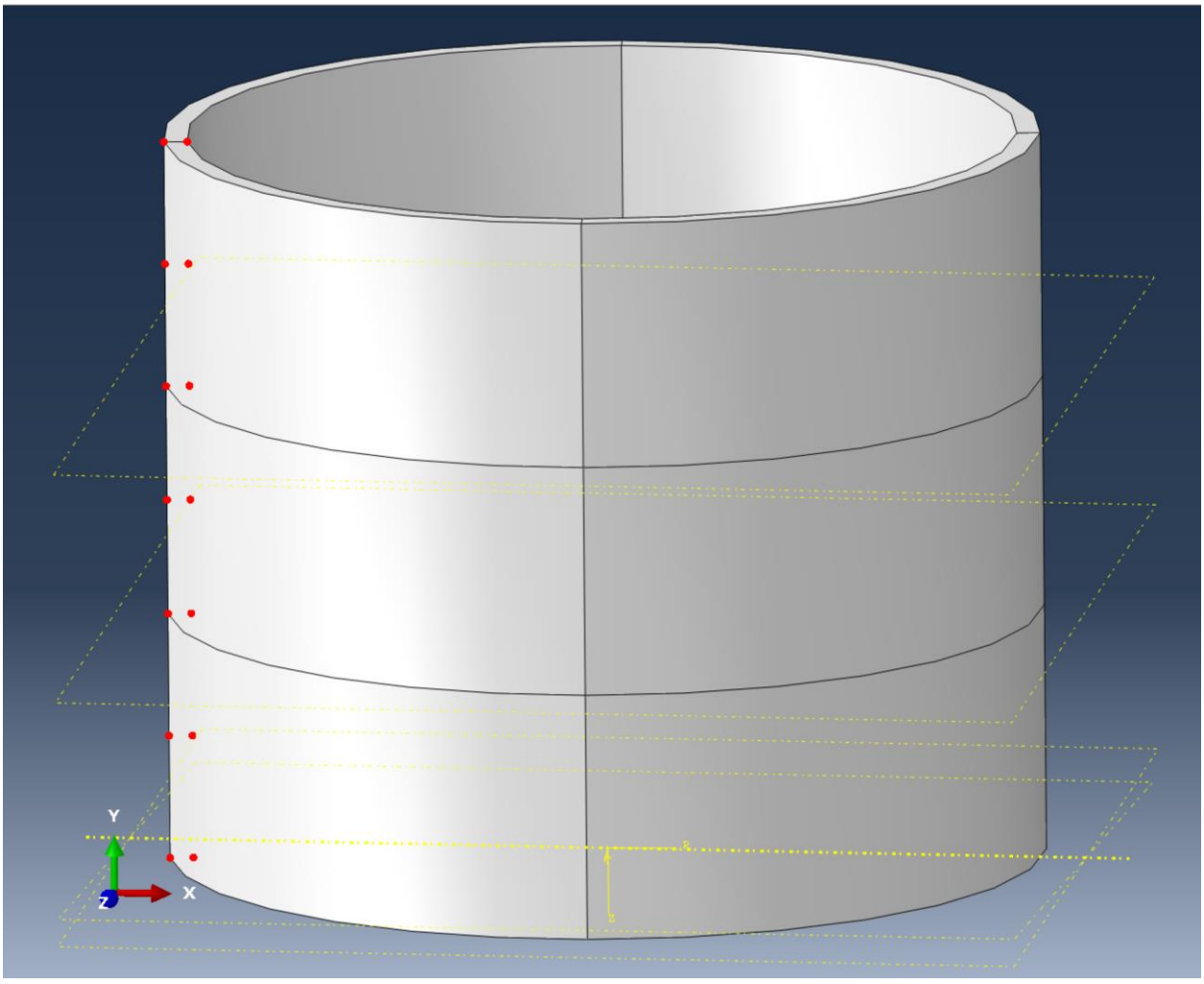

Figure 4.14: Bearing Housing Part Model- Display Group Set Points Highlighted in Red.

The stress values for each of the display group nodes, each having stress in different directions based on attached elements, is mentioned in the Appendix B . The stresses in radial and tangential directions show symmetry across the bearing race width or the bearing housing width. A stress concentration is present at the shoulder intersection of the bearing race end. An exaggerated deformation scale contour of the radial deformation results shows how the deformation is taking place.

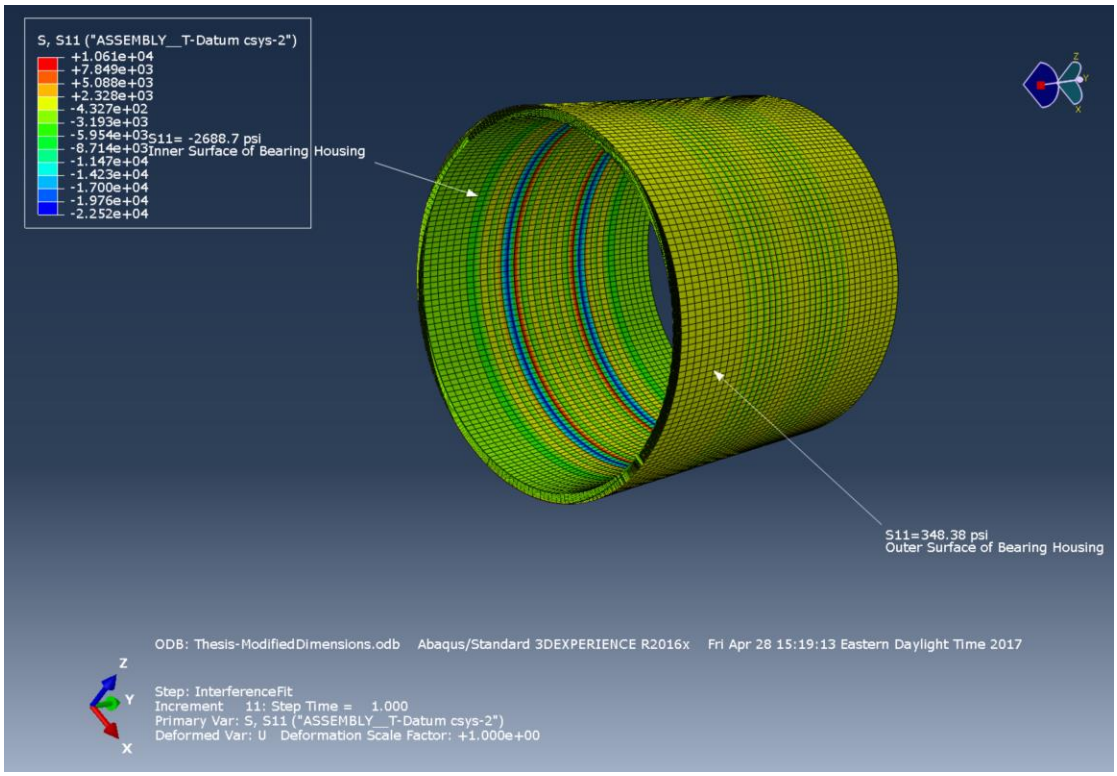

Figure 4.15: S11-Radial Stress for Bearing Housing in Interference fit (Tightest Fit) model.

The results have been transformed to a different local cylindrical coordinate system.

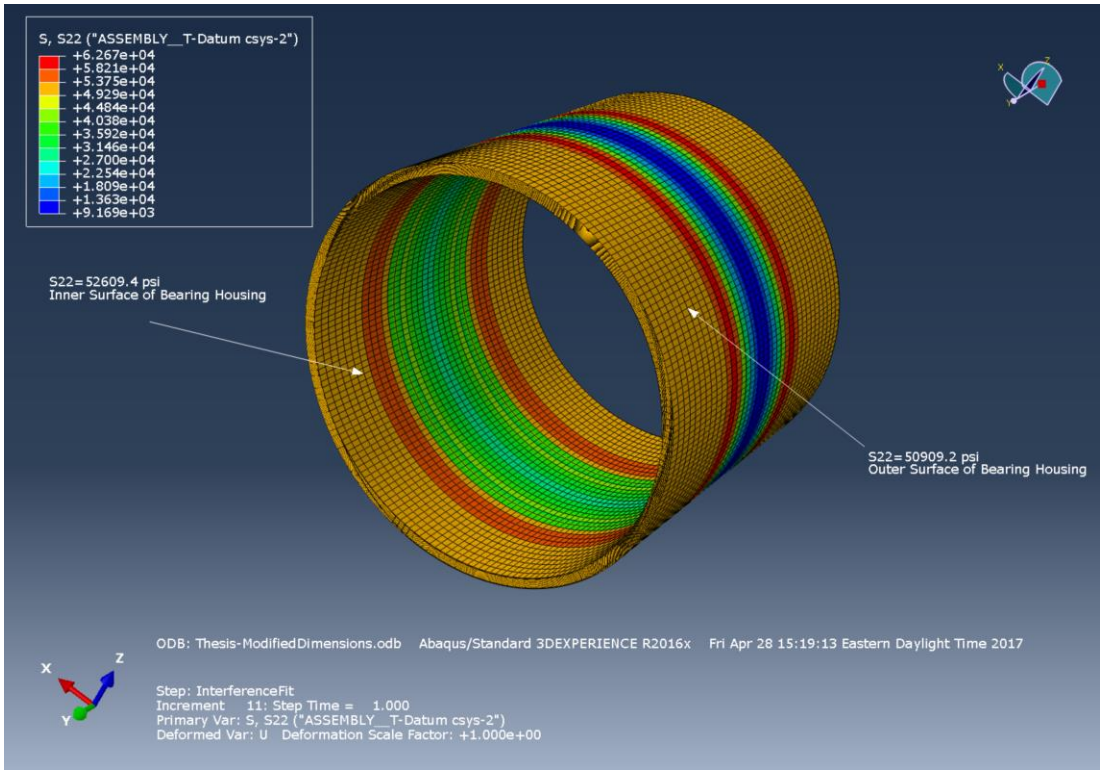

Figure 4.16: S22-Tangential Stress for Bearing Housing in Interference fit (Tightest Fit) model. The results have been transformed to a different local coordinate system.

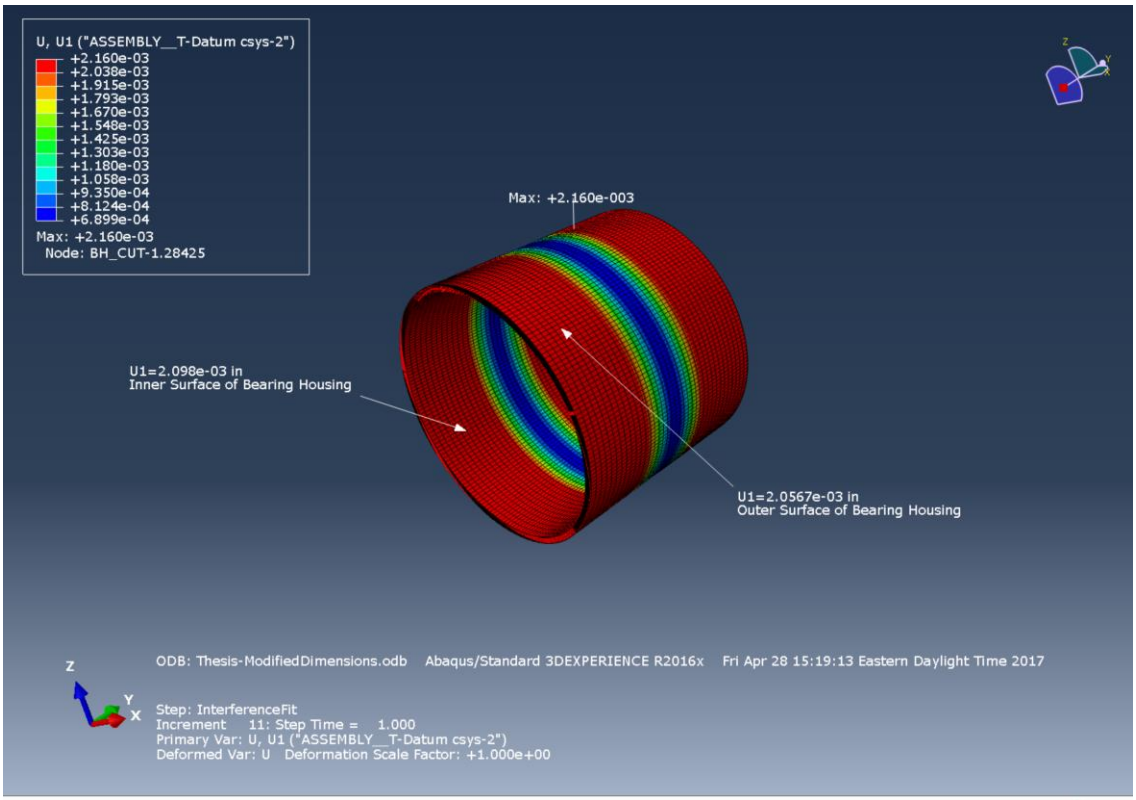

Figure 4.17: U1- Radial Deformation for Bearing Housing Interference Fit (Tightest Fit) Model.

4.3. Summary of Interference Fit Modeling

1. Convergence Study – Establish mesh density and element type

The interference fit problem set a precedent and foundation to establish the mesh density going forward. All finite element problems should be verified with a convergence study to make sure that the mesh density and aggregate stiffness contributed by the elements is representative and accurate. The type of elements used also contributes significantly towards the elastic response, overall stiffness of the component and deformation modes.

To set up a good convergence study, a partitioning strategy was implemented that allowed for gradual increase in mesh density by varying the element size in every dimension. The element type used for modeling the bearing housing is Continuum Shell.

2. Stress concentration

With a mesh density verified from a convergence study and the dumbbell shaped rigid bearing, state of stress and stress at any point of the bearing housing could be probed and assessed. This exercise allowed the study and evaluation of the stress concentration due to two separate bearing races inside the upright. The state of stress and strain was also observed through the wall thickness of the bearing housing

3. Comparison with Hand Calculations

The interference fit problem, like the four bar mechanism, is a simple problem that can be analytically solved and compared with the FE model. The FE model results have accurate modeling to represent stress concentration while hand calculations depend of empirical stress concentration factors. Nevertheless, the results, when compared in Table 5.6 show negligible errors. Hence the modeling technique for setting up the problem in the FE preprocessor is verified.

5. Upright Model Development

5.1. Interference Fit – Upright

The base model is the VTM FSAE 2015 design for a folded sheet-metal upright made from AISI 4130 Steel. The geometry and dimensions were extracted from NX10, a design software package. The inherent coordinates for the front corner suspension have been preserved in this upright model. Sets in Abaqus are logical containers for grouping geometry features, nodes, surfaces, and other entities with a name and are used as references for section properties, boundary conditions, mesh seeds and loads among others. The set names were used to establish connectivity for the edges and surfaces in the upright. The upright has been "defeatured" for the following reasons:

1. Unnecessary detail features which do not contribute significantly to the mechanical behavior
2. Creating a structural mesh for faster computation and more accurate load path representation
3. Accommodate easy mesh partitions which also contribute to faster computation and accurate finite element analysis using integration solvers of Abaqus.

Part Geometry

1. Bearing Schematic – Analytical Rigid Part
2. Bearing Housing - BH_Cut – Elastic Part – As modeled in interference fit model
3. Lever Arm Components - Cut_Lower and Cut_Upper

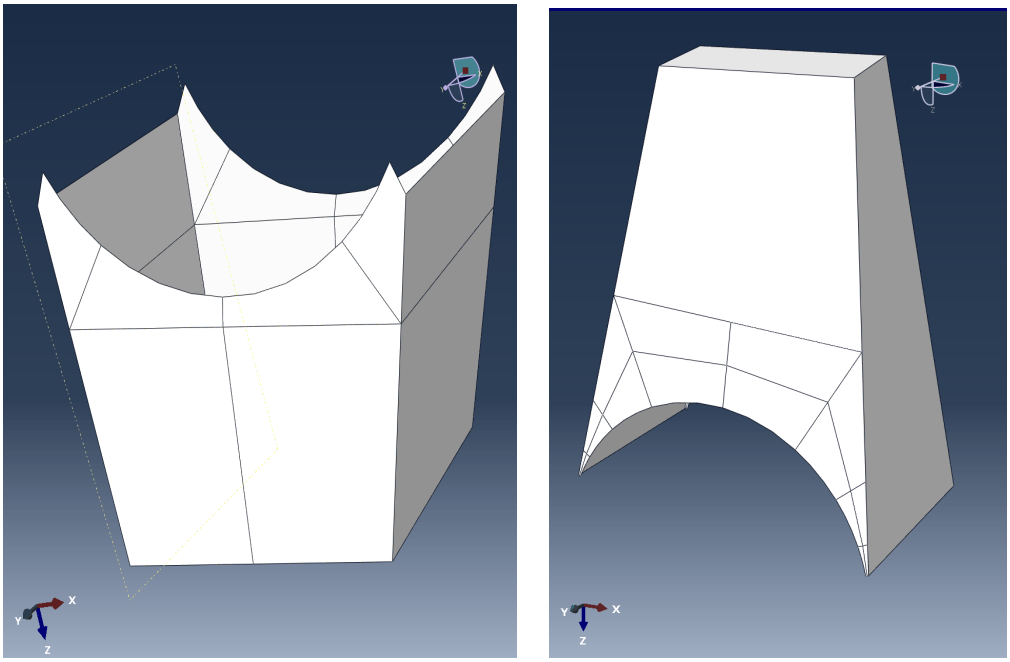

Figure 5.1: Lower and Upper "lever arm" bodies of the Upright Part Geometry Diagrams.

Table 5.1 : Part, Material and Section Properties for components included in the Upright - Interference Fit Model.

	Part	**Part Properties**	**Section Properties**	**Material Properties**
1.	Bearing	Analytical Rigid	N/A	N/A
2.	Bearing Housing	3D – solid- deformable	Shell Thickness = 0.04 in	Steel 4130 E = 3e7 psi, υ=0.29
3.	Upper and Lower Bodies	3D – shell - deformable	Shell Thickness assigned = 0.04 in	Steel 4130 E = 3e7 psi, υ=0.29

The partitioning technique is employed to form a structured mesh and the ends of the curved shells are truncated since elements in the mesh for a surface with a tangential edge get warped or fail mesh verification because of their excessive aspect ratios or obtuse angles between their edges.

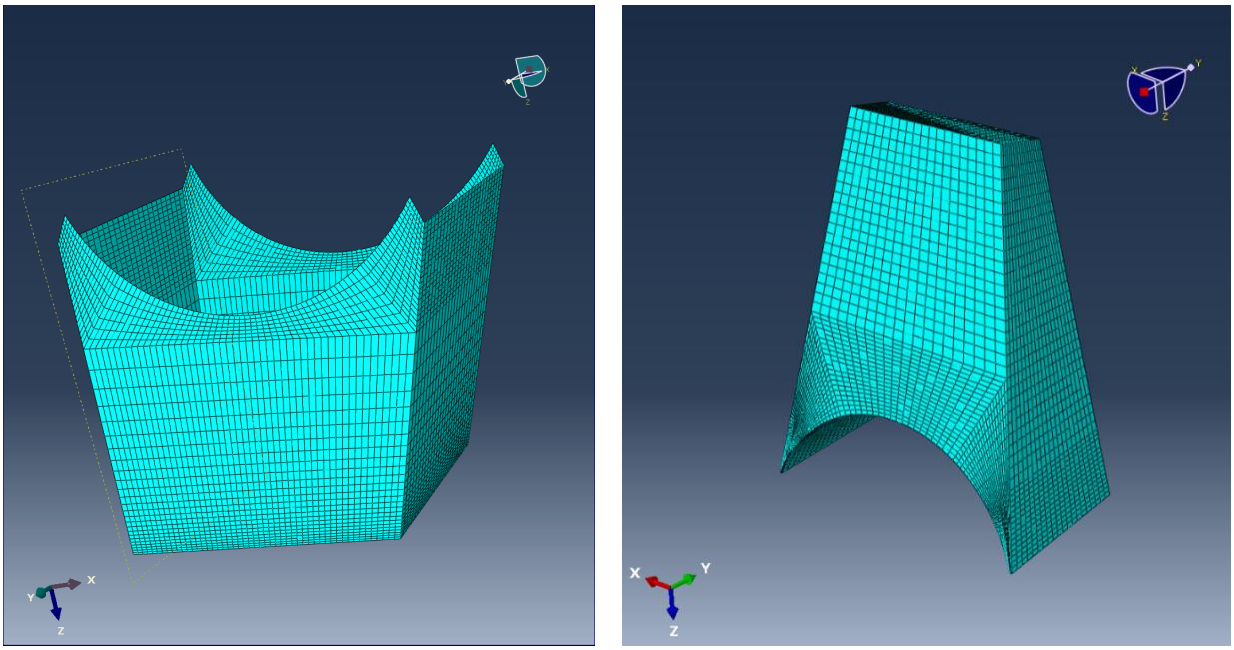

Figure 5.2: Lower and Upper "lever arm" bodies of Upright - Mesh Diagram.

4. Lower Control Arm Connection, Upper Control Arm Connection+Upper Mount

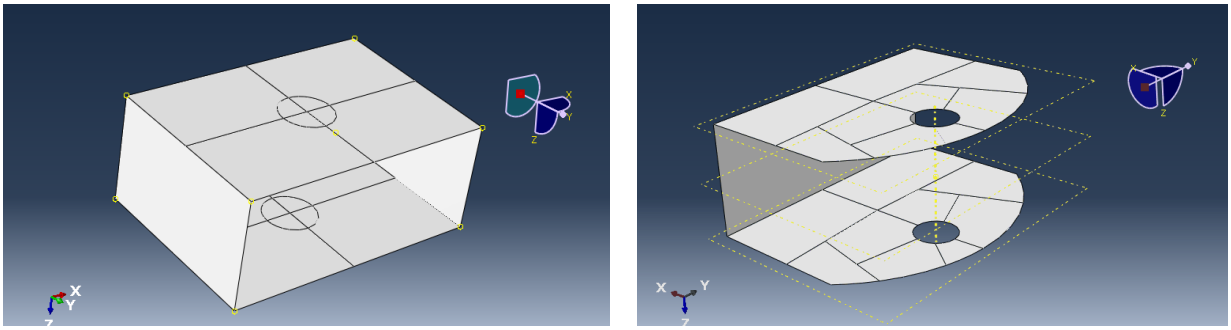

Figure 5.3: Part Geometry of Lower Control Arm Connection and Upper Control Arm Mount.

Apart from the Upper Mount, there is an Upper_control arm (CA) Connection component (shown in Assembly and Appendix) which is a spacer to implement a kingpin inclination angle. These are also conventional shell parts and have similar mesh and physical properties as the “lever arm” components.

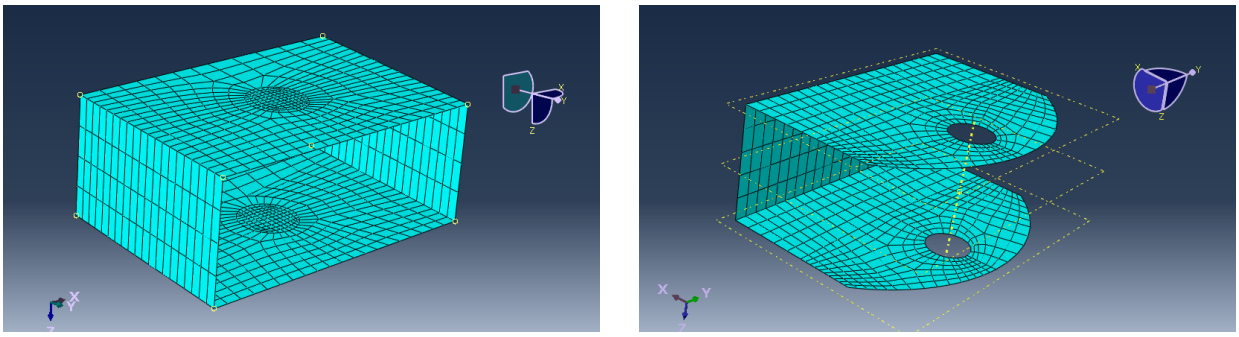

Figure 5.4: Part Mesh Diagram of Lower Control Arm Connection and Upper Control Arm Mounts.

5. Tie Rod Outboard Mount – Similar to construction of other shell components

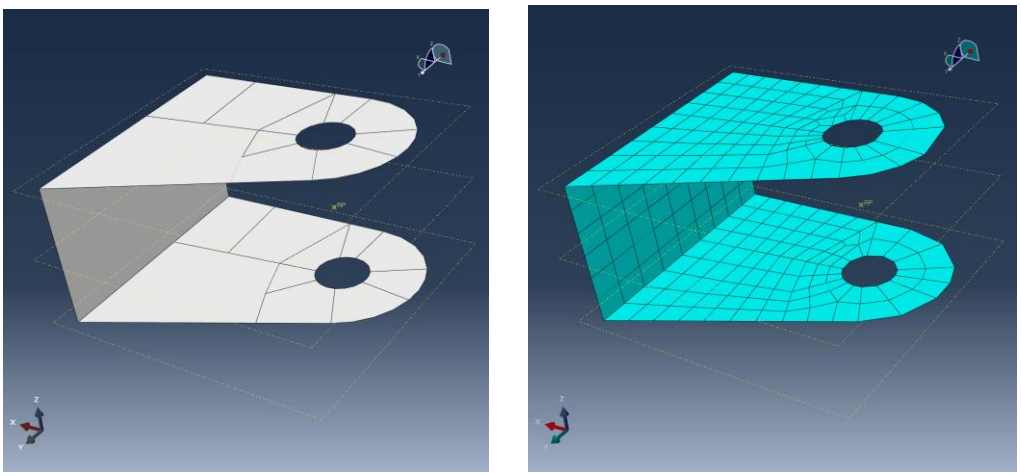

Figure 5.5: Part and Part Mesh Diagram of Tie Rod Outboard Mount.

Material and Section Properties

Table 5.2: Materials and Section Properties for Upright Model to simulate Interference Fit and Weld Joints.

<table>
<tr><td colspan="2">Bearing</td><td>Does not have material or section properties since it is an analytical rigid part</td></tr>
<tr><td colspan="2">Bearing Housing</td><td>Material: AISI 4130 Steel
Yield Stress = 63000 psi, UTS = 95000 psi
For 3D Stress “Brick” elements – Section assigned is Solid, Homogeneous
For Shell elements – Section assigned is Shell/Continuum Shell, Homogeneous</td></tr>
<tr><td rowspan="3">Shell Elements</td><td>Lever Arm Components</td><td rowspan="3">Material: Steel AISI 4130
Yield Stress = 63000 psi, UTS = 95000 psi
Section: Shell/Continuum Shell, Homogeneous
Shell thickness =0.04 in</td></tr>
<tr><td>Upper and Lower Outboard Mounts</td></tr>
<tr><td>Tie Rod Mount</td></tr>
</table>

Step Solver Module and Assembly Module

These module parameters have been preserved from the Interference Fit (only) model.

Interactions Module

All the components of the upright are assembled and welded during fabrication. To simulate weld joints, we use the Abaqus *TIE command to tie (constraining degrees of freedom) components or surfaces together to mimic the ideal weld joints.

A more detailed explanation regarding representation of weld joints is provided in Section 6.6.

Loads and Boundary Conditions Module

No loads were applied on this model, but two different sets of boundary conditions were applied to simulate different scenarios. The behavior and response of the upright is assessed with different boundary conditions on the same interference fit model.

Table 5.3: Loads and Boundary Conditions for Case 1- Bearing Housing Boundary Conditions.

Load	None
Boundary Condition-ENCASTRE	Encastre(Fixed) entire Bearing_Schematic OR Reference Point
Boundary Condition-ZSYMM	Limiting Z-Direction Translation and R-θ plane Rotation for Bearing Housing
Boundary Condition-YSYMM	Limiting θ-Direction Rotation or Tangential Translation for Bearing Housing.

Table 5.4: Loads and Boundary Conditions for Case 2 – Fixed Ends Boundary Conditions.

Load	None
Boundary Condition-ENCASTRE	Encastre(Fixed) applied to the entire Bearing_Schematic OR Reference Point
Boundary Condition-ENCASTRE	Encastre(Fixed) applied to the upper and lower outboard mount plates

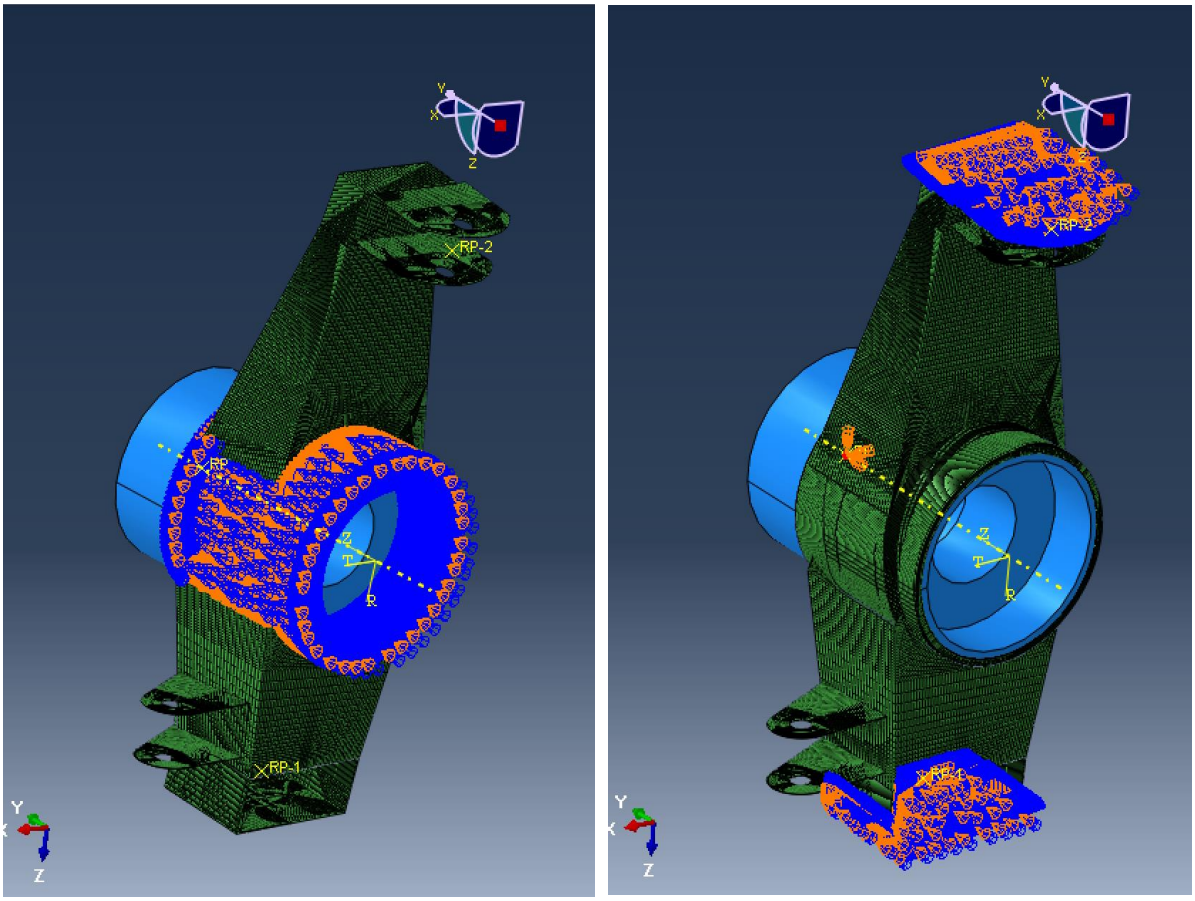

Figure 5.6: Two Cases of Boundary Conditions - Left: Bearing Housing Boundary Conditions, Right: Fixed Ends Boundary Conditions.

Mesh Module

Assembly Mesh Diagram

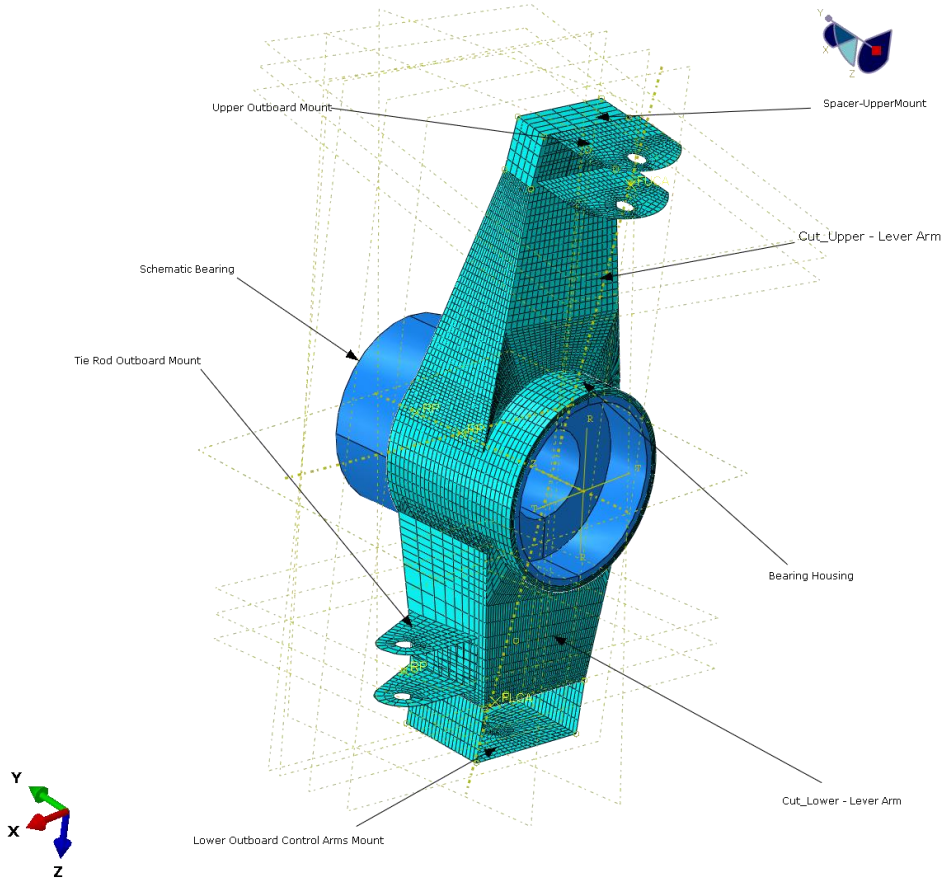

Figure 5.7: Full Upright Model - Assembly Mesh Diagram.

Table 5.5: Element properties of the mesh for different parts of the Upright – Interference Fit model.

Bearing		No mesh – Analytical Rigid
Bearing Housing		3D Stress "Brick" Elements (C3D8R)/Continuum Shell Elements (SC8R)
Conventional Shell Elements	Lever Arm Components	Linear/Quadratic Shell Elements (S4R/S8R) S4R/S8R: A 4/8-node doubly curved thin or thick shell, reduced integration, hourglass control, finite membrane strains.
	Upper and Lower Outboard Mounts	
	Tie Rod Mount	

Results

Abnormal maximum stress values can be explained by inconsistent mesh density because of the inherent geometry of the components or high stress concentration in some areas. A clear example will be the interface of the bearing housing and of the lever arms of the upright (Figure 5.8).

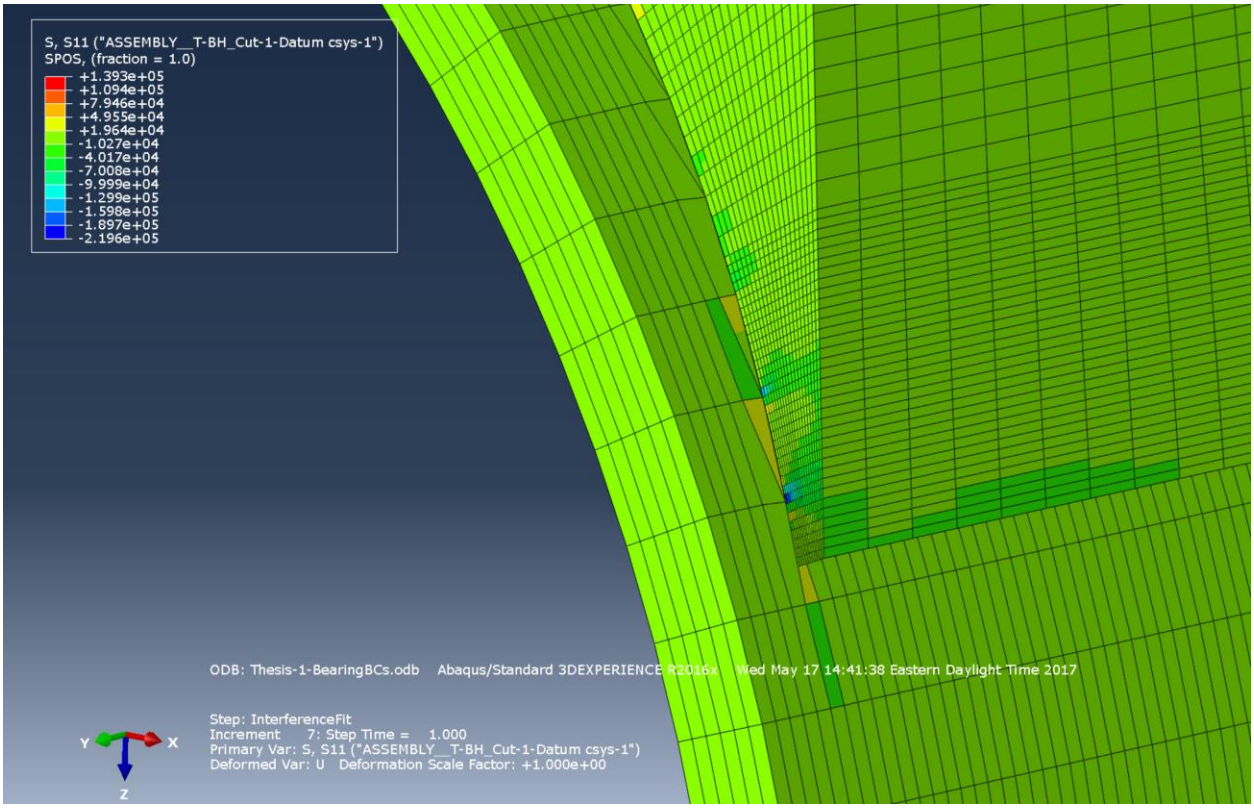

Figure 5.8: Example of Lever Arm and Bearing Housing Interface having stress concentration as well as differential in mesh densities which gives rise to abrupt stress outliers.

Note: To look at results with the same convention of cylindrical local coordinate system, the results have been transformed to make radial as 1-direction, θ as 2-direction and height or Z axis as 3-direction. This has been implemented while looking at results for each of the interference fit models.

Case 1: Bearing Housing Boundary Conditions – Same as Interference Fit Only model

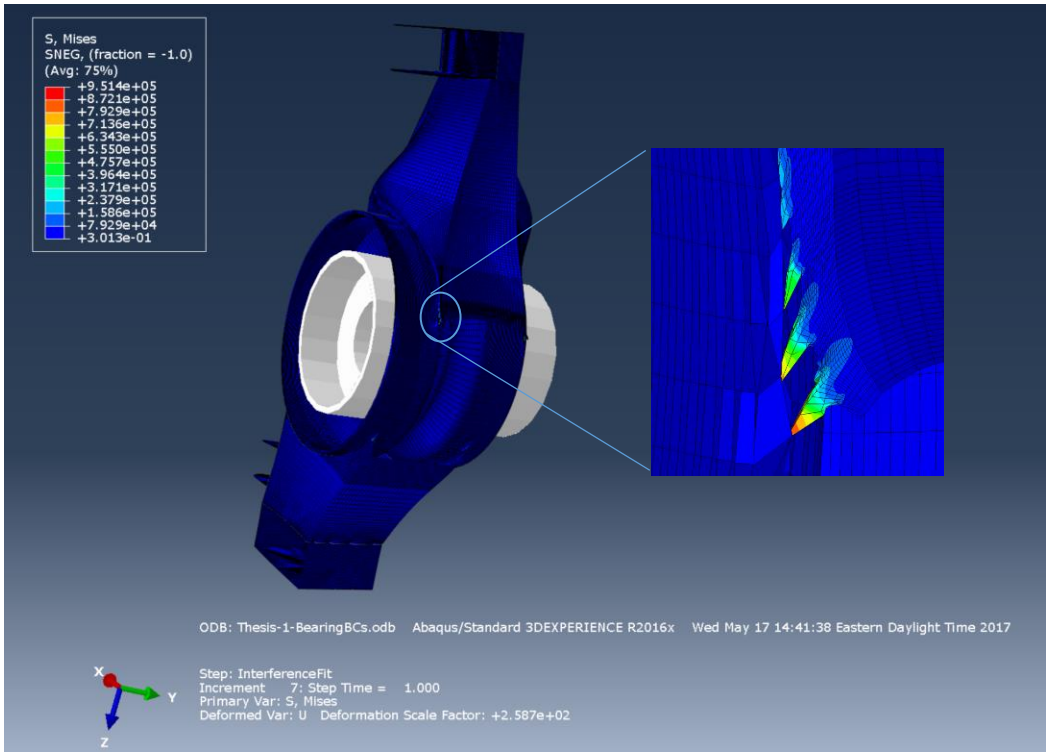

*Figure 5.9: Stress - von Mises- Results for Bearing Housing Cylindrical Boundary Conditions Model - Deformation Factor is 258.7 to display the deformation response of the upright due to interference fit interaction and *TIE constraints between the components*, Magnified image shows how stress concentration response and inconsistent mesh densities at one of the critical areas of loading.

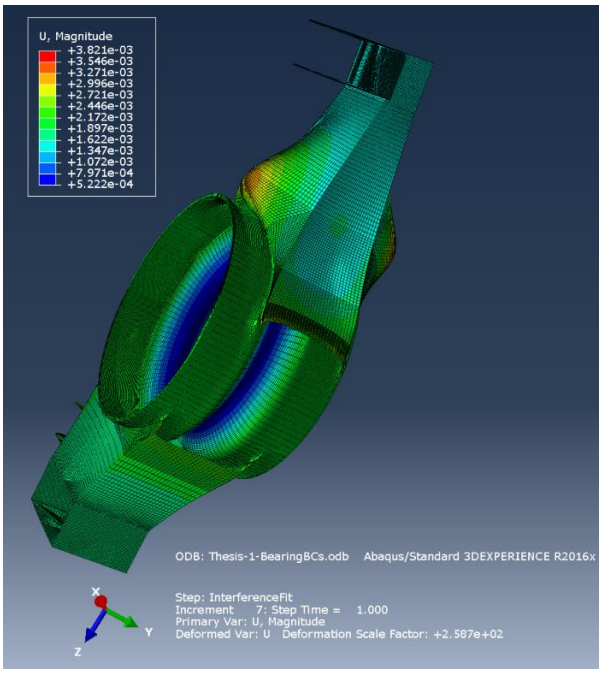

Figure 5.10: Deformation - Magnitude- Response for Bearing Housing Cylindrical Boundary Conditions Model- Deformation Factor is 258.7.

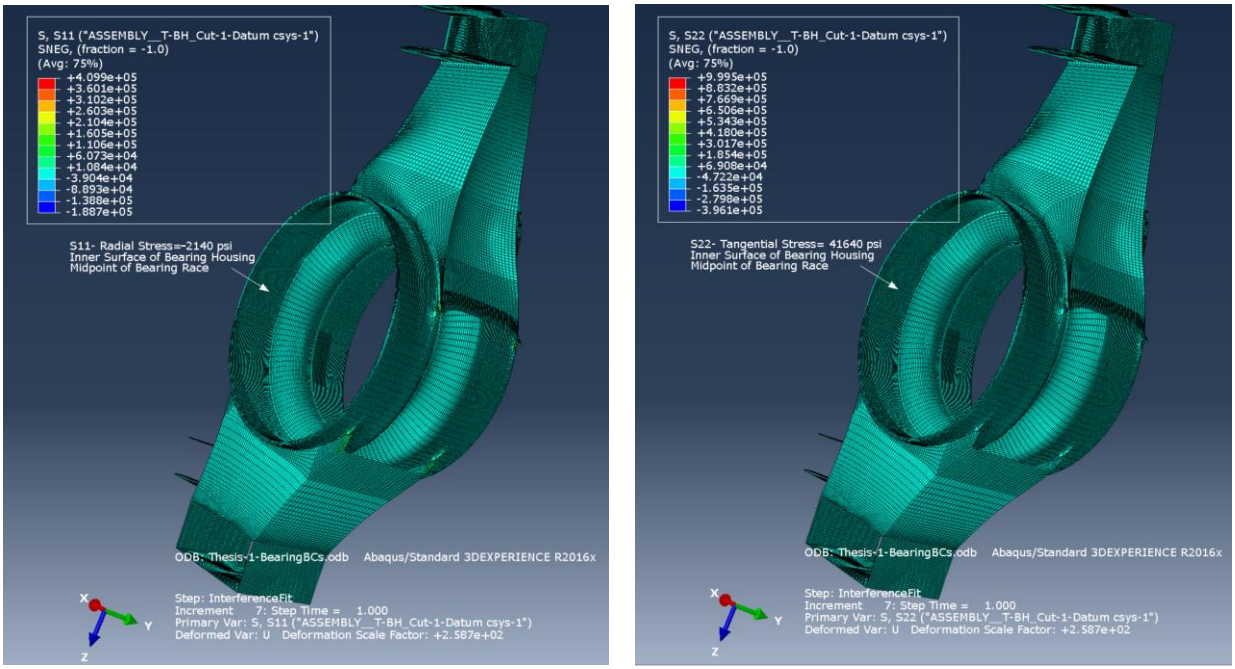

Figure 5.11: S11 and S22- Radial and Tangential Stress Contours for Bearing Housing Cylindrical Boundary Conditions Model.

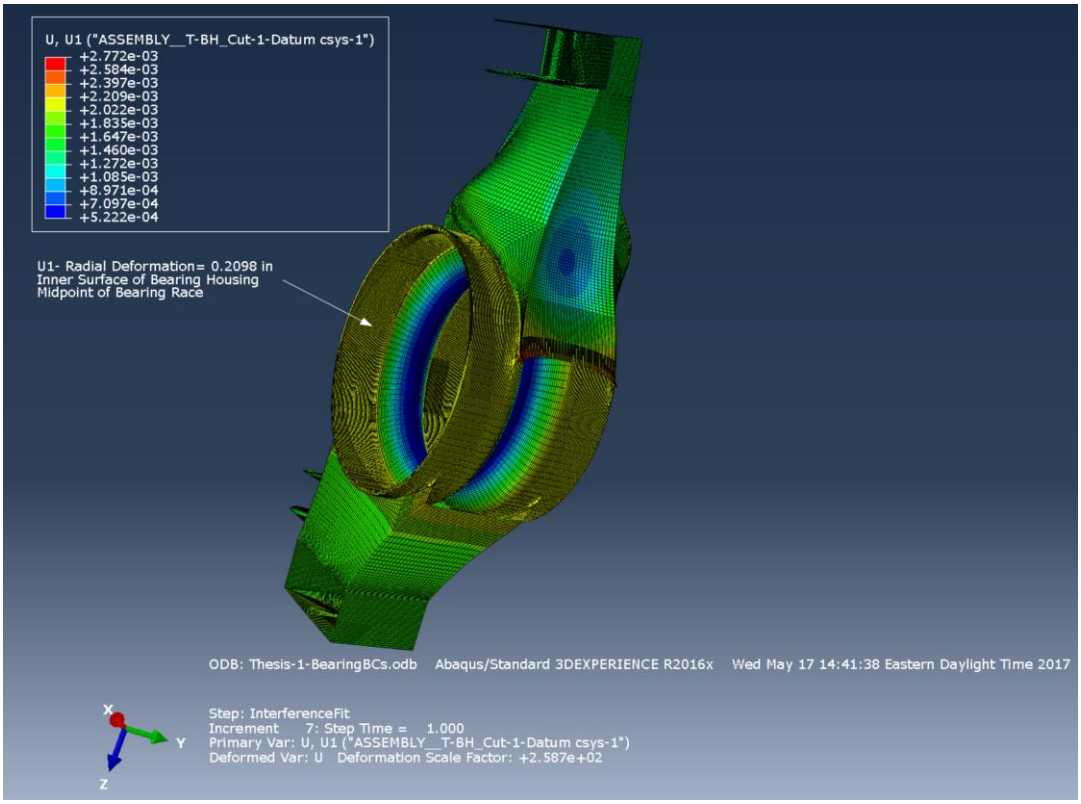

Figure 5.12: Radial Deformation – U1- Response for Bearing Housing Cylindrical Boundary Conditions Model. Deformation Factor =258.7.

Case 2: Fixed Upper and Lower Mounts Boundary Conditions

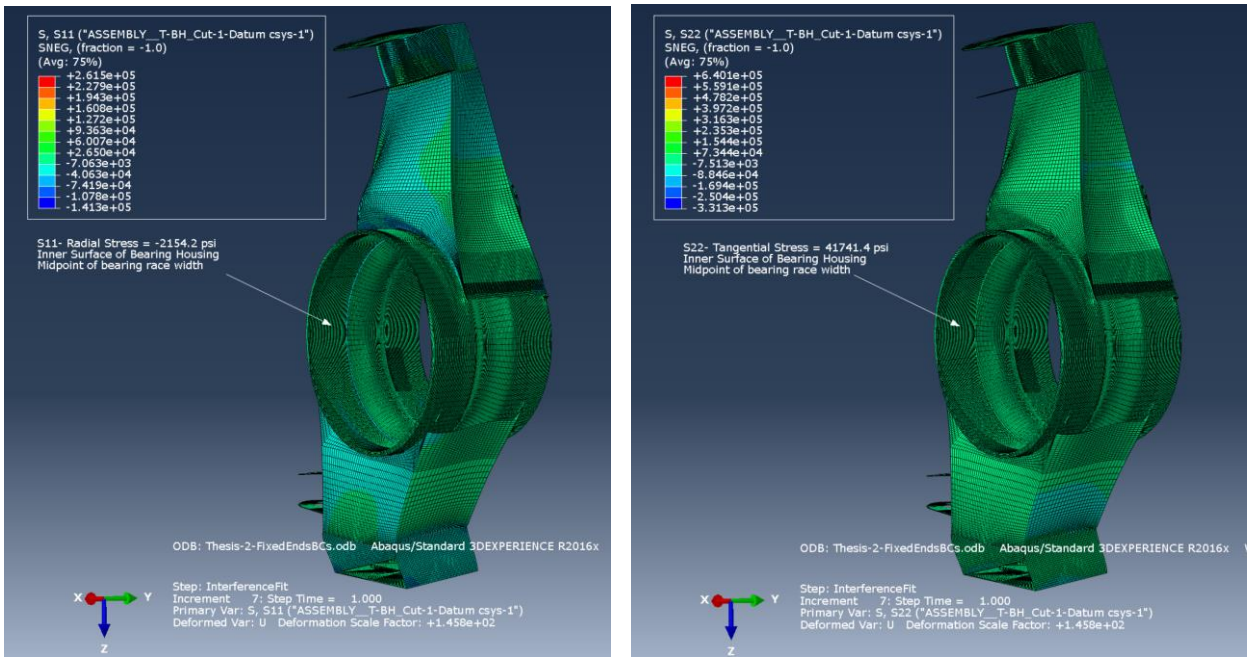

Figure 5.13: S11 and S22- Radial and Tangential Stress Contours for Fixed Ends Boundary Conditions Model- Deformation Factor = 145.8

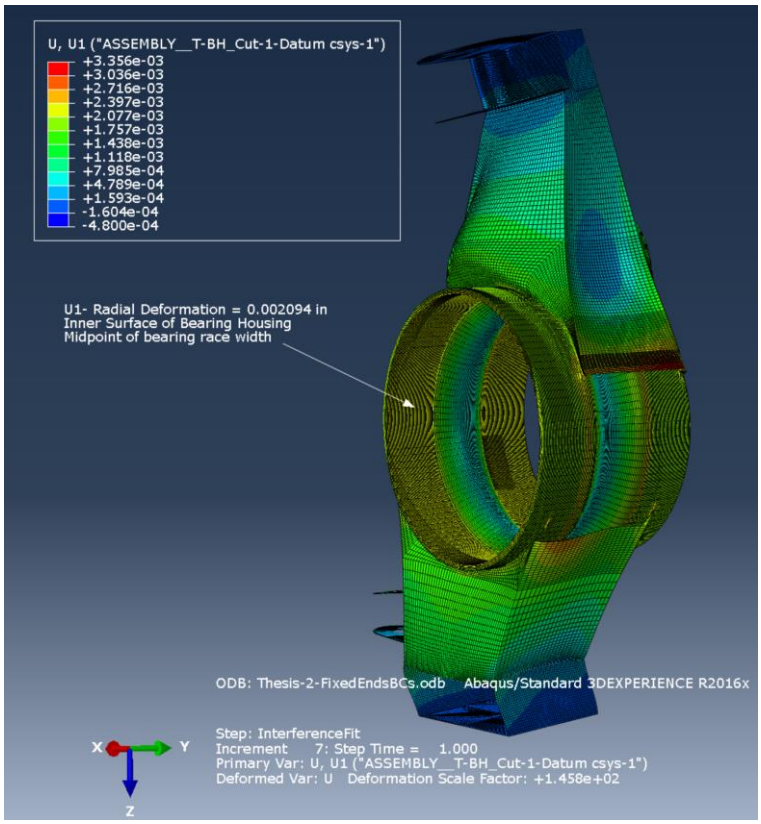

Figure 5.14: Radial Deformation – U1- Response for Fixed Ends Boundary Conditions Model- Deformation Factor = 145.8.

5.2. Comparison and Summary of Results

Since we are extending our interference fit model and adding more parts and assemblies, evaluating the model results are focused on studying the connections. The stresses and deformations at the connections, which are the critical sections, are inspected.

Table 5.6: Comparison of Results between Hand Calculations and Abaqus models to simulate Interference fit response.

	Hand Calculation	**Interference Fit Only**	**Difference %**	**Upright**		**Difference % - From Hand Calculations- Different BC Cases**	
				Bearing Housing BCs	**Fixed Ends BCs**		
Radial Stress (S11)	-2700.4 psi	-2688.7 psi	-0.4%	-2140 psi	-2154.2 psi	-20.8%	-20.2%
Tangential Stress (S22)	49609.1 psi	52609.4 psi	+1.06%	41640 psi	41741 psi	-16.1%	-15.9%
Radial Deformation(U1)	0.0021 in	0.002098 in	-0.0001%	0.002098 in	0.002094 in	-0.0001%	0.001%

Comparing the Hand Calculation and the Simple Interference Fit Only model, we see that the finite element model is consistent with the Hand Calculations. When we introduced the *TIE constraints and build an upright model with underlying assumptions of ideal node-to-node welded joints and encastre boundary conditions on the upright, we notice that the model response (stress and deformation) are different because the stiffness matrix has changed. The Upright Model is also a completely different problem relative to the hand calculations-which is the reason for the large percentage of difference in results. Comparing these different problems all for the same phenomenon but different geometries verifies the direction of solution.

1. Overall the addition of welded joints and different components changes the stiffness matrix. More stiffness results in higher stress values at the lever arm ends of the upright (since the displacement from the expansion of the bearing housing is equal).
2. Stress concentration influences the stress contour maps.
3. Bending moment due to the kingpin inclination of the upright
4. The finite element model incorporates finite sliding between the inner surface of the housing and the bearing. Additionally, the friction between the two surfaces also dissipates some energy if there is relative motion like a “stick-slip” phenomenon.

The upright model will be extended to add more components of the suspension assembly. The model response will be studied for different loading scenarios that the FSAE car would be expected to be subjected to.

6. Development of Quarter-Car Suspension

6.1. Representation of Suspension Members

During the design phase for the FSAE competition, the control arms, tie rod and pull rod are assumed to be individual pinned-pinned truss members. This may be true for the pull rod and tie rod, but both control arms have two members welded together at their outboard ends. This will likely allow bending loads in the members of the control arms that may make them more prone to buckling. The bending loads, if significant enough, may cause large amounts of deflection that will cause the suspension to camber out excessively, causing an undesirable drop in the lateral capacity of the vehicle [3]. If the bending loads on the controls arms are excessive and non- uniform across upper and lower CA, the immediate concern would be failure of the suspension. Additionally, camber gain could be higher than expected from a kinematics study. Excessive camber gain would result in the reduction of contact patch which may cause instability and even excessive tire wear while cornering.

Borg [3] represents the suspension members as pinned-pinned trusses in the hand calculations. Hence, a very large factor of safety is applied to account for any unknown bending and buckling stresses. Buckling failure is an unlikely phenomenon however it is not a thorough design until all loads, specially bending, are investigated.

Suspension systems are typically designed to sustain tensile and compressive loads. But bending loads in the upper control arm are prominent as it supports the pull rod at an offset (overhang). The VT FSAE suspension team decide to use a pull rod but bending loads are experienced on the supporting suspension member of the push rod as well. To minimize the bending loads, the pull rod mount is located as close to the upper ball joint as possible.

Another reason for bending is the gusset as well as the welded joints at the vertex of control arms. The two members in each control arm are attached such that they are not free to independently rotate at the outboard end. The gussets are added specifically to reduce the bending stresses at the welded joint as well as to reduce the effective free length of each of the members to reduce the chances of buckling.

Since a finite element solver like Abaqus includes BEAM elements with shear flexibility, this research explores applying BEAM elements to all the suspension members. The cross section and material properties are preserved according to VT FSAE design.

6.2. Representation of Spring-Damper

The spring damper system is a part of the corner (quarter-car) suspension assembly and is one of the components that govern the multibody dynamics of the suspension system. There is a decent amount of literature about how the spring damper assembly, called shock absorbers, contribute to the characteristic behavior of the vehicle on the road and the subjective comfort parameter of the passenger. As part of the finite element model, the spring damper system is not modeled with complete detail but enough detail to represent the multibody dynamic constraints it provides.

6.2.1. Truss

The spring damper assembly can be modeled as a rod of length equal to the length of the spring (locked displacement at stroke length), preserving the geometry of the suspension system. Preserving the geometric coordinates is important since it contributes to the installation ratio of the spring-damper. The spring stiffness is adjustable since the FSAE team uses the Ohlins TTXII spring damper assembly.

Figure 6.1: Ohlins TTX II.

Section and Physical Properties

The spring representation as a truss requires section properties that require elastic properties.

Representation of Spring Stiffness:

$$k = \frac{AE}{L} \tag{11}$$

$$\therefore E = \frac{kL}{A} = Spring\ Stifffness\ \times \frac{Length\ of\ Spring}{Cross\ Sectional\ Area(\pi r^2)} \tag{12}$$

Hence, the computed value of the effective modulus of elasticity is used so that the truss element emulates the spring.

Table 6.1: Spring Characteristics when modeled as a TRUSS element.

Spring Stiffness (k)	285 lb/in
Stroke Length (L)	2.1 in
Radius of Spring Representation Bar (r)	Assumed as 1 in
Spring Model Elasticity	Calculated to be 190.5 lb/in^2

Unfortunately, this representation does not include any definitions for damper properties by Section Assignment.

To emulate the viscous damper used by the FSAE team, the damping parameters used in the discrete dashpot elements in the Interactions module act in parallel to the spring.

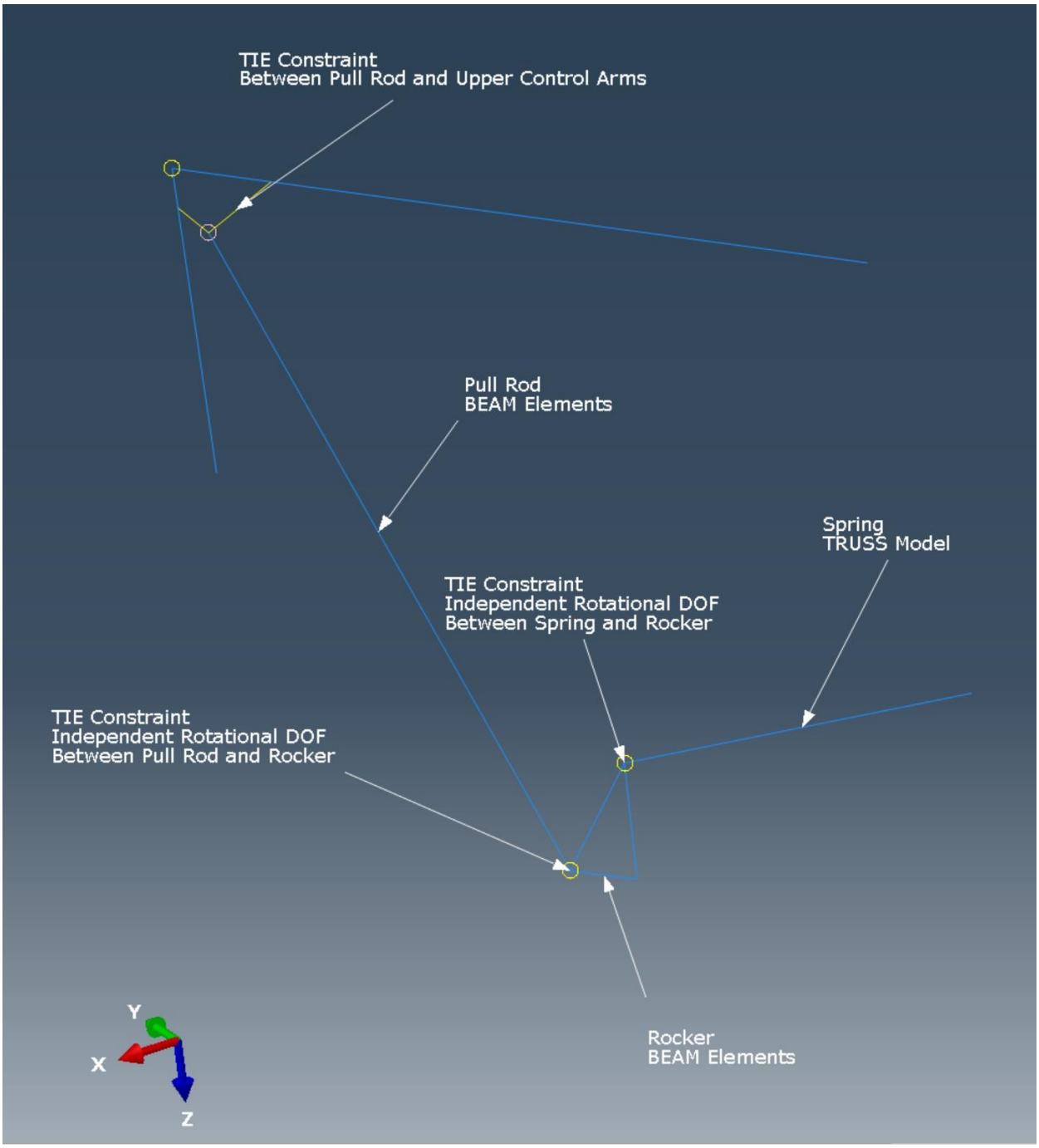

*Figure 6.2: Assembly of Pull Rod, Rocker and Spring where the Pull Rod and Rocker are modeled as Beams, the spring is modeled as a truss and *TIE constraints with independent rotational DOF is applied to spherical joints between them.*

6.2.2. Connector – AXIAL

Springs and dampers can also be modeled with AXIAL connector elements with a datum rectangular coordinate system created to orient the local x-axis along the line connecting the bell crank and spring with degrees of freedom definition in the following table.

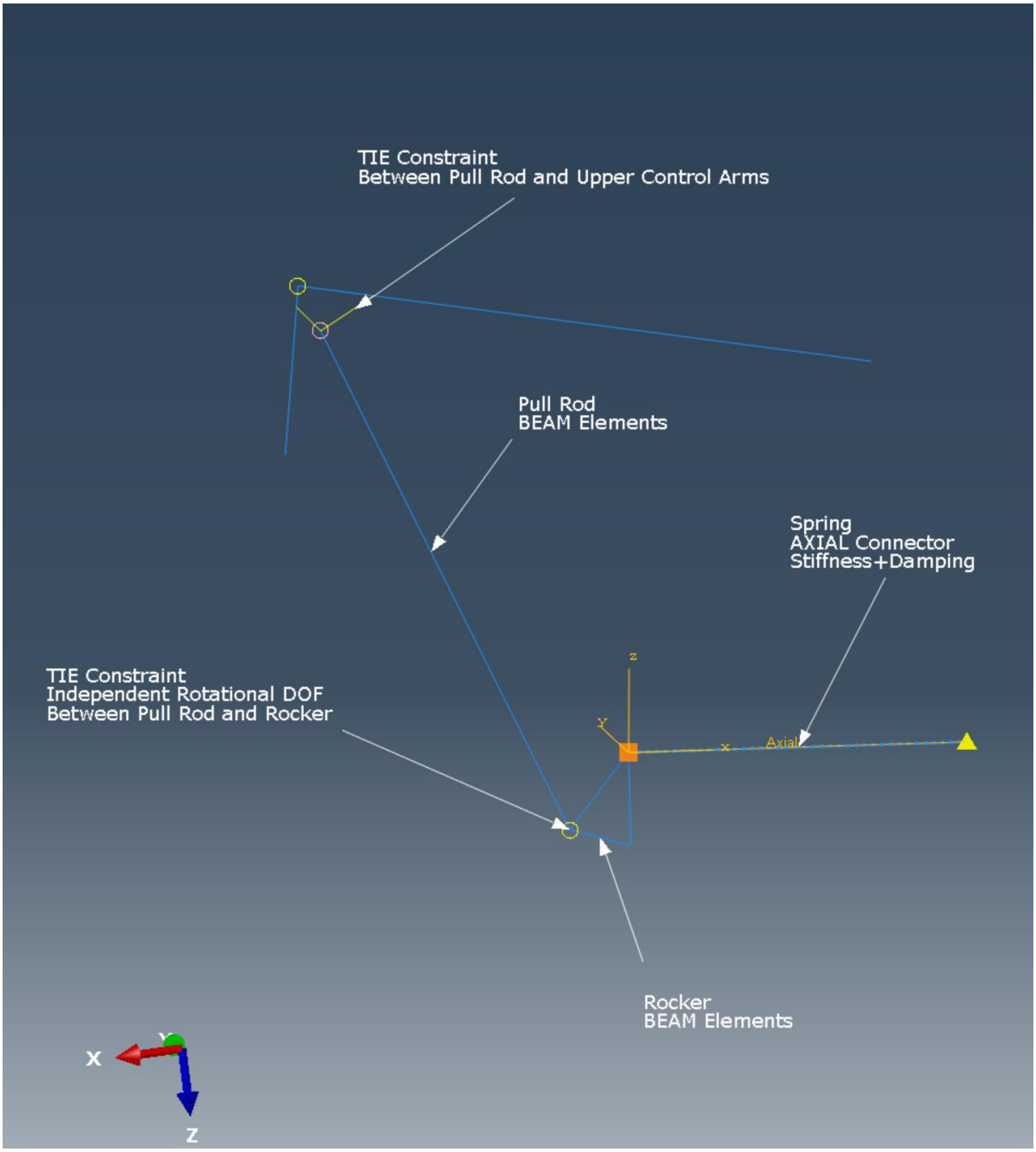

*Figure 6.3: Assembly of Pull Rod, Rocker and Spring where the Pull Rod and Rocker are modeled as Beams, the spring is modeled as an AXIAL connector element and *TIE constraints with independent rotational DOF are applied to spherical joints at the ends of the pull rod. A local coordinate system is established for the connector element with the X-Axis aligned to Spring length.*

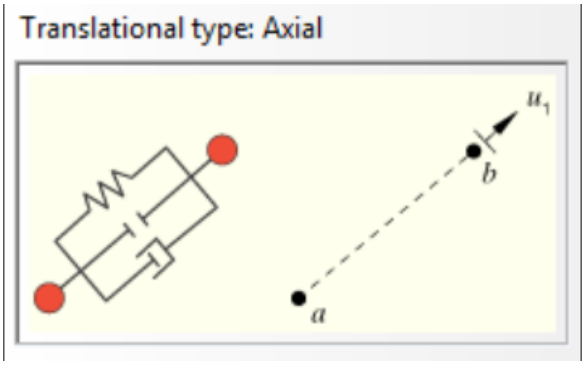

Figure 6.4: AXIAL Connection.

Table 6.2: AXIAL connector Degrees of Freedom.

Available Degrees of Freedom	Local U1
Constrained Degrees of Freedom	N/A

These elements are defined with nodes at the bell crank pickup points and the points in space where they are mounted. In Figure 6.3 the spring/damper is the AXIAL element on the right side of the bell crank rocker. The AXIAL connector elements are given elastic and damping properties reflecting springs/dampers on the vehicle with limits on their relative displacement. Table 6.3 outlines the spring/damper properties. Limits on relative displacement for the connector elements are prescribed based on initial relative distance between nodes. Therefore, when the stops are specified the initial distance between the nodes needs to be calculated and then added or subtracted to the allowable movement.

Table 6.3: Spring Characteristics when modeled as an AXIAL connection.

Front Spring Constant	285 lbf/in
Front Damper Constant	10.5 lbf-s/in
Front Spring Limit	2.25 in

Table 6.2 shows the only available degree of freedom in the local x-direction with no constrained degrees of freedom. The connector element definitions to follow for the bell crank and spring attachment point will account for the restriction of motion needed. With no constrained degrees of freedom there can still be relative motion between the nodes, but only the local x-direction can be assigned properties.

6.2.3. Special Element – Establishing "Best Practice" for Spring Representation

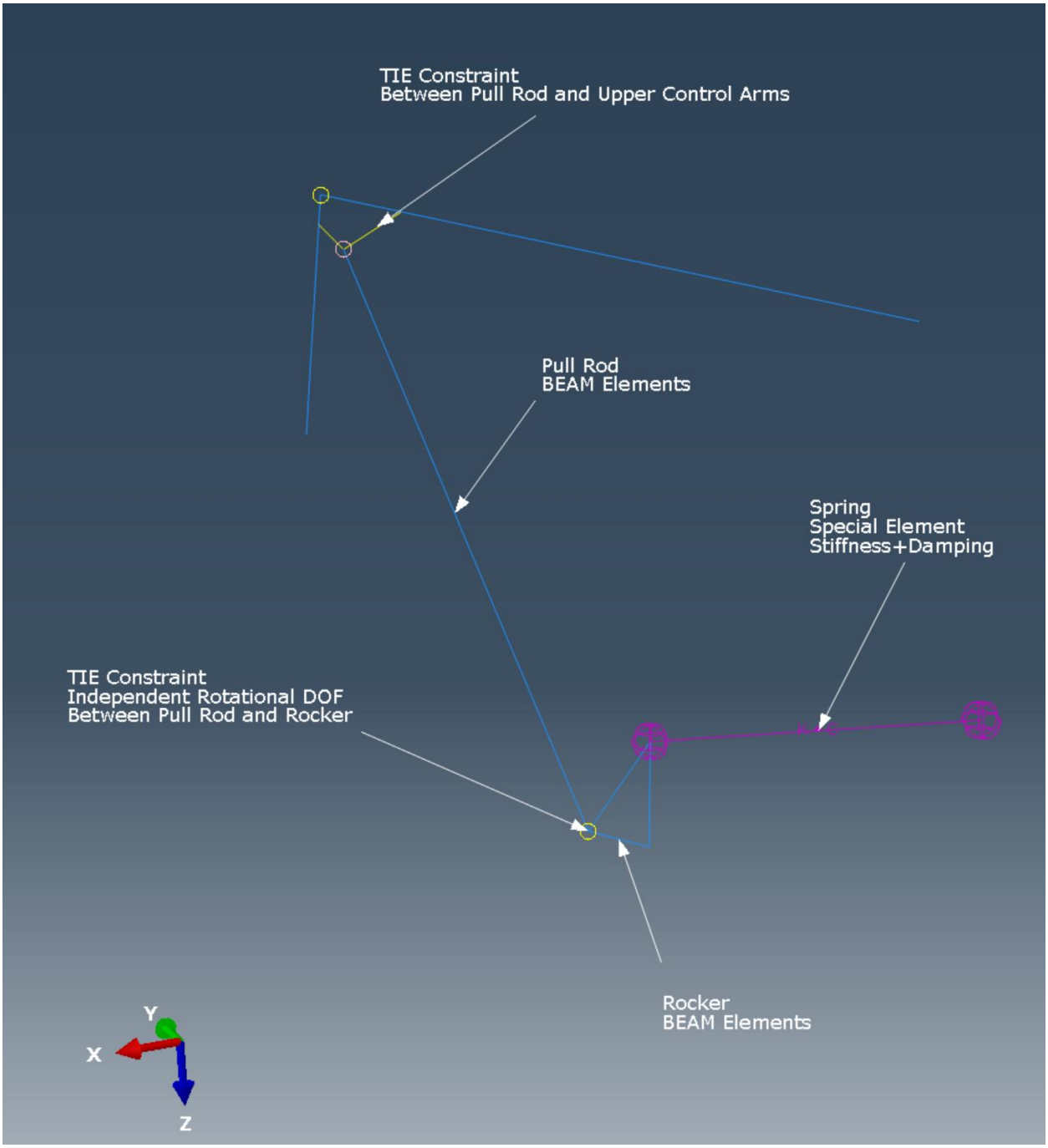

Figure 6.5: Assembly of Pull Rod, Rocker and Spring.

*Where the Pull Rod and Rocker are modeled as Beams, the spring is modeled as a SPECIAL element for SPRINGS AND DASHPOTS and *TIE constraints with independent rotational DOF is applied to spherical joints at the end of the pull rod.*

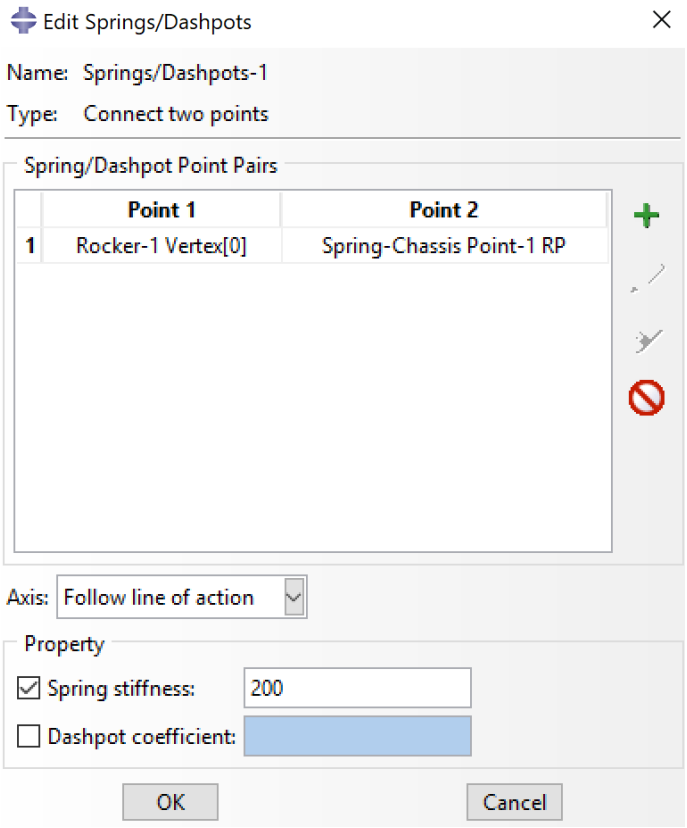

Figure 6.6: Dialog Box for Special Spring Element.

The special element to represent the shock absorber or spring-damper assembly is chosen above the truss element and the AXIAL connector element. As we have set up a library of options for spring representation, the special element provides easy set up – no datum coordinate system set up, no indirect material properties (plug in value of elastic modulus derived from spring stiffness or spring rate) and this element is computationally stable and easy-to-modify. This establishes as the best practice to model the spring-damper assembly in Abaqus FE modeling. With this practice, the spring can be modeled as a simplified singular element preserving its behavior and properties without the complex meshing and modeling effort.

6.3. Representation of Rocker- Rocker Connector Element Model

The rocker, the bell crank, in a pull rod double wishbone suspension system can be modeled by using elastic beam elements and setting up a combination of boundary conditions, constraints and interactions to emulate a representative model. Below is the CAD design of the rocker on the VT 2015 FSAE car.

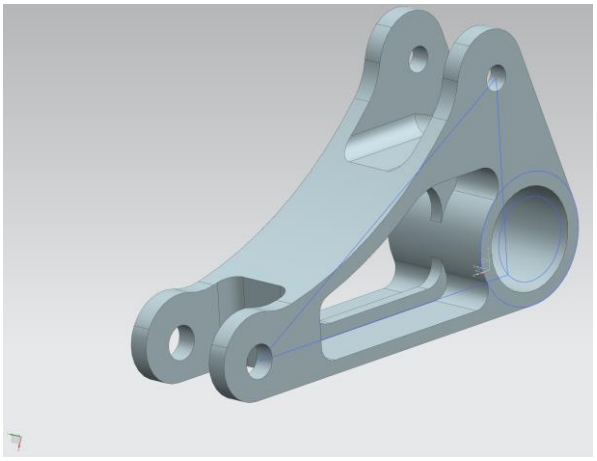

Figure 6.7: Rocker CAD model on NX 10.

Beam Element Model

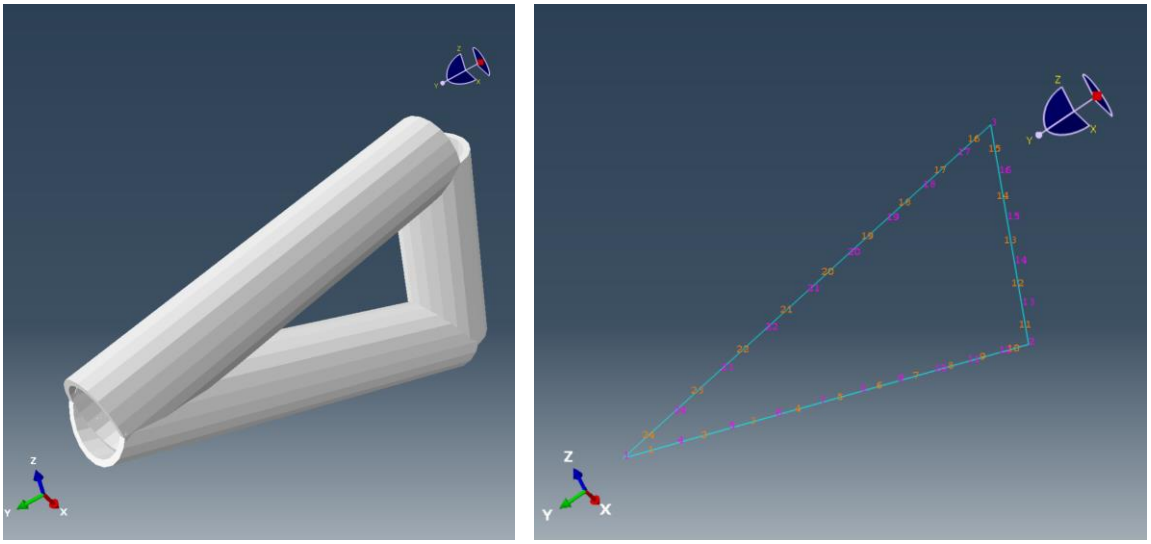

Figure 6.8: 1. Equivalent Mass Beam Element Rocker Model on Abaqus and 2. Part Mesh Diagram of Rocker.

To create a corresponding beam element model, the geometric coordinates are preserved for kinematic accuracy but with pipe sections which were designed with specific dimensions to preserve equivalent mass. The rocker is not the focus of this study, but a certain subjective level of stiffness equivalency was preserved by making it mass equivalent with a common uniform cross section. The mesh module also mentions that multiple elements were used in the formulation instead of single element for each rocker member so that the model is more flexible. The focus of the rocker model is that the kinematics and inertia are well represented and not the elastic flexibility.

Mesh Module

Table 6.4: Mesh Characteristics of Rocker Beam Model.

Element Type	Beam – B31 – 2 node linear shear flexible beam in space
No. of elements	24

B32 – Quadratic shear flexible beam element would have been the best choice for modeling the rocker. This is because quadratic formulation is more accurate and is less stiff than the linear element. The linear element was chosen for this part which acts as a kinematic link more than an elastic member because of its short length beams (high stiffness) and free rotational degree of freedom.

Interactions Module

The rocker has heim joints and spherical bearings connecting it to the pull rod and the spring. The heim joints and spherical bearings are rotationally free to move for a spherical cone of compliance. Some representations for the heim joint (in their particular kinematic situation with relatively large diameter spacers) could consider it a UJOINT formulation since it is an easily available preset connection in most FEA codes.

Rocker Interactions can be set up either using *TIE Constraints (with independent rotational degree of freedom) or using connector elements.

1. Tie Constraints

In this model, we use tie constraints defined between the rocker and the pull rod as well as between the rocker and spring. Tie constraints are easy to imagine joints as welded; however, in this case we do not constrain the rotational degrees of freedom in a typical weld joint. The connector elements were chosen to model the joints.

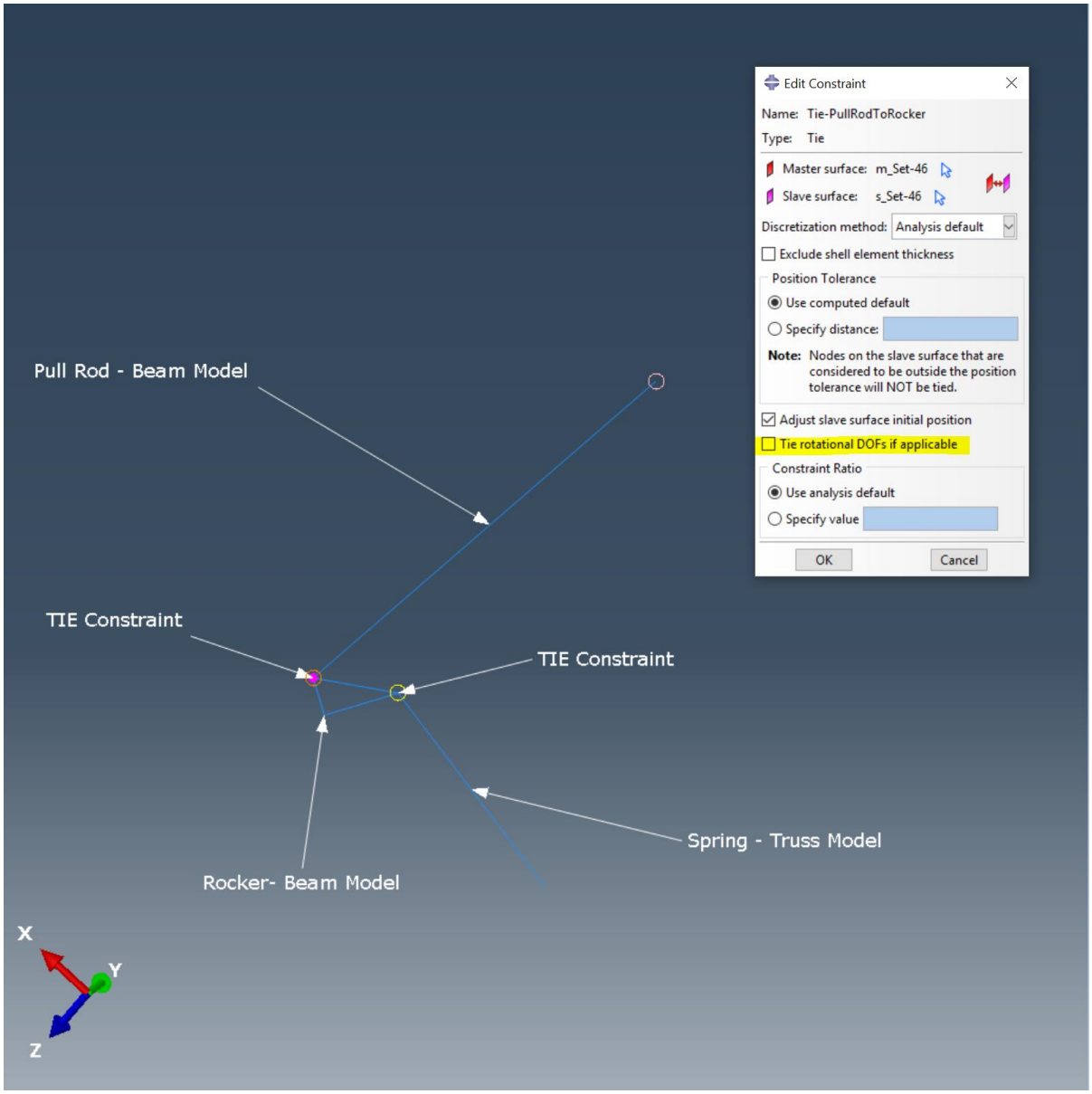

*Figure 6.9: Assembly of Pull Rod, Rocker and Spring where the Pull Rod and Rocker are modeled as Beams, the spring is modeled as a TRUSS element and *TIE constraints with independent rotational DOF is applied to spherical joints between the components.*

2. Connector Elements

a. UJOINT Connection

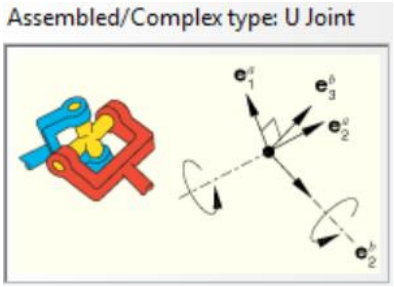

Figure 6.10: UJOINT Connection Diagram.

For all connector elements, since we define them using degrees of freedom, we must create a new coordinate system for each connection. For the UJOINT connection between the pull rod and the rocker, we create a local coordinate system with the local y-axis pointed along the axis of the pull rod. While the joint is not actually a universal joint, it does provide the necessary restrictions on the degrees of freedom to prevent the pull rod from spinning about its own axis.

Table 6.5: Degrees of Freedom Table for UJOINT connection.

Available Degrees of Freedom	UR1, UR3
Constrained Degrees of Freedom	U1, U2, U3, UR2

b. AXIAL Connection for the Spring

As we covered in the representation of the spring, we can also define the connector element representing the spring-damper assembly connected to the rocker. The details of the formulation was covered in Section 6.2.2.

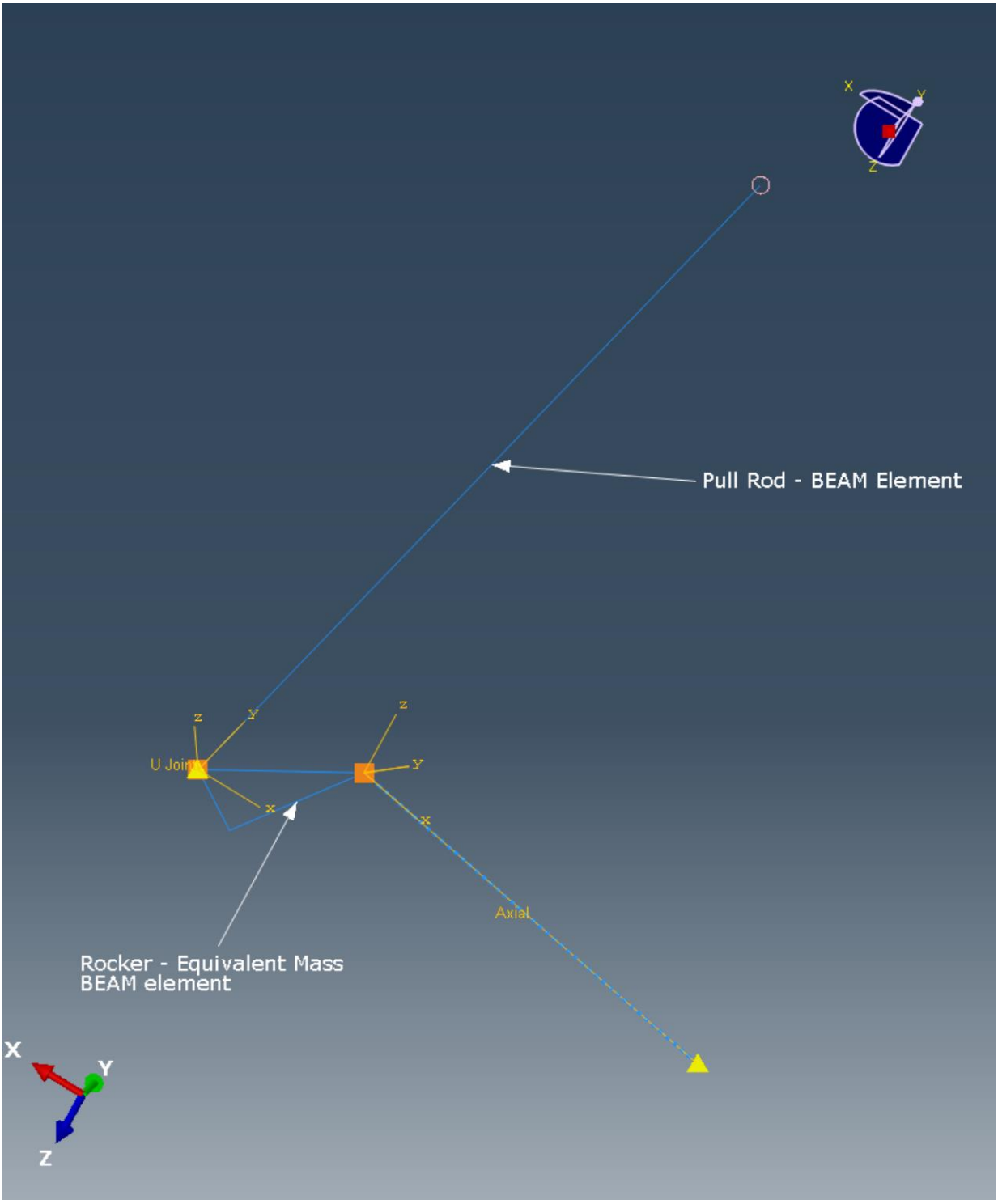

Figure 6.11: Assembly of Pull Rod, Rocker and Spring where the Pull Rod and Rocker are modeled as Beams, the spring is modeled as an AXIAL connector element and a UJOINT connection is applied between the rocker and pull rod.

Summary of modeling Rocker and Rocker Connections

The rocker in quarter-car suspension is important to model the kinematic connection of the wheel assembly to the shock absorber. Since this is an elastodynamics model, the inertia and elasticity of rocker is preserved by using a mass-equivalent BEAM element model. The rocker connections are modeled with CONNECTOR elements – UJOINT on the pull rod attachment, boundary condition for ROTATION NORMAL TO IT'S PLANE at the chassis attachment point and the SPECIAL element for the spring applies a spherical joint at the spring attachment.

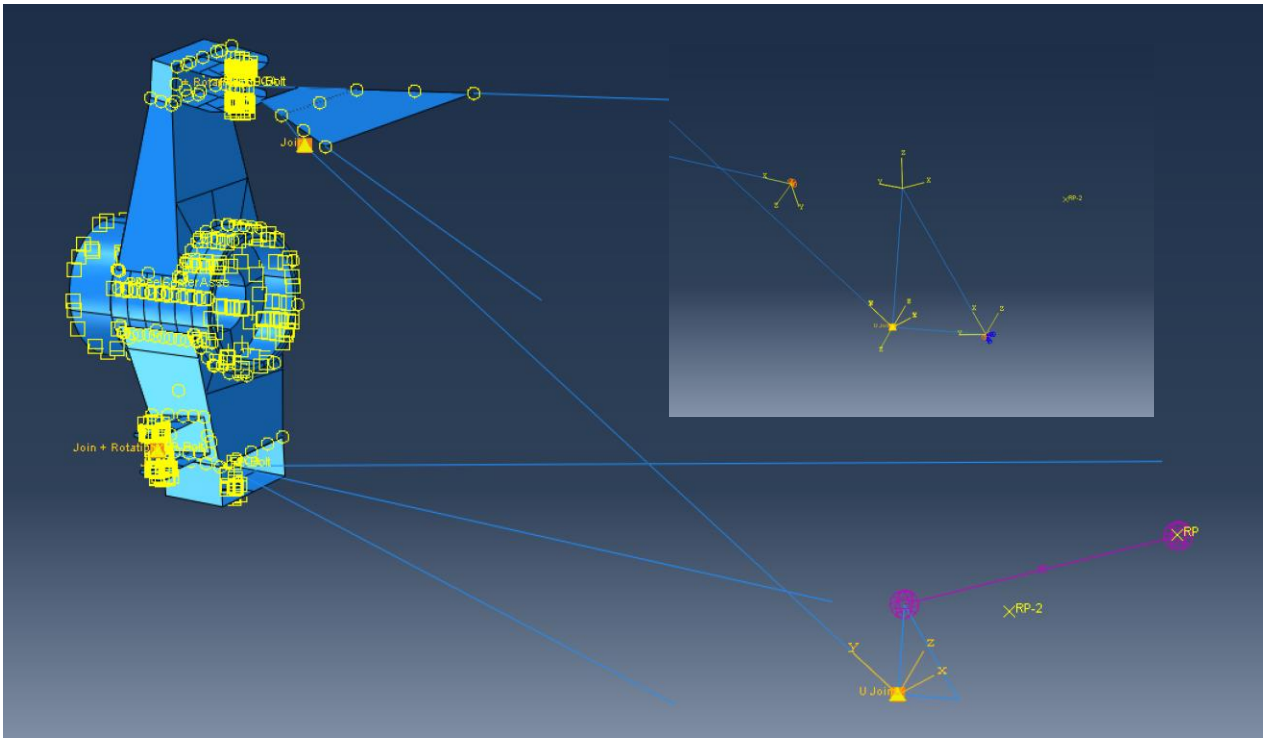

Figure 6.12: Best Practice - Rocker Representation for Pull Rod Double Wishbone Suspension – Magnified Image shows how the Boundary Condition is set up with a Datum Coordinate System – Z axis Normal to Rocker Plane.

6.4. Representation of Pull Rod + Pull Rod Mount – Installation Ratio

The pull rod is modeled as a beam element with section and material properties applied as per accurate FSAE designs. The pull rod connections can be modeled in different ways:

1. Rocker Connection

   *TIE constraint and the UJOINT connection element for Pull Rod connection with Rocker is discussed in Section 6.3.

2. Control Arm Connection

   The pull rod connection with the upper control arm can be modeled in 2 different ways based on computational flexibility and scope of thesis.

   a. Coupling constraint

      The pull rod is connected to the control arms using a universal joint or a rose (heim or spherical) joint representation as shown in Figure 6.14. These joints are represented accurately based on kinematics using the coupling constraint. The coupling constraint, however, if used to join 2 elements without accurate representation of the pull rod mount, would result in inaccurate behavior. The pull rod mount is a major reason for bending loads and a coupling constraint works between nodes in 1D elements. Hence it cannot represent the deformation mode caused by the gusset plate, the clevis mount and the heim joint bolted connection of the pull rod.

   b. BEAM model of the Pull Rod mount and *TIE constraints

      Below is a representation of an equivalent mass Pull Rod Mount that is welded (*TIE Constraint) to the upper control arm - Figure 6.15. This mount is designed according to the motion ratio that is a part of the ride and roll rate calculations which govern how the suspension designer would like to make the car react or behave to cornering and bump load scenarios.

      Since the pull rod mount is modeled with 1D deformable elements, it will also contribute to the overall suspension behavior. This is an accurate representation with elastic members instead of rigid body dynamics.

The pull rod mount is TIED to the control arms and connected to the pull rod using the JOIN connector element.

3. JOIN Connector element for Pull Rod Mount Connection to the Pull Rod

   The JOIN elements represent spherical bearings that exist on the 2012 car restricting all translational degrees of freedom while allowing all rotational degrees of freedom (Figure 6.13). Because the JOIN element has all relative rotational degrees of freedom available a local coordinate system definition was not required, and the global system was used instead. The actual heim joints (spherical joints) have physical limitations from the bolts and the clevis distance to rotate but it has not been included in this formulation.

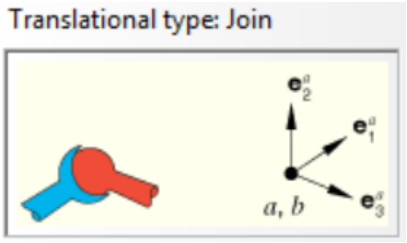

Figure 6.13: JOIN connection diagram.

6.4.1. Established practice of representing Pull Rod and Pull Rod Mount

The final representation of the Pull Rod is a BEAM element formulation with UJOINT connector element at the rocker attachment point and JOIN connector element at pull rod mount attachment.

The Pull Rod Mount is modeled as a triangle with BEAM element formulation which has a *TIE connection with the Gusset Plate. This represents the clevis mount welded to the gusset plate.

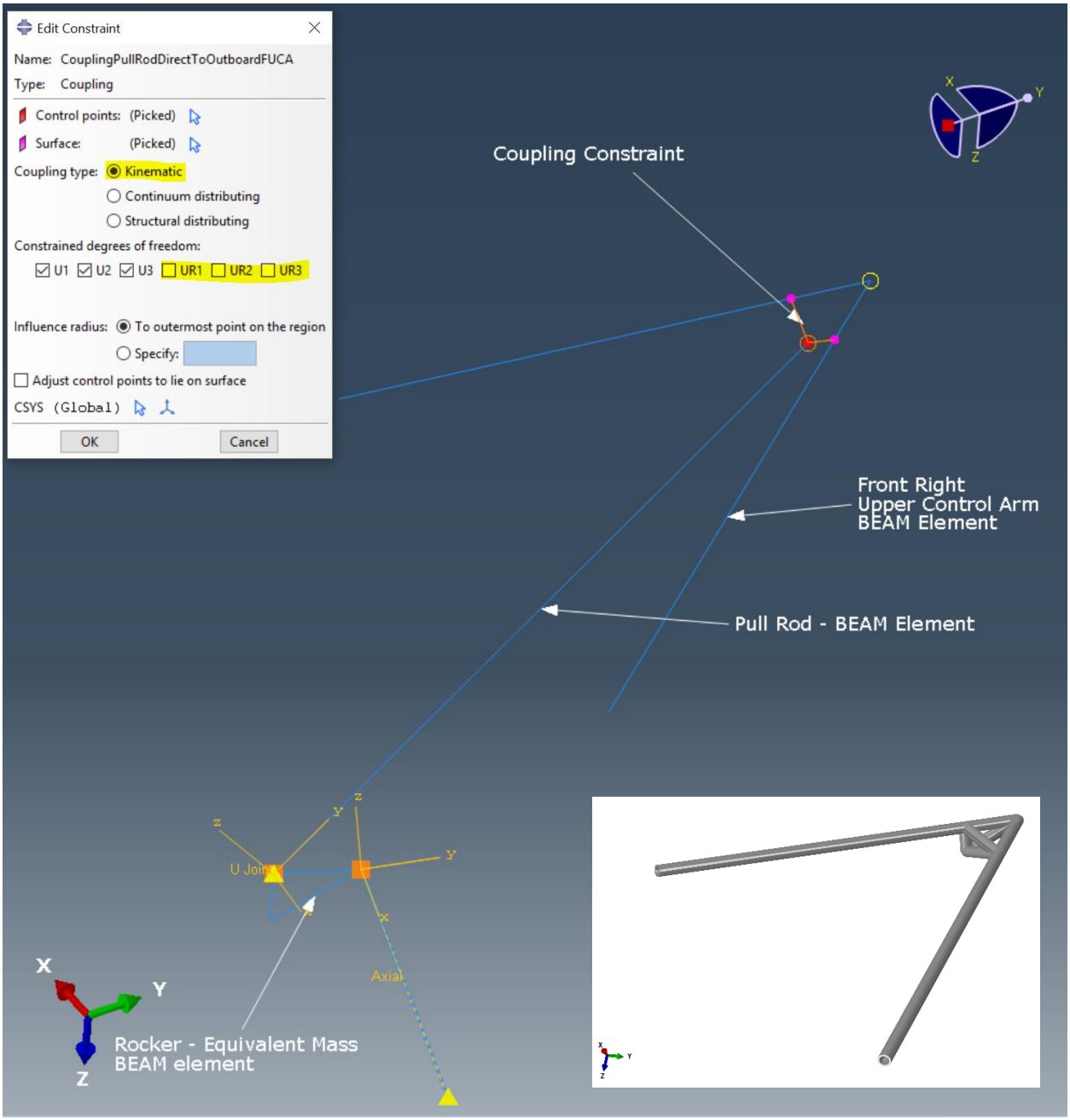

Figure 6.14: Coupling Constraint between the pull rod and control arms.

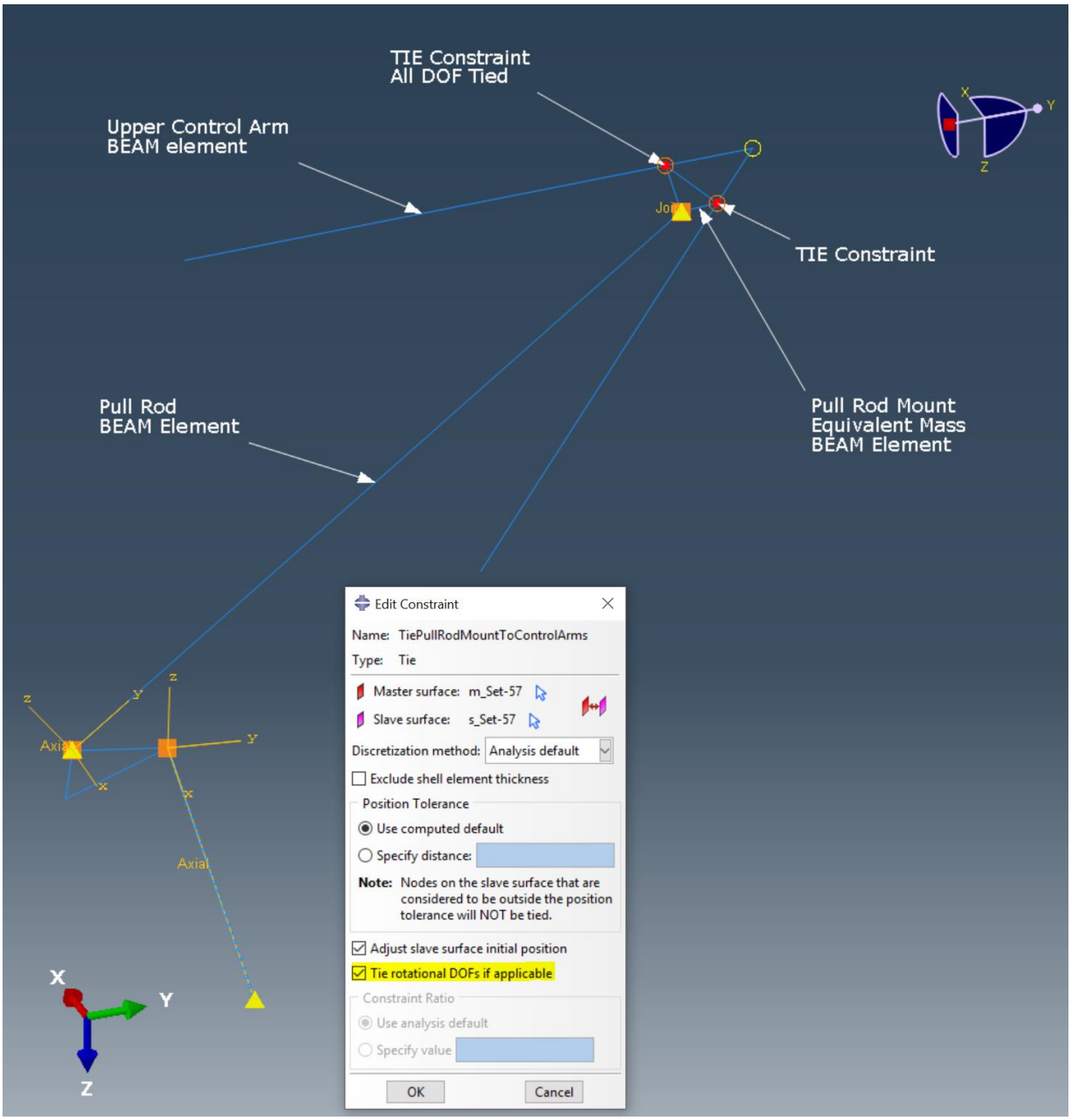

Figure 6.15: Tie Constraint (Weld) between Pull Rod Mount and Control Arms - Note: Gusset Plate has not been modeled.

6.5. Representation of Gusset Plate for Pull Rod Mount

The gusset plate for the pull rod mount is designed to carry bending loads from the pull rod mount but it also creates/allows bending loads in the control arms.
The gusset plate mesh is consistent, with the pull rod mount and the control arms, resulting in a compatible mesh.

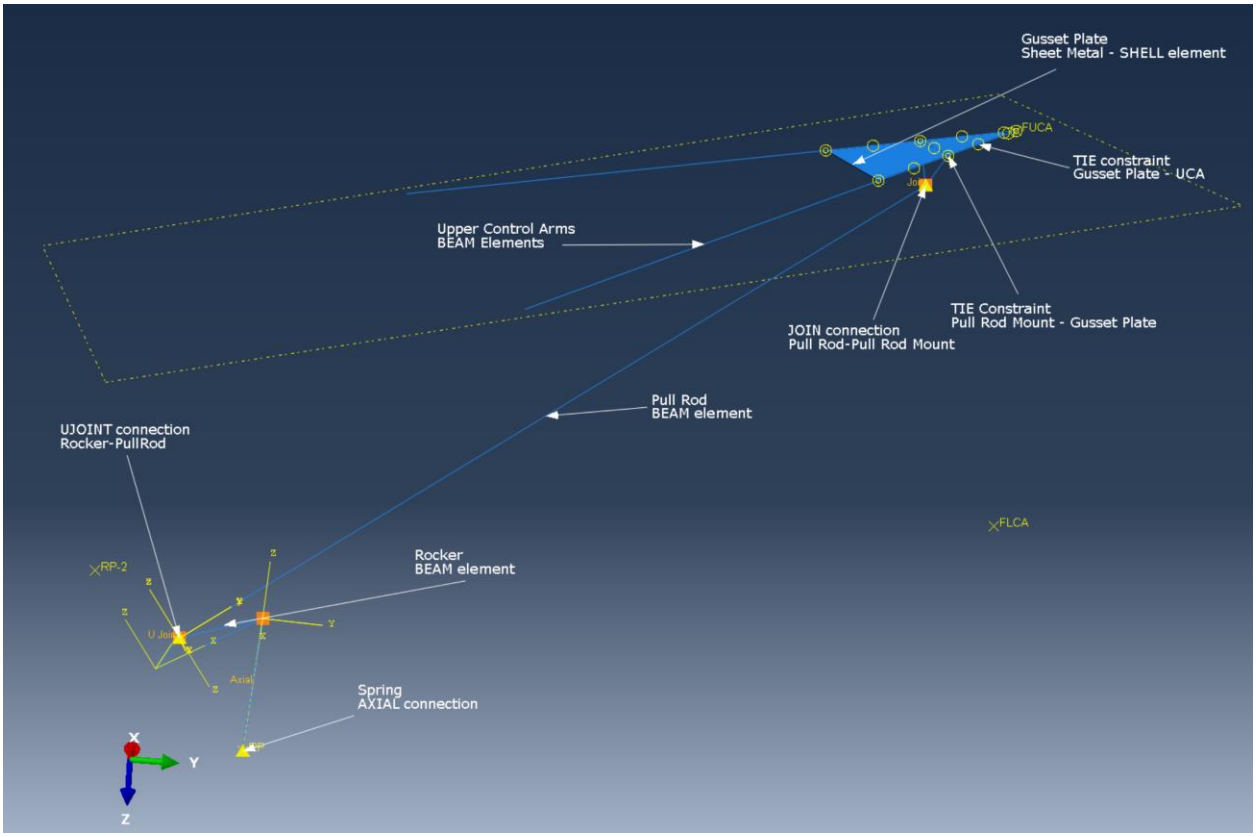

Figure 6.16: Overview of Pull Rod and Pull Rod Mount Connections and Representations in FE Model.

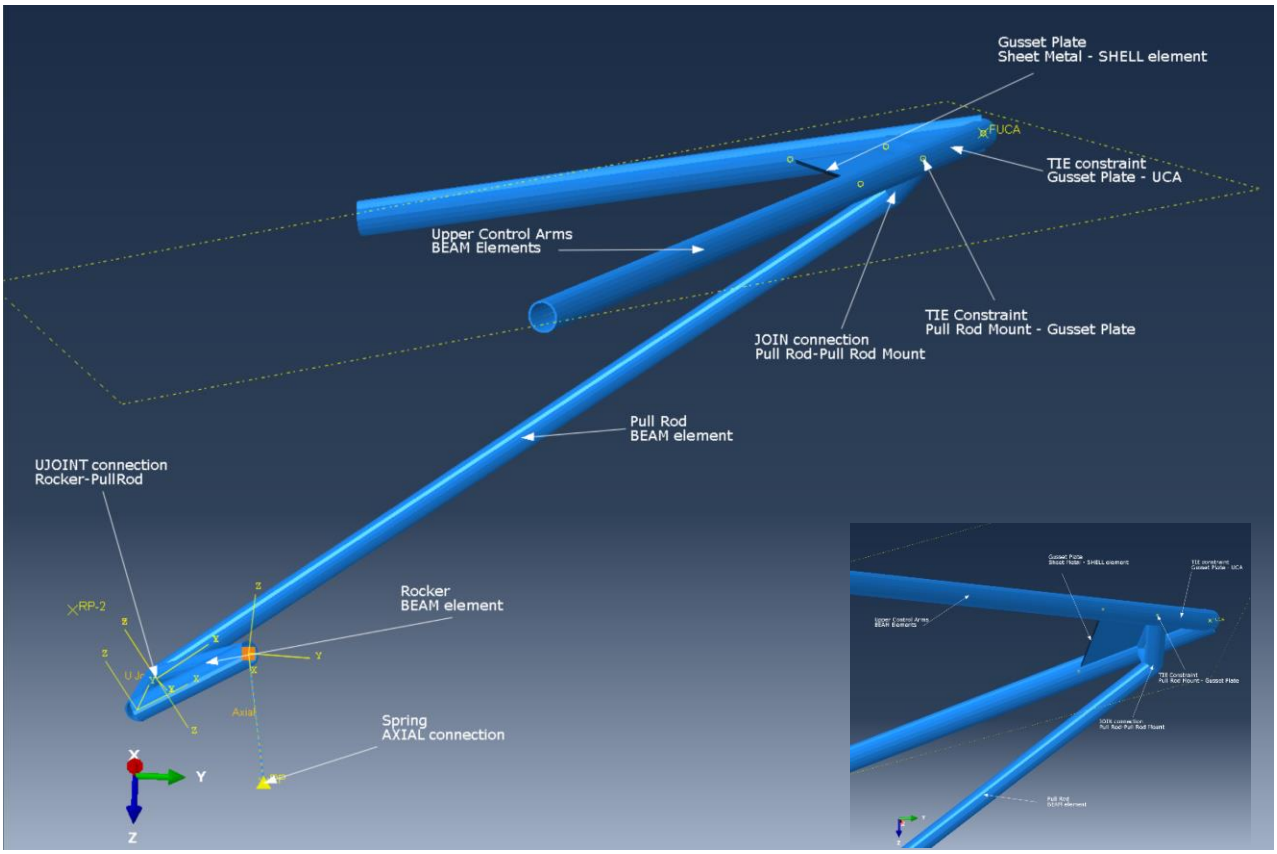

*Figure 6.17: Gusset Plate Model for Pull Rod Mount - *TIE constraint between Control Arms and Gusset Plate as well as between Gusset Plate and Pull Rod Mount.*

6.6. Representation of welded joints

Welded joints are typically represented using the *TIE command in Constraints if they are different parts. The shell model of the upright is designed and manufactured as a folded sheet metal component which is welded together for assembly. The *TIE command emulates a weld joint by writing multi-point constraints between all displacement dof, which is used for general purposes.

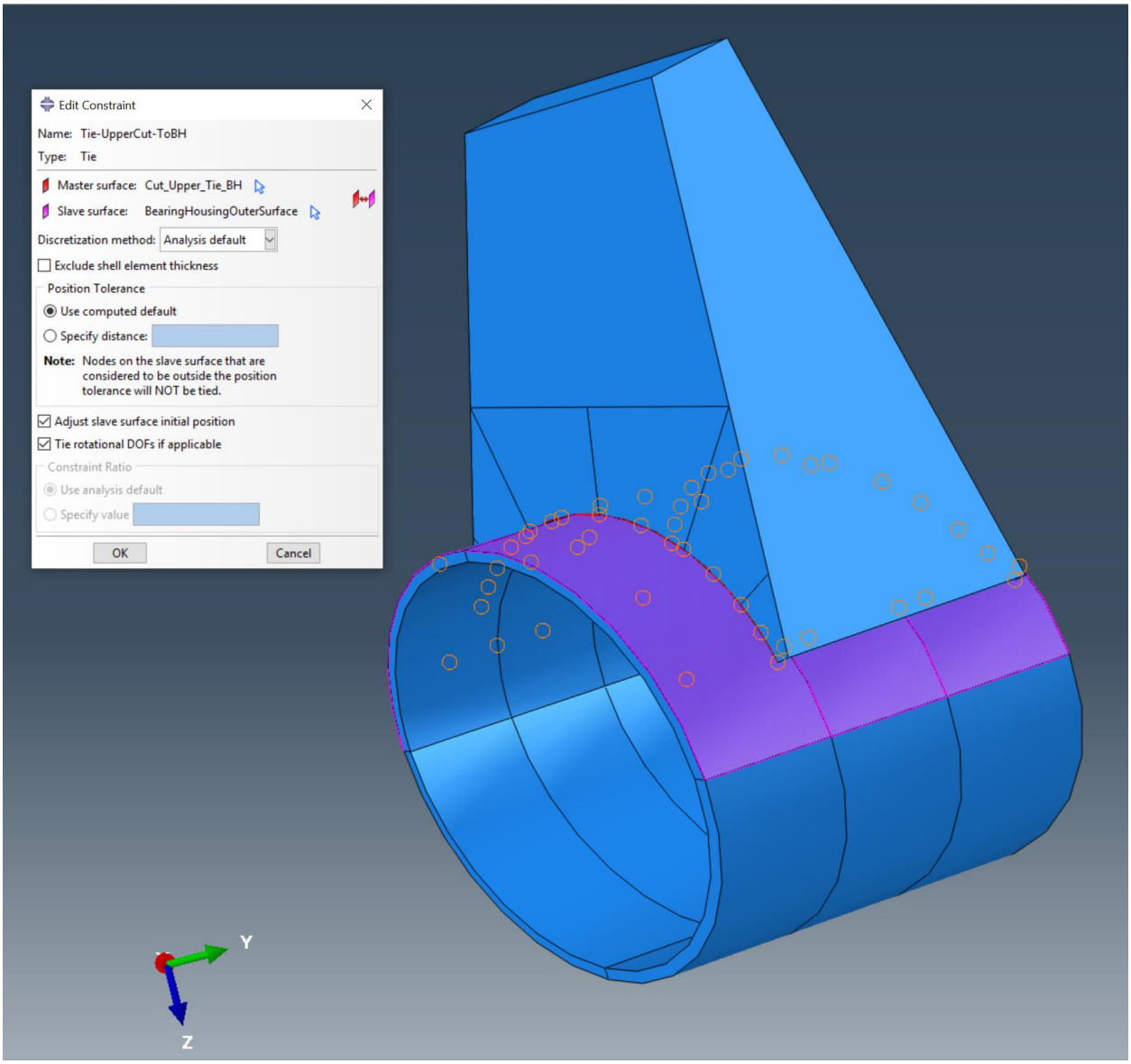

*Figure 6.18: Welded Joint between Upper Lever Arm of the Upright and Bearing Housing modeled as a *TIE constraint.*

6.7. Representation of Spherical Rod End Bearings

Spherical bearings are implemented with rod ends for the outboard suspension points. Along with spherical bearings, heim joints are also employed for other suspension joints. They allow limited spherical rotational motion. Below is a summary of joints in a typical double wishbone push rod suspension geometry.

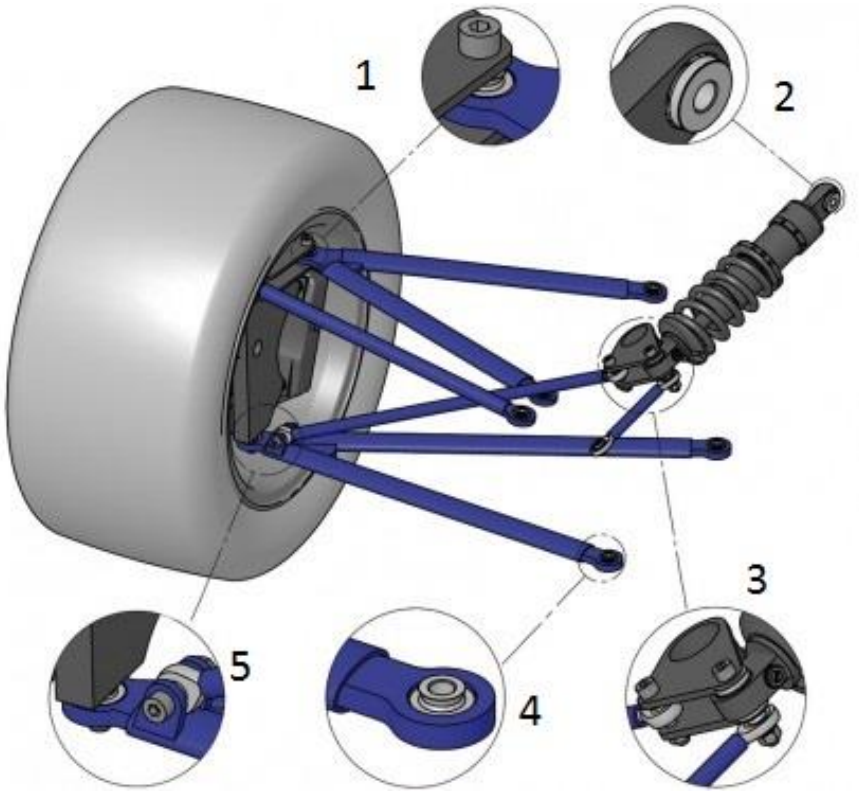

Figure 6.19: Double Wishbone Push Rod Suspension – Different connections involved.

1. Spherical Bearing inside a tab: This is typically used for outboard points of the suspension instead of simpler heim joints to prevent rod ends in bending. For an explanation of rod ends in bending, refer to [24]. A shank bolt is inserted in the spherical bearing.
2. Bolted Joint at the Inboard spring mount: This is a pin joint. Some spring-damper assemblies have a spherical joint at this location. Spherical joints allow for easier installation as well as preventing the spring from bending and snapping on impact or crash situations.
3. Pin Joints for rocker. These can also be spherical joints to prevent bending deformation.
4. Rose Joint or Heim Joint staked inside the suspension member pipes: These are easy to install and have a spherical bearing inside a custom threaded bolt housing.

5. Rose Joint at the pull rod mount (discussed in Section 6.4)

In Abaqus, there are different representations in the connector sections to model the interaction and constraints at the joint. To model the bolts interaction with the upright mount tabs, the bolts are modeled as analytical rigid revolute parts, which represent the bolt head, the bolt shank and a nut. Washers, bushings and spacers are not modeled which are used to provide compliance and help the fastener serve its purpose. There is no "gap" between the bolt and the sheath- consider it a hard bolt stack with washers or bushings.

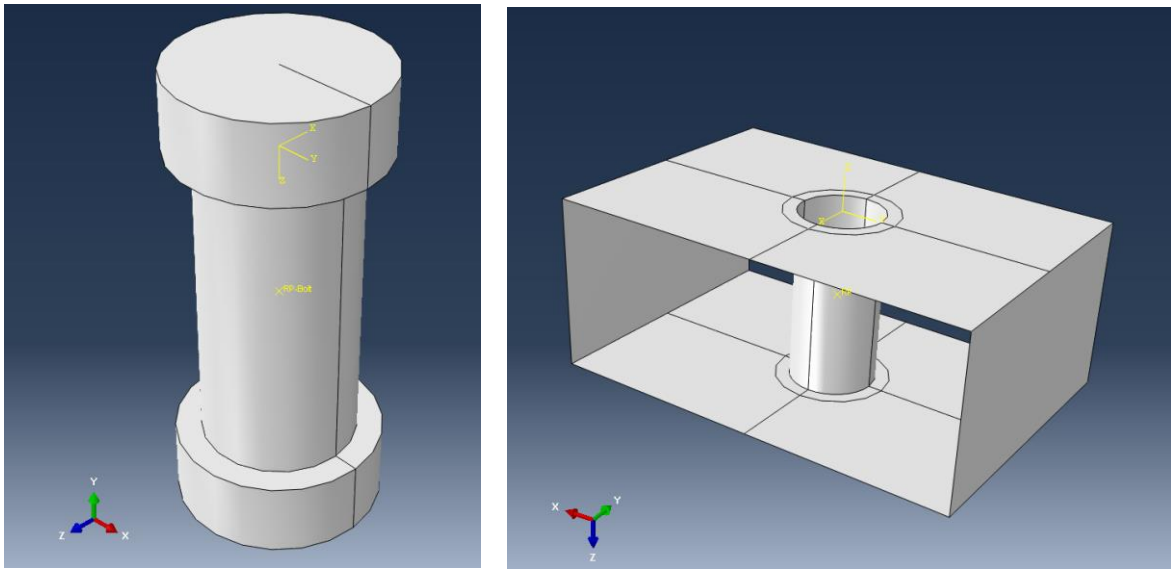

Figure 6.20: Part Models -Analytical Rigid Bolt and Partitioned Shell Model of the Mount with the sheath.

Modeling the interaction between bolts that are analytical rigid solids and holes in upright mount tabs, which are edges for shell elements, is challenging. To resolve modeling surface contact between a surface and an edge, bolt "sheaths" were created as part of upright mount tabs so that the bolt surface and the sheath surface can be given surface-to-surface contact.

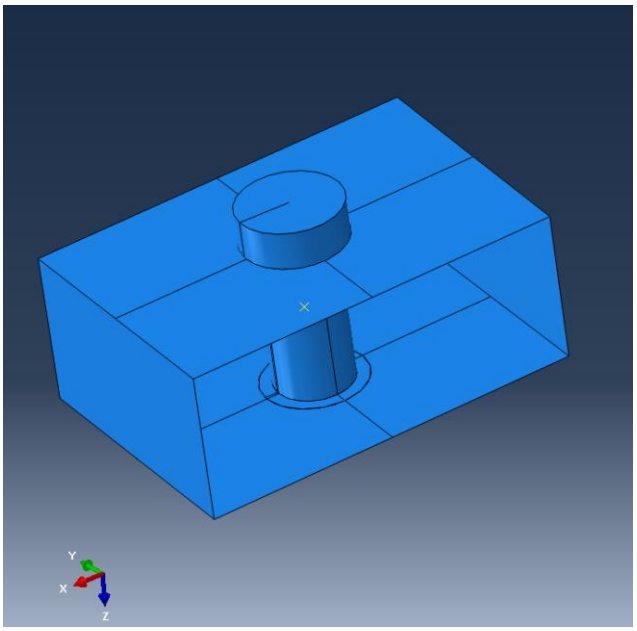

Figure 6.21: Assembled Bolt and Mount.

In Abaqus, a reference point on an analytical rigid solid is by definition tied to the entire body. A connector element made of JOIN+ROTATION is established between the vertex of a control arm or the end of the tie rod and the reference point on the corresponding outboard bolt. This is the established best practice to efficiently and effectively model a heim joint using FE techniques.

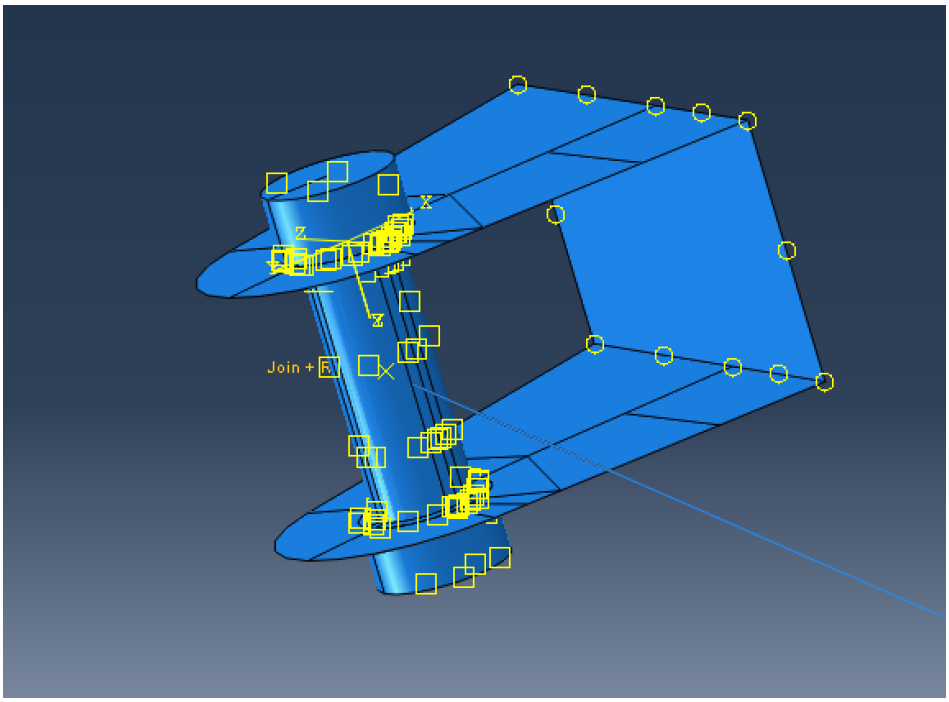

Figure 6.22: Assembly of Steering Mount and Bolt with Interactions and Connector elements for the Tie Rod.

7. Dynamic Loads Development

7.1. Major Areas of Concern with Loading

The upright is subjected to large bending stresses from the suspension members and wheel bearing loads, while also needing to handle the braking forces created by the brake caliper, which is mounted to the upright. This thesis does not focus on braking forces from calipers but longitudinal forces from braking are considered.

The first area of concern modeling the suspension assembly is that suspension members are typically modeled as two-force members or truss elements. This is not accurate as the control arms have two members that are fixed to each other in all degrees of freedom at the outboard end. There is often a gusset plate welded in place at this connection, designed to decrease the effective free length of these members to address buckling concerns and packaging constraints (rear suspension also includes the drive axle). This type of connection will induce some bending in the control arm members under load. At this time, it is unknown how great this bending moment is; therefore bending loads cannot be neglected until proven insignificant.

The next area of concern is mounting the pull rod. The pull rod acts on the upper control arm via a bracket welded to the gusset connecting the two members. This creates a bending load on the members due to the pull of the spring acting through the pull rod. All suspension members will exhibit large displacements with small strains during suspension movement. This means that the geometry of these members and the direction of loading will change as the vehicle is subjected to different loading conditions. This geometry change may create differential loads within the members. Some of the loading scenarios may move the suspension to the bump stops. Hitting a bump stop will increase the load within the pull rod and will apply bending to the suspension members. This scenario is very important to analyze as it is a common occurrence on a rough racetrack or during an off-track excursion.

The worst-case suspension load scenario in this study is taken as combined cornering and braking - the tie rod is actuated to steer the wheel while the brakes are actuated to slow the vehicle down. The loading scenarios are discussed in detail in the Section 7.2.

7.2. Load Calculations

Hand calculations used to determine suspension loading begin with tire data obtained from the FSAE Tire Testing Consortium (TTC) data. Tire data from 2009 Tire Testing Consortium for Hoosier LC0 tire is used to determine the forces and moments at the contact patch of the tire under the various loading scenarios to be analyzed. These forces are transferred to the wheel center, providing the forces and moments applied to the wheel bearing on the upright [3]. Table 7.1 specifies the loads on the wheel center on the right front corner of the FSAE vehicle.

Table 7.1: Forces and Moments classified by load case scenarios.

SAE Coordinate System	Loading Scenario	Left Hand Corner (1.4 g) + Full Load Transfer	Braking (1.4g) + Full Load Transfer	5 g Bump	Cornering + Braking
	Forces (lbf)				
	X	0	-502.7	0	-324.4
	Y	-425.1	0	0	-301.9
	Z	-270.7	-299.9	-676.5	-272.9
	Moments (lbf-in)				
	X	-126.6	-136.3	0	270.8
	Y	0	-5026.3	0	-3243.8
	Z	4251.9	0	0	3018.9

Each of these loading scenarios is calculated from the tire data using the estimated load transfer and desired vehicle performance from Borg's thesis [3]. These loads form the basis for the structural analysis of the suspension members. The maximum internal loads for each member that occur in each of these loading scenarios are determined and these loads become the critical design loads for the suspension components. Each member is then designed to withstand the maximum load it will see from these loading scenarios with a factor of safety. The factor of safety is decided based on which load case the member come close to yielding (failure criteria) and how abusive that load is. Another failure mode that is more relevant in FSAE is fatigue. Since steel has a well-defined S-N curve, the dynamic stresses can indicate towards the life expectancy of the suspension component. Factors of safety are decided on a case-by-case basis. The suspension members are and must be designed for both strength to withstand critical loads as well as provide necessary compliance. However, depending on the load scenario the design direction would start with either or both criteria.

7.3. Dynamic Implicit – Activate Displacement vs. Pseudo Time

In general, obtaining a closed form solution to a set of nonlinear algebraic equations is not possible with the exception for the simplest case of a single nonlinear equation. For that reason, an approximate solution to a system of nonlinear algebraic equations is sought by using the incremental analysis of a nonlinear boundary value problem. The principal idea of incremental analysis is very simple: imagine that the total external load is applied in terms of several increments, which are all sufficiently small to permit that the nonlinear problem under consideration be approximated by an equivalent linear problem. The implicit solver will thus replace (in each increment) a set of nonlinear algebraic equations with the linear equations, which can be solved numerically. This kind of approximate solution to a nonlinear problem is constructed through a solution sequence of equivalent linear problems and will thus remain linear in each increment. A simple way to handle the incremental analysis is by introducing a so-called pseudo-time parameter denoted as 't', which is used to describe a loading program.

The label pseudo-time for parameter 't' implies that it plays the same role as time in describing the loading sequence, except that the problem remains placed within the framework of quasi-static analysis where inertia effects are neglected.

The main goal of the incremental analysis is providing the value of the displacement increment corresponding to the chosen load increment.

At every step increment, the equilibrium equation is

$$[k]\{u\} = \{F\} \tag{13}$$

And the incremental form is

$$[\Delta K]\{\Delta u\} = \{F_{ext}\} - \{F_{int}\} \tag{14}$$

where

$$\{u_{k+1}\} = \{u\}_k + \{\Delta u\} \tag{15}$$

7.4. Development of Nonlinear Dynamic Implicit Model

The objective of this model development is to refine and study the results of the finite element solution. A finite element model with separate load case scenarios i.e. loads and boundary conditions, is submitted for solution to the Abaqus nonlinear implicit dynamic solver.

Table 7.2: Loads Specifications for Dynamic Implicit Model.

Load	**Concentrated Force on Wheel Center**
Cornering Forces	Forces in lateral and vertical directions (Y and Z) as centrifugal and steering forces and lateral load transfer (Rolling)
Braking Forces	Forces in longitudinal and vertical directions (X and Z) as deceleration and longitudinal load transfer (Pitching)
Load	**Concentrated Moment on Wheel Center**
Cornering Moments	Rolling Moment – Around X-direction Steering Moment – Around Z-direction (Yaw)
Braking Moments	Pitching Moment – Around Y-direction

Table 7.3: Boundary Condition Specifications for Dynamic Implicit Model.

Boundary Condition	**Region of Application**
Constrained DOF: U1, U2, U3	Suspension members (control arms) inboard points
Constrained DOF: U1, U2, U3, UR1, UR2	Rocker (Pivot Point) – Local Datum Coordinate System (as shown in Figure 7.6)
Constrained DOF: U1, U2, U3	Suspension Spring-Damper – Inboard point
Constrained DOF: U1, U2, U3	Tie Rod Inboard End– For Interference Fit Step
Constrained DOF: U2, U3	Tie Rod Inboard End– For Load Step
Prescribed Displacement: U1= 1 in	Tie Rod- For Load Step with Load Curve plugged in as an Amplitude vs. Time – in Tabular form – Local Datum Coordinate System (as shown in Figure 7.7)
Constrained DOF: UR3	All Analytical Rigid Bolts – Global Coordinate System

A detailed series of load diagrams follows the above tables.

1. Cornering Forces on Wheel Center

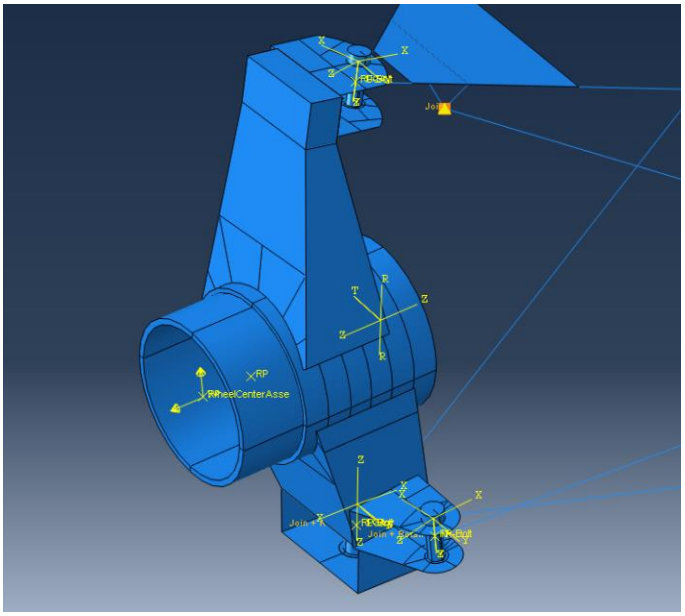

Figure 7.1: Lateral – Centrifugal and Vertical – Load Transfer forces applied on wheel center during vehicle turning.

2. Cornering Moments on Wheel Center

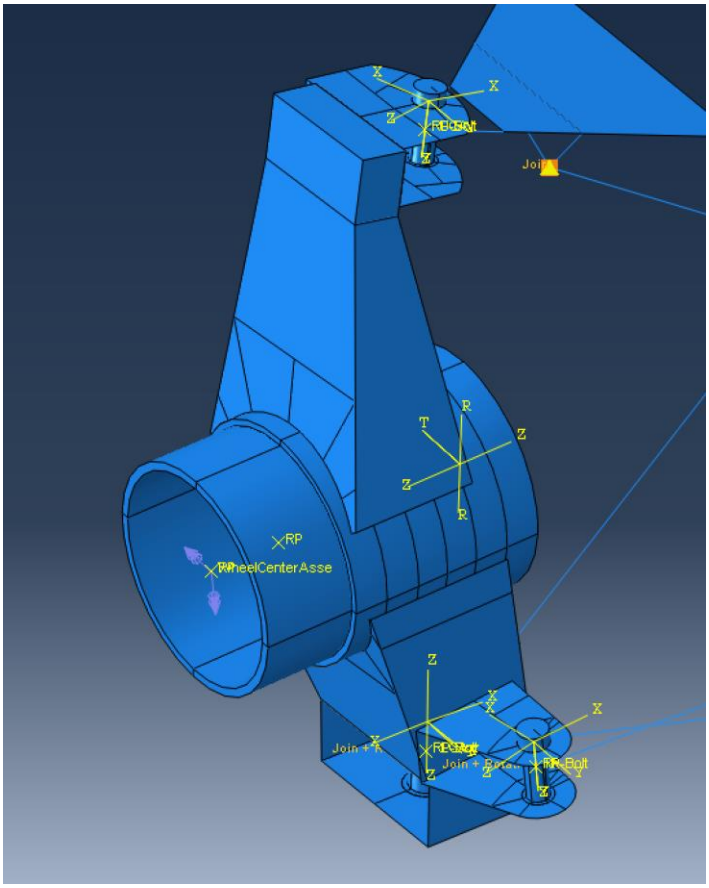

Figure 7.2: Yaw and Roll Moments applied on wheel center during vehicle turning.

3. Braking Forces on Wheel Center

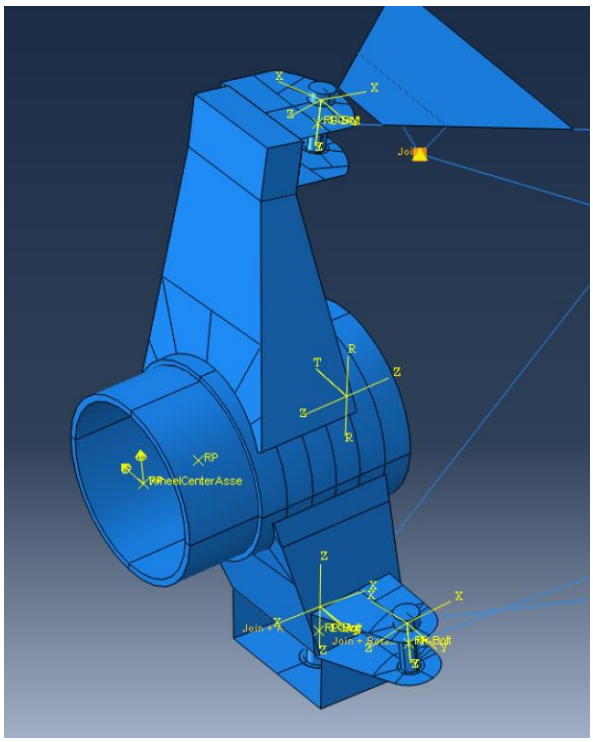

Figure 7.3: Vertical - Diving and Longitudinal - Deceleration forces applied on wheel center during vehicle braking.

4. Braking Moment on Wheel Center

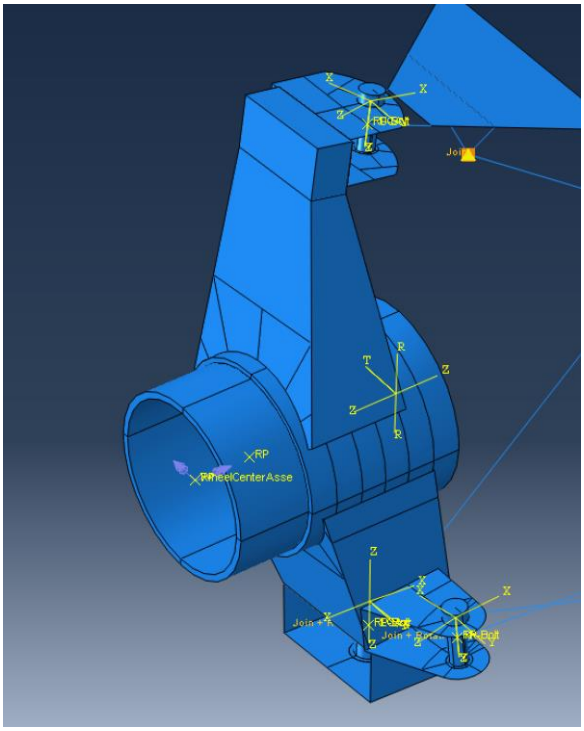

Figure 7.4: Pitching moment applied on wheel center. A slight rolling moment arises because of vehicle asymmetry about X-axis.

5. Pinned Boundary Condition: Inboard Points

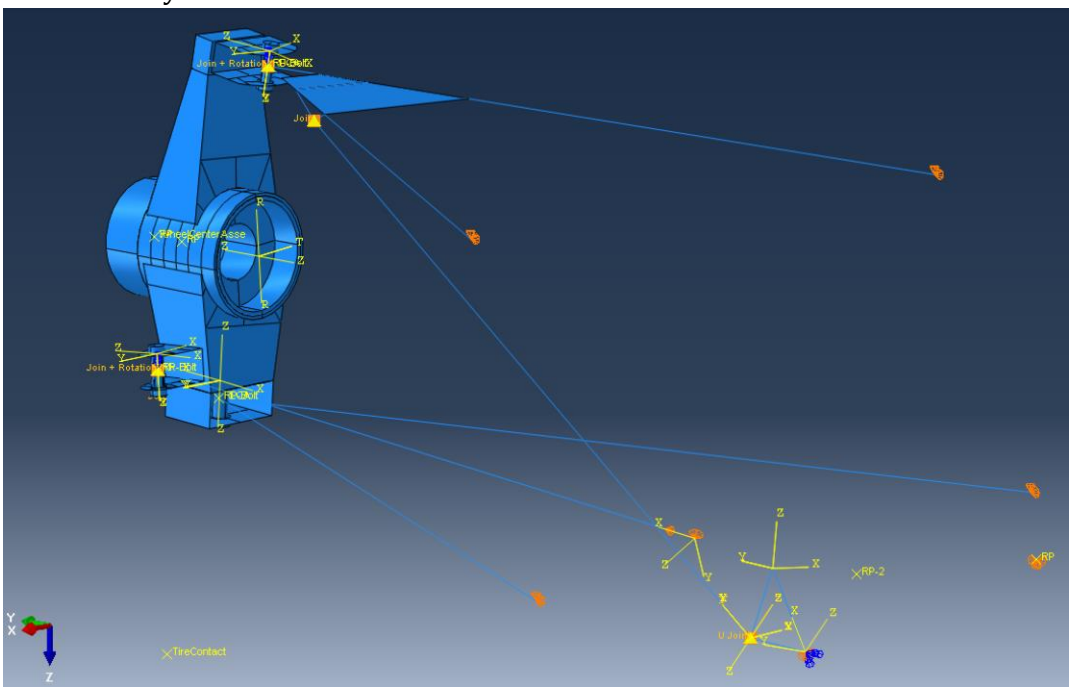

Figure 7.5: Constrained DOF for inboard suspension points.

6. Rocker – Free Rotation about the axis of the pivot bolt – Rotation about local Y and Z-axis constrained

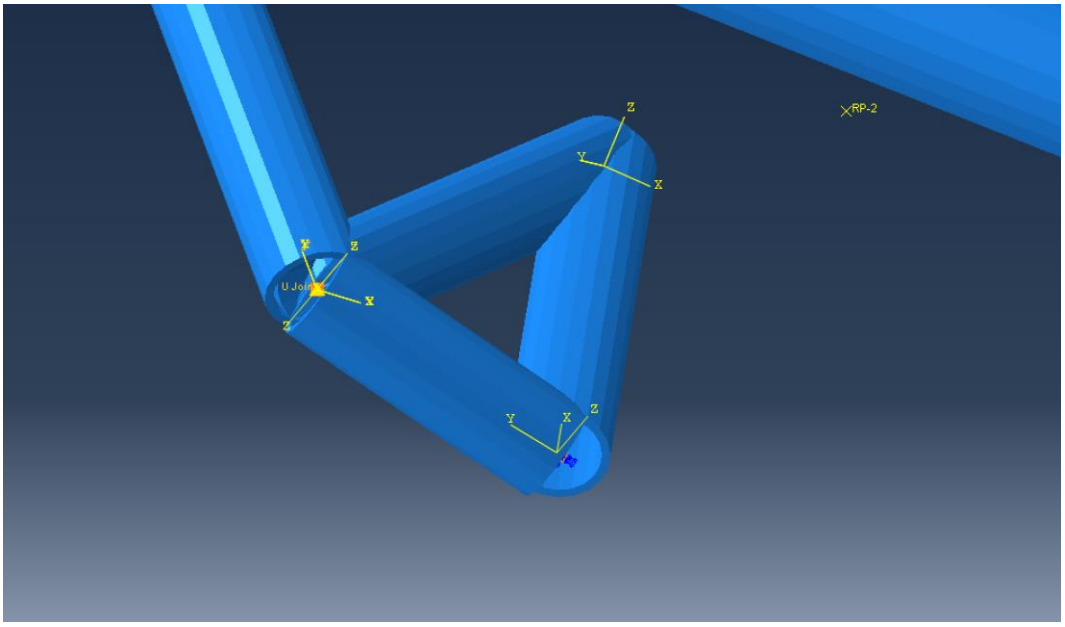

Figure 7.6: Degrees of freedom for the rocker – Free UR3 for local coordinate system axis which is normal to the rocker plane.

7. Tie Rod Constraints: Pinned Boundary Condition during Interactions Step, Prescribed Axial Displacement during Load Application Step

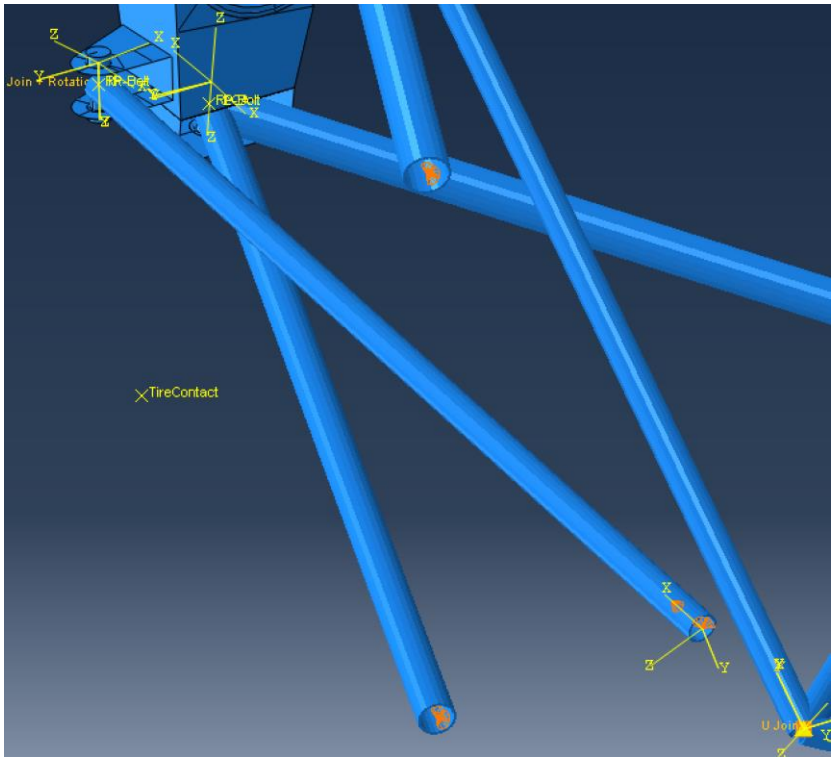

Figure 7.7: Tie Rod constrained as pinned during Interference Fit Step and then articulated to emulate steering for Load Application Step.

8. Bolts – Axial Rotation Constrained

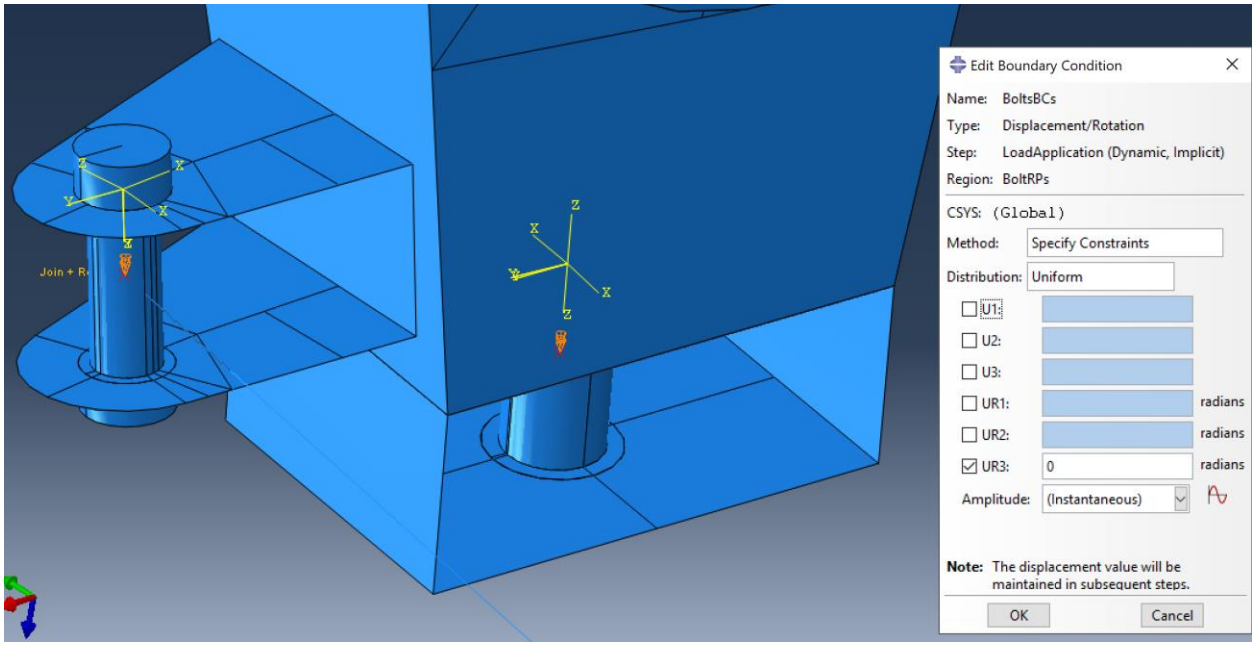

Figure 7.8: Each analytical rigid bolt constrained so that it does not spin around its own axis.

7.5. Results for steady state dynamic load case scenarios

a. Constant Speed Turning + Lateral Load Transfer

To simulate turning and lateral load transfer, the loads were applied as periodic oscillating loads to simulate turns in both directions.

The amplitude and direction to move the tie rod was made to synchronize with the loading amplitudes and directions.

For turning, the loading curve was multiplying the directional loads with the multiplier as below. The timeline only includes the loading step.

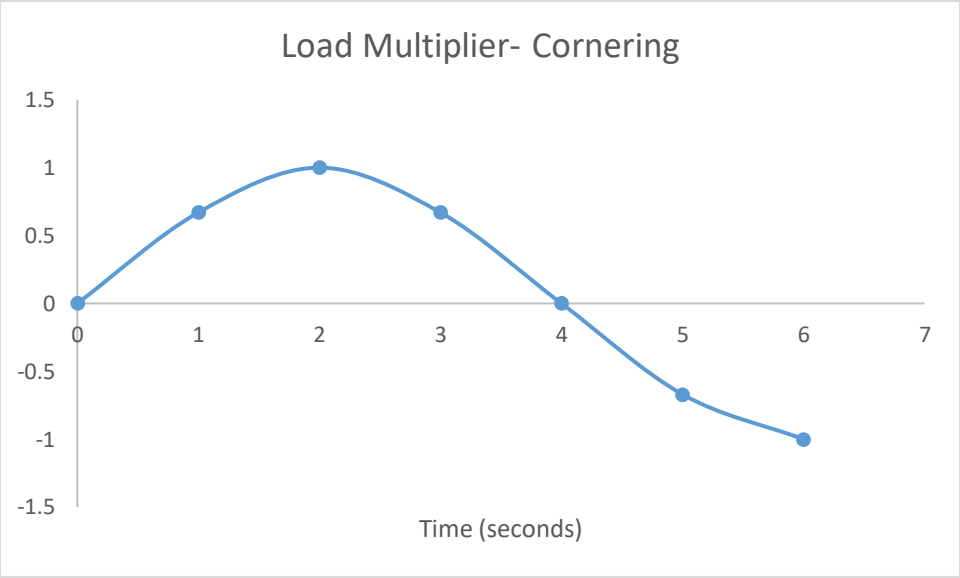

Figure 7.9: Chart showing timeline of load multiplier for steering loads and displacements during Load Application step.

This load multiplier is used for forces, moments and prescribed displacements associated with turning. It translates to the wheel starting from the neutral steering position to full right turn, back to the neutral steering position then to full left turn. The vertical loads will increase during the right turn (outer wheel – lateral load transfer) and decrease during the left turn. This load curve works in sync with the articulation of the upright.

Simulation for Constant Turning

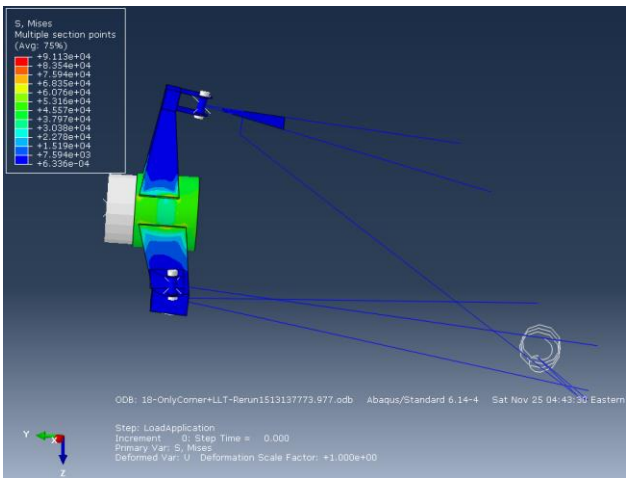

Time= 0s

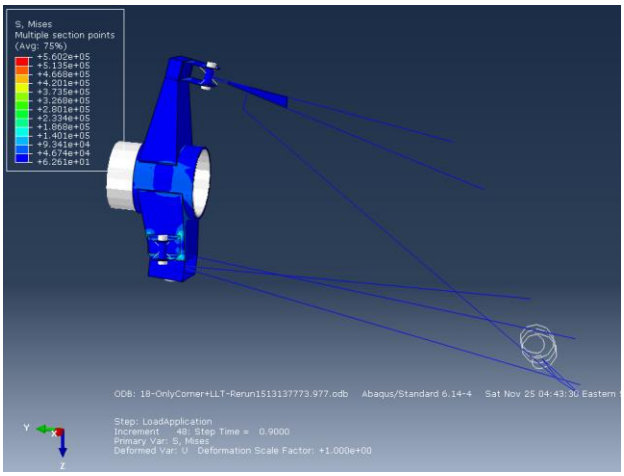

Time = 1s

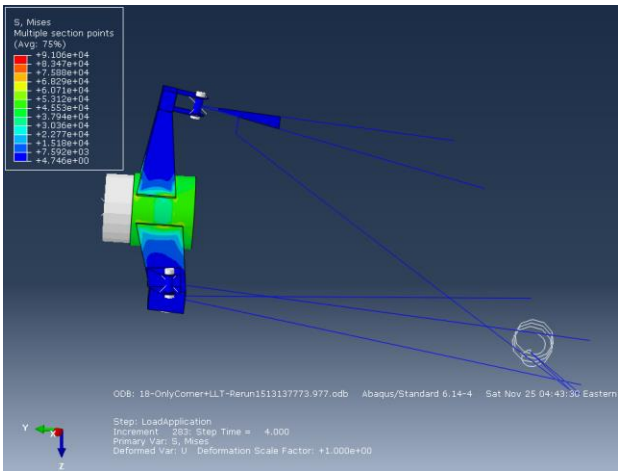

Time = 4s

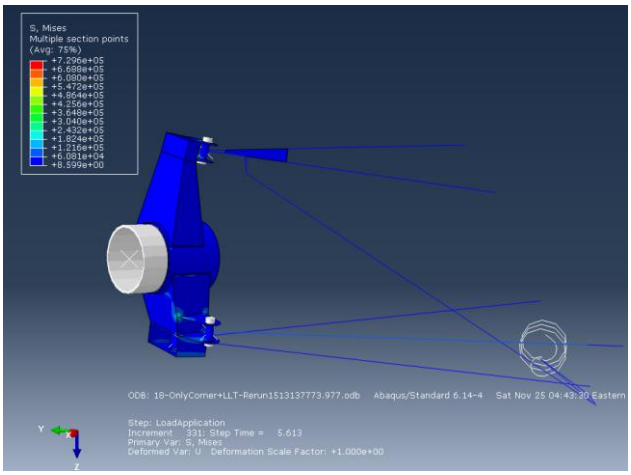

Time= 5.6 s

Figure 7.10: Simulation of Quarter-Car Suspension for Constant Speed Cornering Load Scenario for Step Time = 6 s.

b. Braking + Diving Load Transfer

Simulation for Only Braking Loads – Vertical forces and Pitching Moments

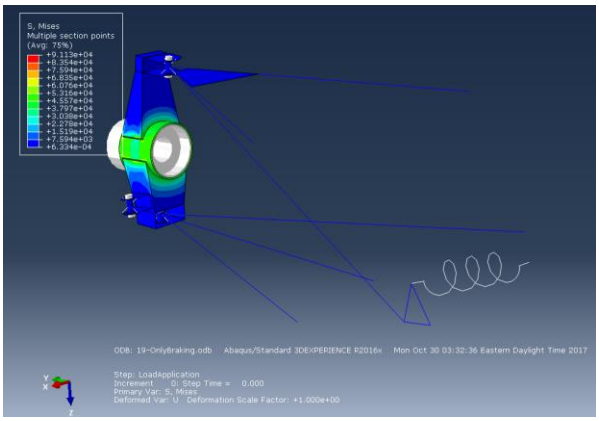

Time = 0s

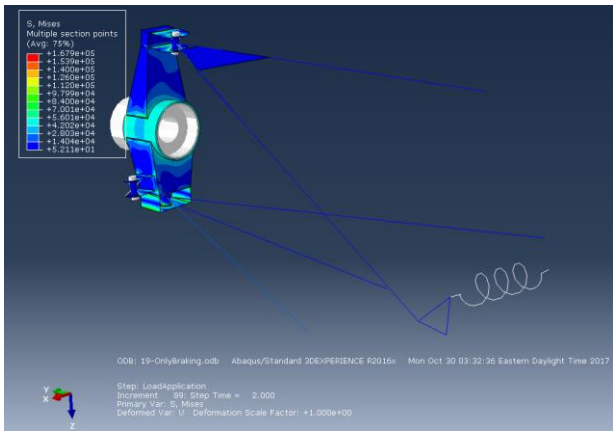

Time = 2s

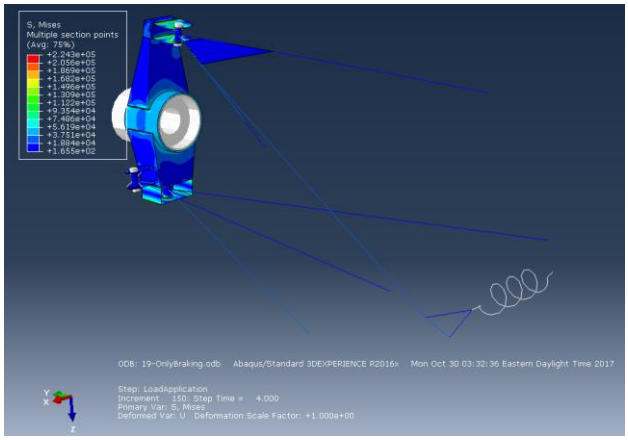

Time = 4s

Figure 7.11: Simulation of quarter-car suspension for Braking Load Scenario for Step Time = 4 s.

c. 5g Bump

Simulation for instantaneous 5g bump vertical force

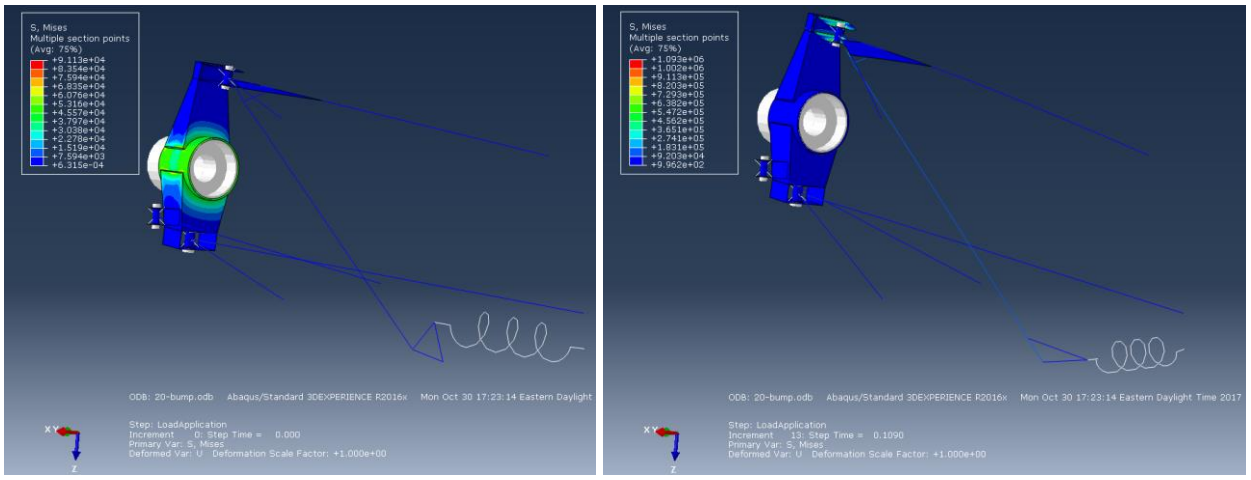

Time = 0s Time = 0.1s

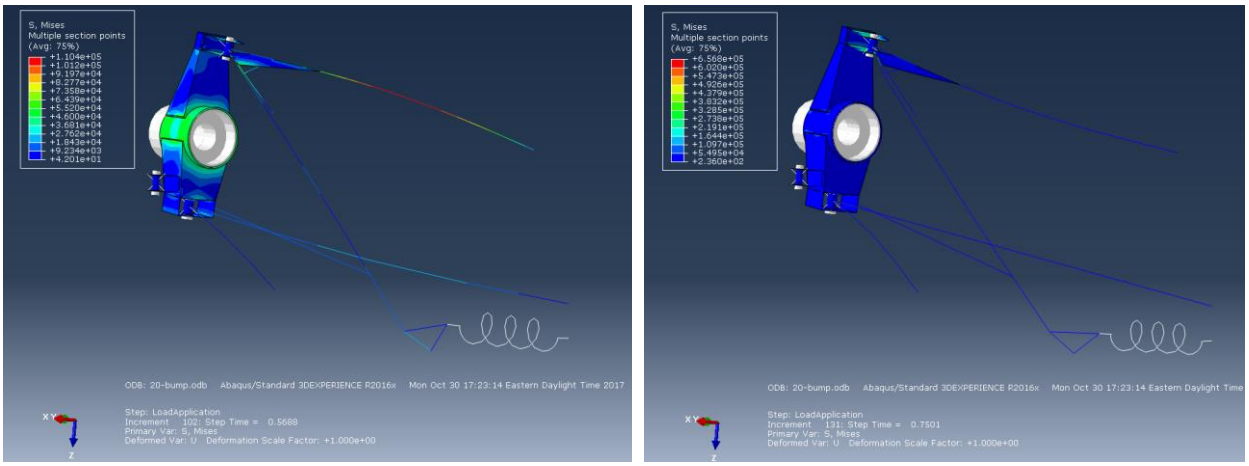

Time = 0.56 s Time = 0.75 s

Figure 7.12: Simulation of Quarter-car Suspension for 5g instantaneous bump load scenario for Step Time Duration = 1s.

d. Cornering +Braking

The Load Application Step consists of Load Multipliers for Cornering and Braking Loads individually. By loads, it is implied that the load multiplier is applied on forces, moments and prescribed displacements.

The cornering+braking load case is the most abusive on the suspension system and consists of extreme loads. Stress timelines on parts of the upright will be investigated to understand the dynamic elastic response of the folded sheet metal parts and of the suspension members.

Simulation:

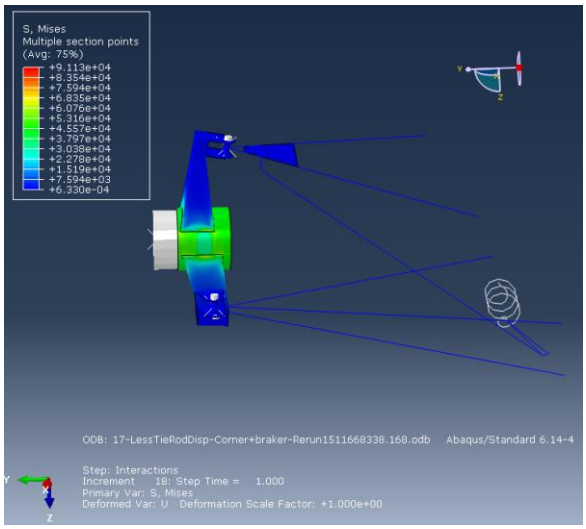

Time = 0s

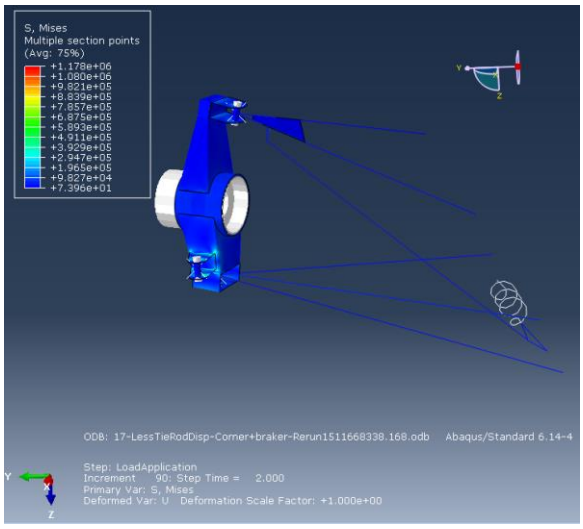

Time = 2s

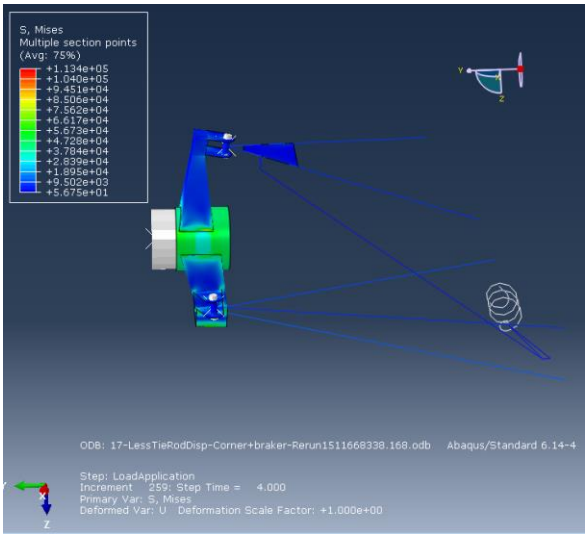

Time = 4s

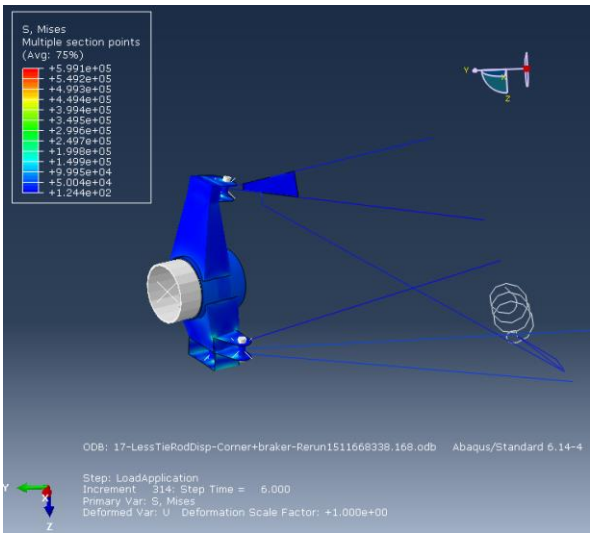

Time = 6s

Figure 7.13: Quarter-car Suspension System - Articulation at every 2 seconds of Load Application for Cornering+Braking Loads.

Results:

Certain elements on the suspension members and especially the critical sections of the upright are probed for stress timelines in order to evaluate the dynamic response of each part and its interaction. The results of some of the critical sections will be discussed in detail.

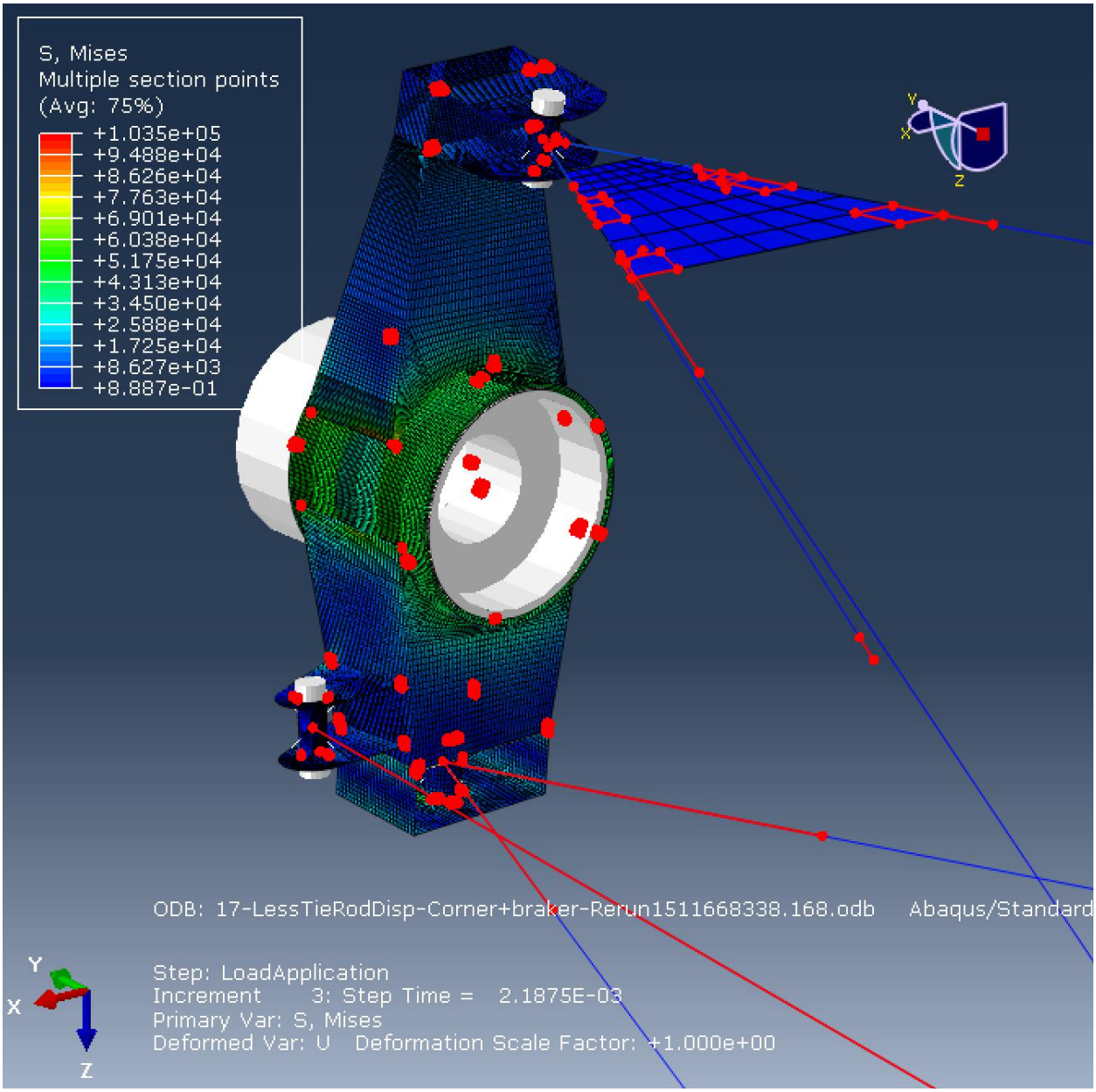

Figure 7.14: Critical Section elements on the Upright highlighted in red.

Critical Section – Bearing Housing: Certain elements with stress concentration and interactions with other attached parts are selected and their stress timelines are plot.

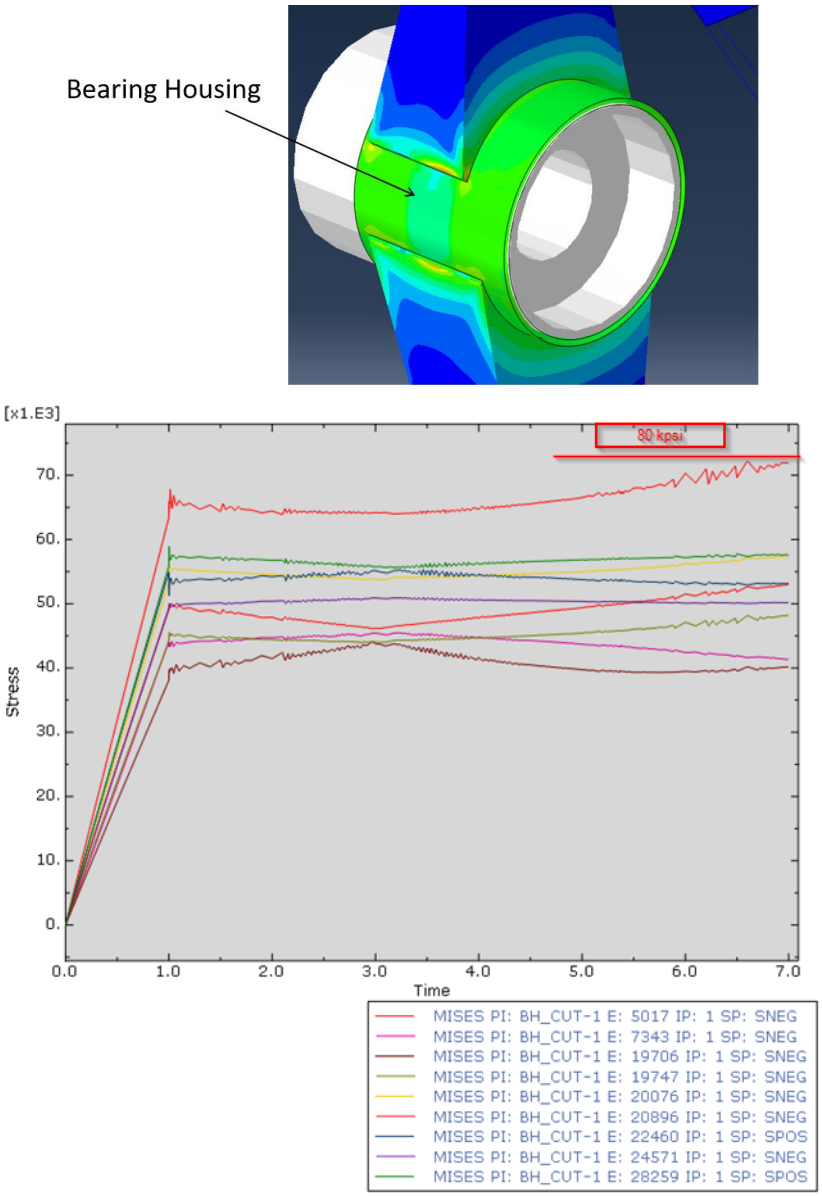

Figure 7.15: von Mises Stress (psi) vs Time (s) for critical section brick elements on the Bearing Housing.

In the 1st second of the simulation, the housing experiences interference fit stresses which linearly increase. This is reasonable, as the rigid bearing will expand the housing as a linear function of interference. As the wheel center on the rigid bearing exerts oscillating forces on the bearing housing, the stresses will oscillate.

Note the linear stress for the 1st second due to the interference fit expansion. Stress slopes change based on the distance of the element from the center of the bearing. The bearing housing encounters minimal varying cyclic loads. However, some element entities reach stress beyond yield

strength (S_{yt} =63000 psi) under the abusive cornering+braking loads. The stresses observed can be attributed to the stress concentration and/or mesh density incompatibilities (Section 4.3 – Results).

Critical Section- Cut_lower: Certain elements on the Cut_lower are chosen because of their shared nodes with the bearing housing, tie rod mount and the lower mount to observe the stress generated and overall behavior.

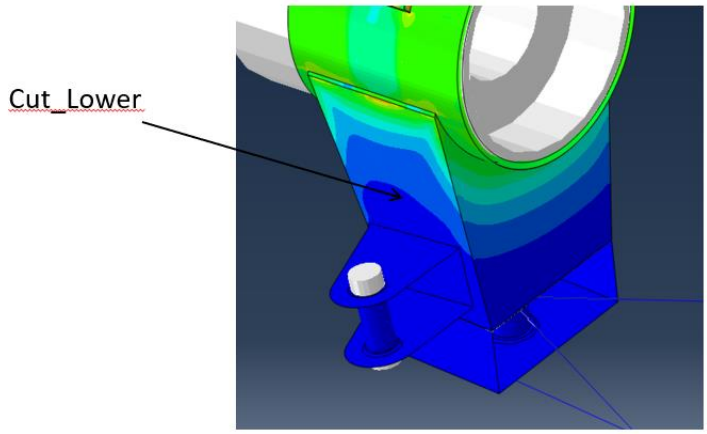

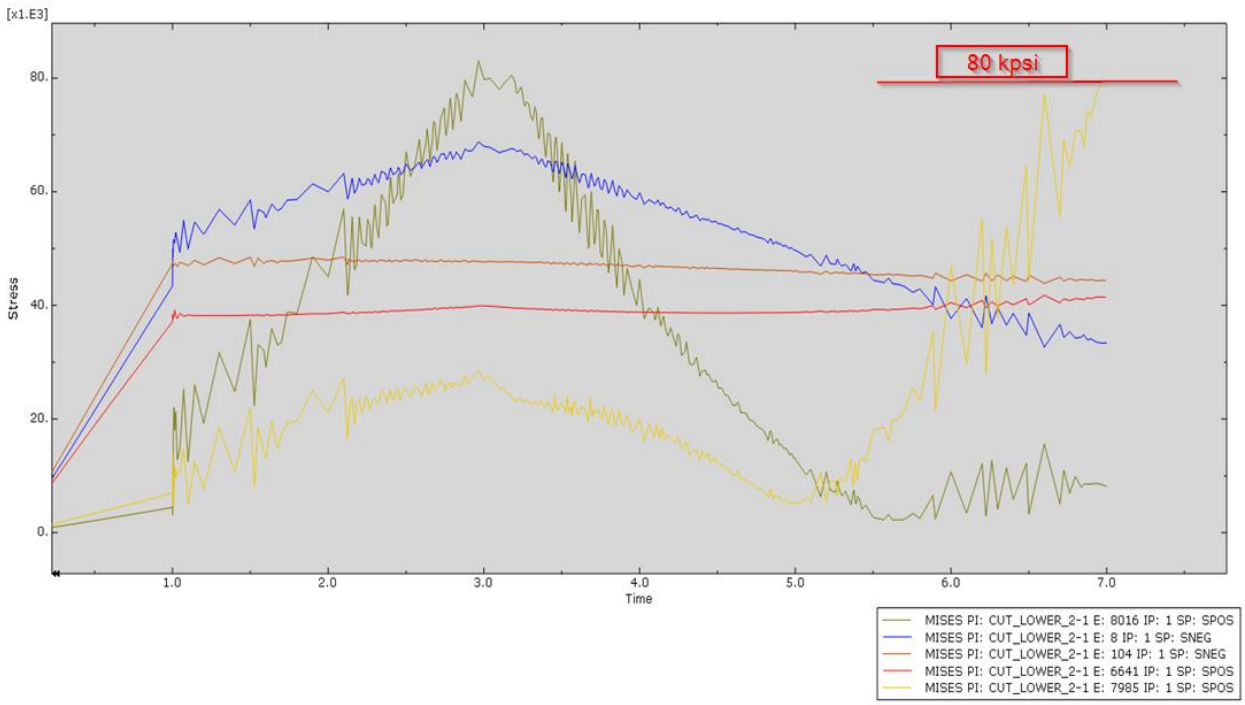

Figure 7.16: von Mises Stress (psi) vs Time (s) for critical section shell elements on the Cut_Lower part.

The elements #6641 and #104 are close to the bearing housing. The elements #8016 and #7985 are close to the steering mount and element #8 is close to the lower mount.

The elements that are close to the bearing housing do not experience oscillating stress due to turning as much as the elements closer to the steering mount.

The stress for regions near the steering mount fluctuates and responds to the cyclic nature of the load. These results exhibit that this component must not only be designed for structural strength but also protect it from fatigue failure and fatigue crack propagation. Maximum stress for infinite life of steel components is considered when the endurance stress (S_e) is less than half of ultimate tensile strength of the material (S_{UTS}) which is also a coarse estimate made in absence of real data and is limited to different dimensions and aspect ratios for sheet metal steel. This part does not need to be designed for infinite life, hence based on the stress the part can have an estimate finite life enough for the endurance race and other dynamic events of the competition.

$$S_e = \frac{S_{UTS}}{2} \tag{16}$$

$$S_e = \frac{95000}{2} = 47500\ psi$$

Hence cyclic stresses should be limited to ±47500 psi for infinite life with AISI 4130 steel sheet metal. The component Cut_Lower experiences loads and stresses (peak 83000 psi) higher than the prescribed endurance limit stress. The stress is cyclic in nature for the abusive load case of quick tight cornering and braking. The vehicle on the track may not even encounter this load case scenario and hence a decision to redesign for fatigue strength must be taken with careful considerations. If a redesign is discussed, the finite element model results can show the direction towards an upright that is built for durability.

With physical testing and real loads plugged into the finite element model, a more accurate estimate of the life expectancy of the component and overall suspension system can be made.

Critical Section- Cut_Upper: Elements chosen for Cut_Upper are on the same lines are Cut_Lower. Cut_upper component does not encounter sinusoidal cornering forces as much as Cut_Lower as elastic energy is absorbed by lower components.

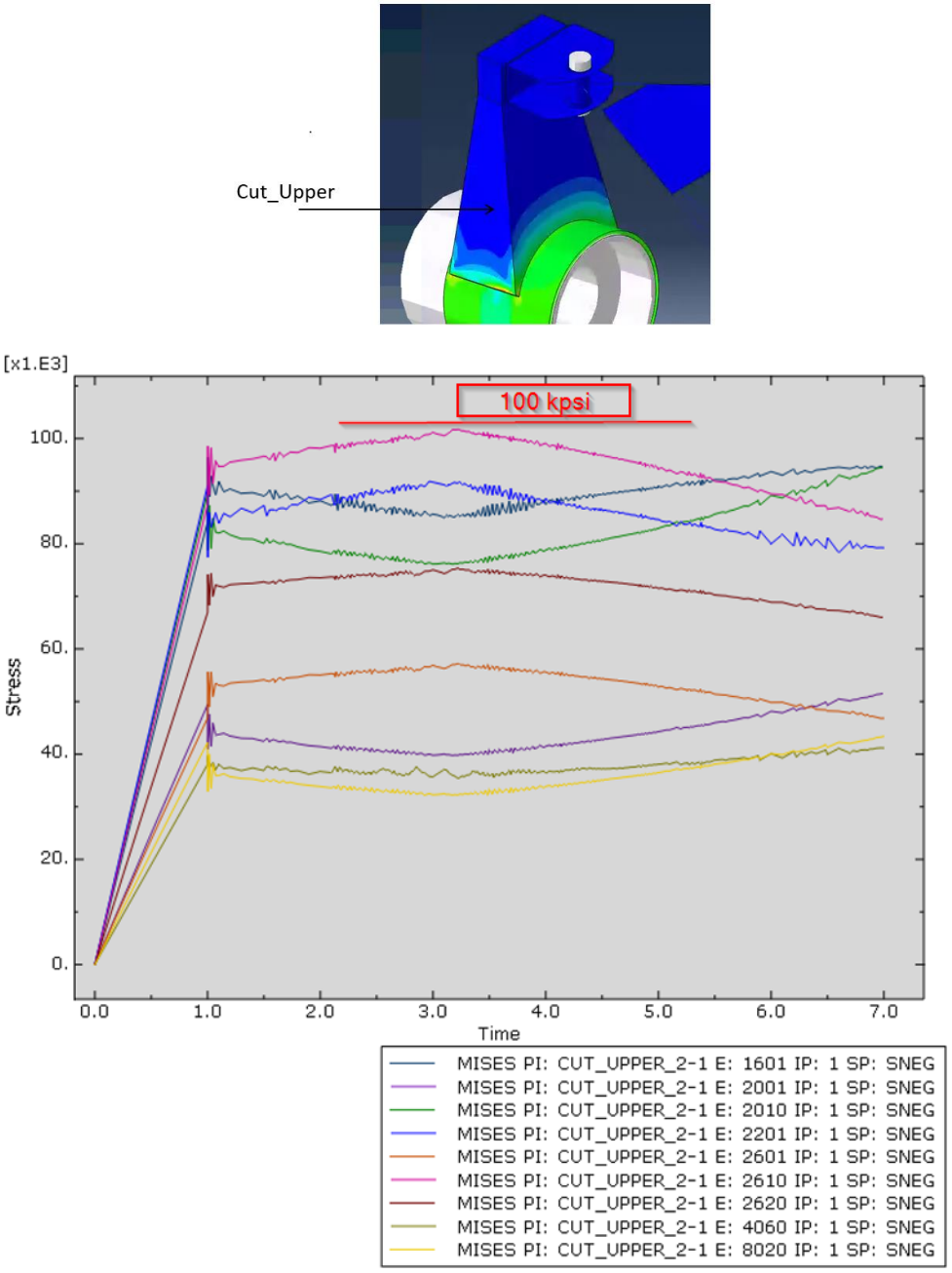

Figure 7.17: von Mises Stress (psi) vs Time (s) for critical section shell elements on the Cut_Upper part.

Like the Cut_Lower component, the elements close to the bearing housing have little variation in stress during cornering. This part also experiences minimal cyclic stresses in this load case. Even without variation, the static stresses on some elements on Cut_Upper component is higher than the

ultimate tensile strength of the 4130 Steel. The Cut_Upper component is stiff and resists torsion as well as bending caused by the tie rod actuation.

Critical Section – Front Lower Control Arm

The elements on every end of the two beam elements are chosen to observe and analyze their beam deformation behavior – axial as well as tension. The elements have been identified in the figure and legend below.

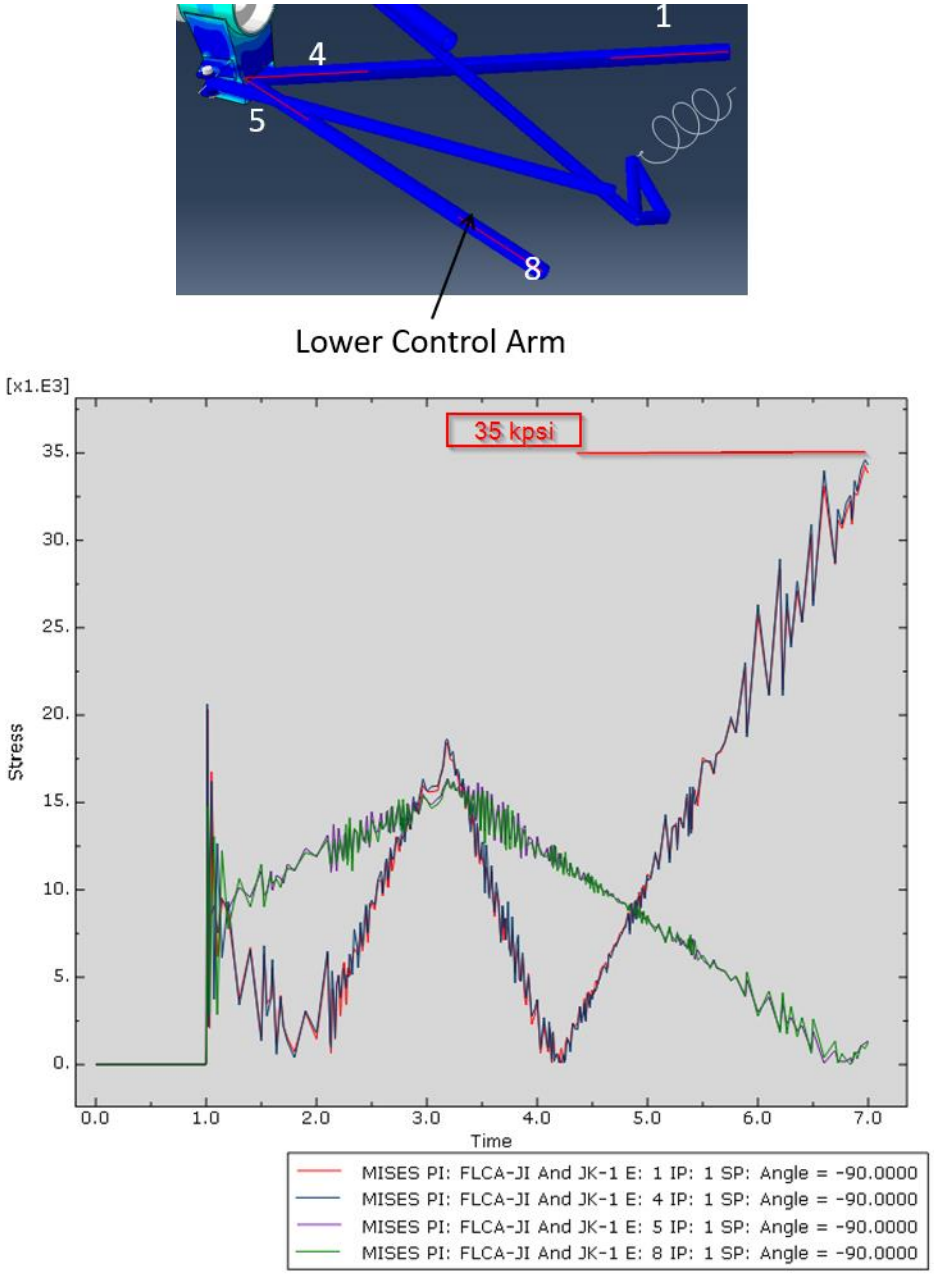

Figure 7.18: von Mises Stress (psi) vs Time (s) for critical section beam elements on the FLCA (end elements). The probe elements are indicated in the above figure of the lower control arm.

From the above stress timelines, it was evident that the end elements of JI and JK beams individually showed different behaviors in left and right cornering simulations. These results can be employed to design to the lower control arm for member loads. The static and cyclic stresses are under the yield strength for the LCA with a maximum factor of safety of ~1.85 (static yield).

Critical Section – Front Upper Control Arm

The elements at the intersection and where the beam elements meet the gusset plate (that supports the pull rod) and are chosen to observe and analyze their beam deformation behavior – axial as well as tension. The elements have been identified in the figure and legend below.

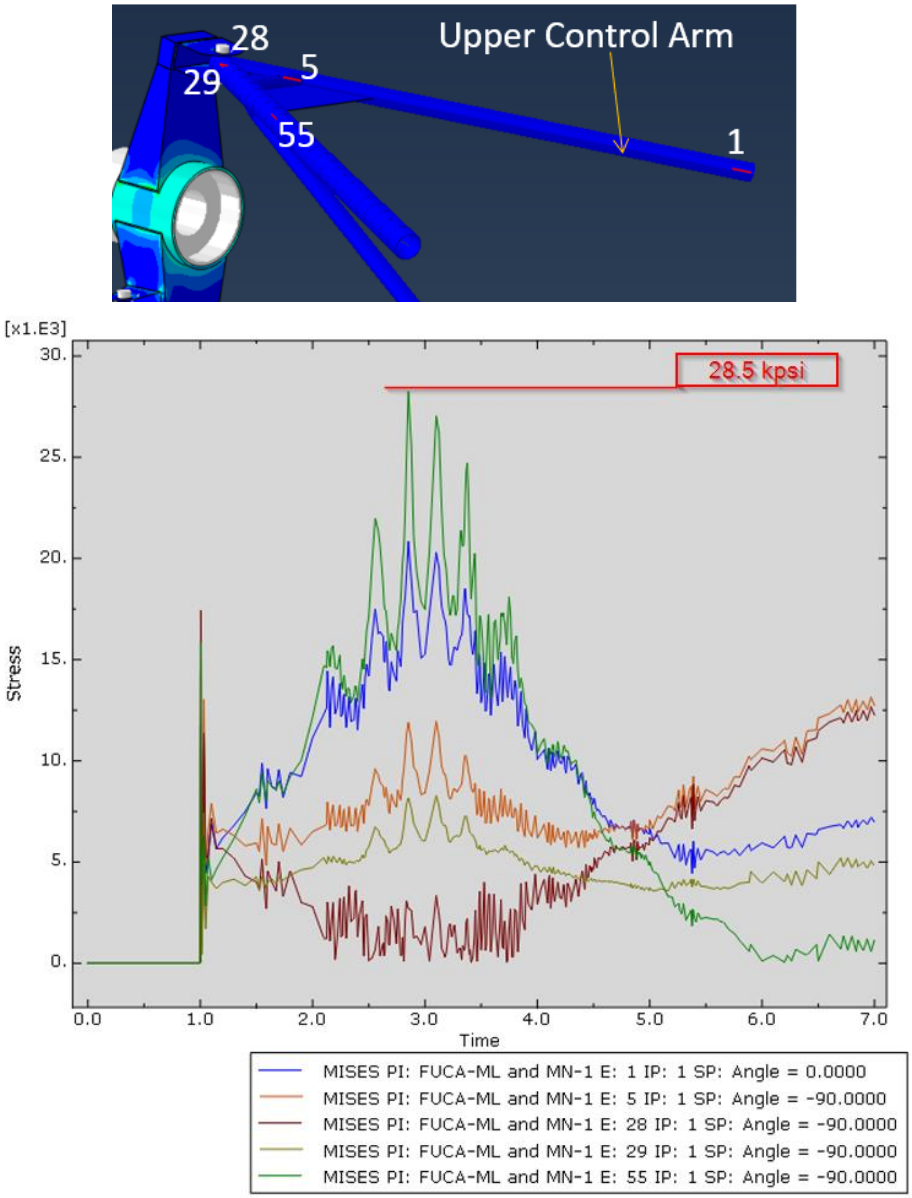

Figure 7.19: von Mises Stress (psi) vs Time (s) for critical section beam elements on the FUCA.

Apart from the control arm members, the elements attached to the gusset plates add another force transfer and bending equation to this problem. The stress timelines indicate that these control arms react with sensitivity to the cornering cyclic loads and must be designed well for axial and bending strength. The UCA stresses are under the yield strength of the material with a factor of safety of 2.24 for static yield.

Critical Section - Lower Control Arm Connection Mount

The Lower CA Mount is close to the steering mount. The stress timeline is indicative of sensitive response from the cyclic cornering loads. The stress experienced is also high – the magnitude is 10 times more than the lower control arm and the Cut_lower component. The component is constrained by the bolt inside the bolt sheath and the weld to Cut_lower attached when the load is applied.

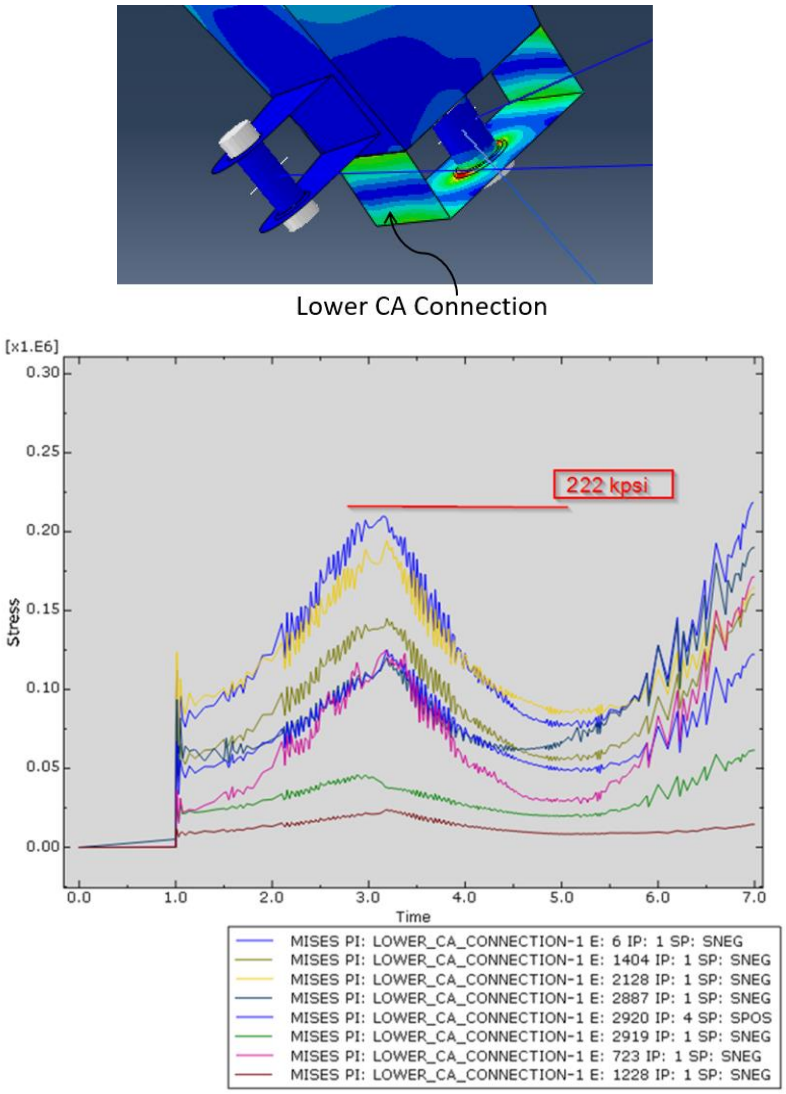

Figure 7.20: von Mises Stress (psi) vs Time (s) for critical section shell elements on Lower Connection.

The higher stress values indicate this component needs some gussets which can distribute the load evenly and reduce stress concentration. It will also ensure increasing the strength and life of the component. The stresses in the Lower CA Connection are particularly high (~7 times the yield strength) because of the transitive constraints on the component and overall stiffness of the bolt interaction. The stress concentration can be minimized with good spacers and fillets in the design.

Critical Section - Steering Mount on Upright

The steering mount experiences the maximum stress because of cantilever deformation mode and stress concentration. The mesh in these components is dense as to study them and the results have convergence to 95% for the interference fit model. The higher element density also makes the component stiffness converge towards actual stiffness and that helps determine reinforcements.

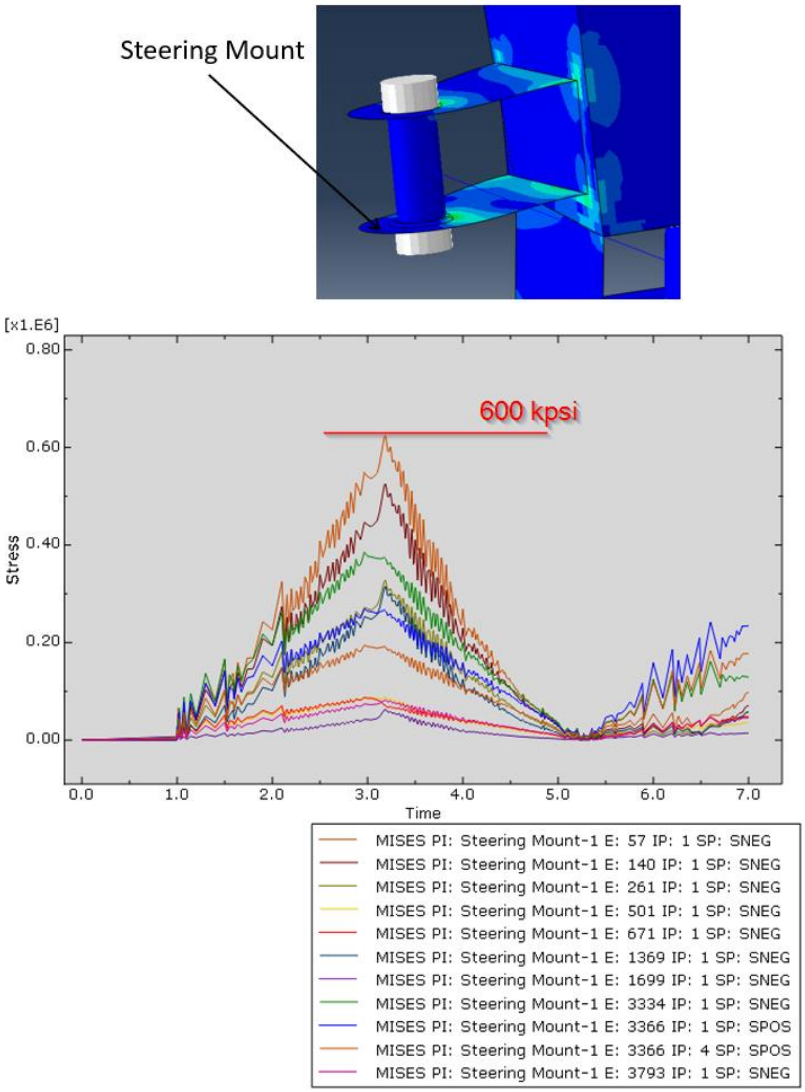

Figure 7.21: von Mises Stress (psi) vs Time (s) for critical section shell elements on the steering mount.

Critical Section - Upper Mount and Upper Control Arm Connection Block on Upright

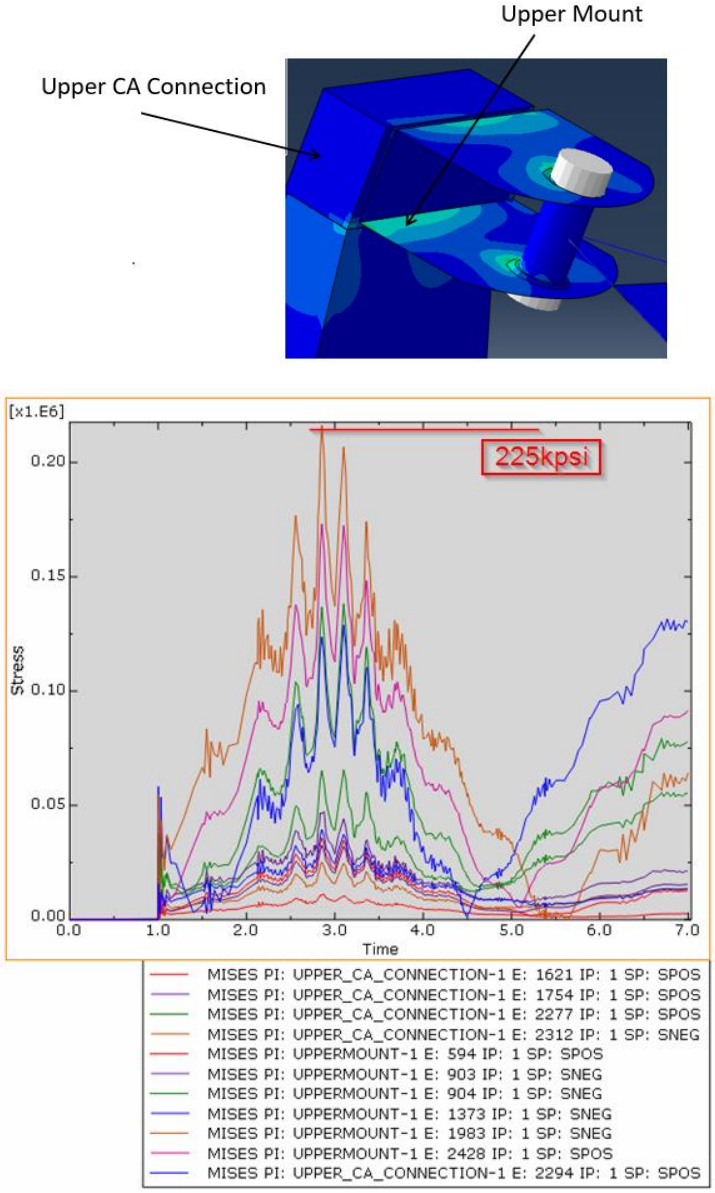

Figure 7.22: von Mises Stress (MPa) vs Time (s) for critical section shell elements on the Upper Mount and Connection.

Shell elements on the upper connection experience stress from the load transfer from the control arms trying to turn the pull rod. The pull rod is applying restoring force from the spring in response to braking (pitching) and cornering (Lateral load transfer) forces. The pull rod is also experience forces from the steering tie rod link trying to bend the upright while turning it.

All the 3 mounts on the upright are stiff since they resist turning (bending and torsion) deformation of the upright. With each small steer angle induced by the tie rod, the camber gain, change in caster angle and kingpin inclination, elements are loaded to bend and twist to the extreme abusive load case – cornering+braking.

Critical Section- Tie Rod

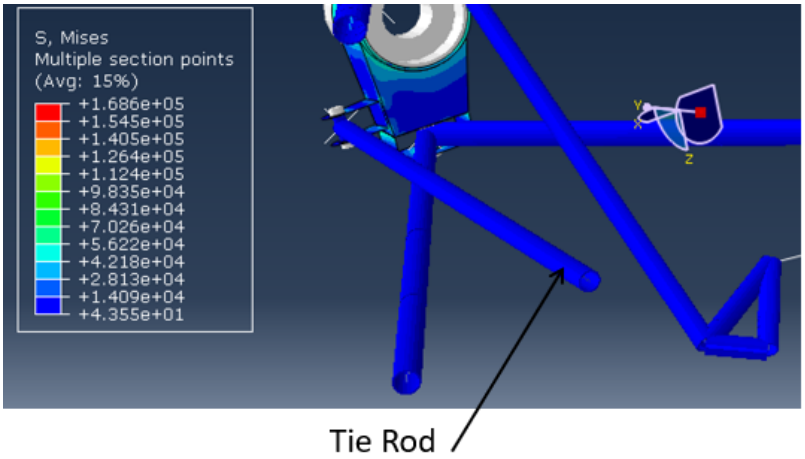

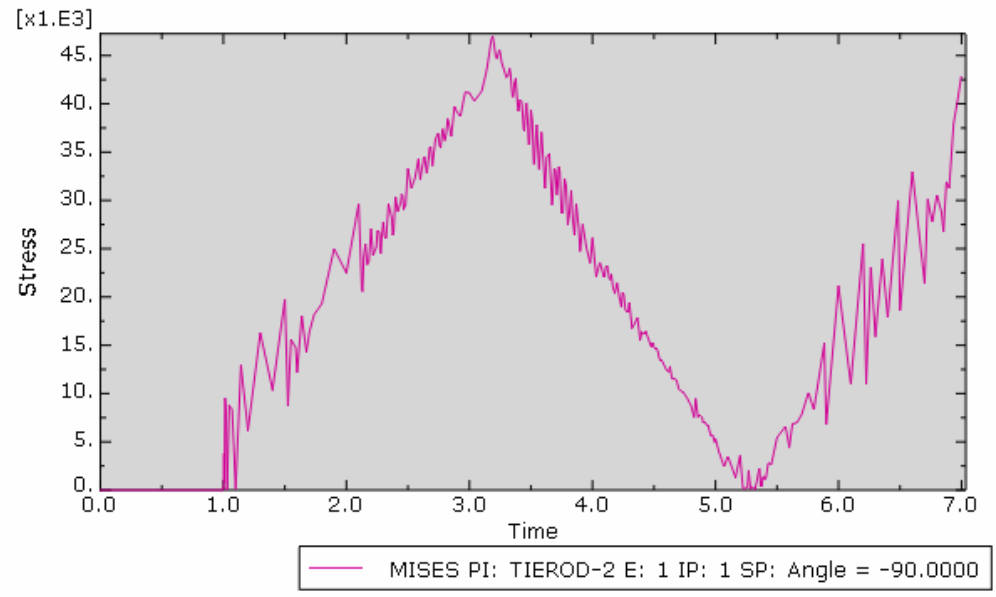

Figure 7.23: von Mises Stress (MPa) vs Time (s) for critical beam elements for the Tie Rod.

The tie rod is modeled as a single element beam since it is not the focus of the study compared to the upright. The tie rod component plays the role of actuating the cornering simulation while experiencing wheel center forces that induce stress. The tie rod design must incorporate considerations for buckling, bending and the heim must be installed correctly to minimize "follower" bending loads. The "follower" bending loads are longitudinal and vertical forces that try to bend the tie rod no matter which cornering position it is in.

8. Conclusions and Recommendations

8.1. Contributions to Suspension Analysis Problem

8.1.1. Finite Element Elastodynamic Analysis

The finite element model and simulation developed in this research answers questions about the direction and magnitude of motion when the suspension mechanism articulates. The model is also capable of solving for different vehicle maneuvers like cornering/turning and braking at the same time.

The model extracts the state of stress and strain and how the elastic response contributes to the motion of the mechanism. The elastodynamic analysis includes stress concentrations near joints, bending in suspension members as well as how the rocker and the spring articulate. The simulation yields internal loads (reaction forces and moments) as well as shows the state of stress and stress vs. time for critical sections.

The addition of elastic members includes the complex deformation modes, the inertial effects to deformation, elastic compliance and accurate representation of constraints to the model parameters.

8.1.2. Meshing Strategy and Technique

The ability to use shell elements – continuum and conventional shell elements, beam elements and properly represent the joints where they interface – effectively was achieved. The model acts as a framework for other elastodynamic problems where components can be defeatured while still preserving its elastic behavior and attitude with connections and interactions.

The use of unique techniques to model the connections as surface contacts, tied components or using certain connector elements also requires refinement and debugging. These practices have been set up as best practices for representation

8.1.3. Best Practices for Modeling and Simulation

The quarter-car suspension model has been refined, iterated and debugged to build an effective representation of the suspension and produce simulations of representative behavior in different vehicle maneuvers. The quarter-car suspension model is popular as a vehicle dynamics problem. Hence, this framework will contribute towards establishing the best practices while modeling elastodynamics of suspension systems. The representation of

the spring, representation of heim joints (spherical joints, rose joints, rod ends) as well as the different connector elements are examples of established practices.

8.1.4. Scalability

The framework model can be scaled to bring more detail or defeature components without losing their elastic behavior or representation. For example, the gusset plate and the pull rod mounts can be modeled in much more detail but because of the kinematic constraints, the behavior and upright response will still be repeatable with that representation.

8.2. Discussion of Loads Analysis

To support the claim that a component or system has been designed for strength and/or compliance, we must first establish static and dynamic load case scenarios. The questions to be asked must consider at least the following questions:

a. What is the worst load case scenario? Is it static, steady-state or transient dynamic?
b. Can we translate this scenario into measurable loads?
c. Is there a safety factor based on manufacturability or service required?

Establishing critical load cases and predicting those loads on a vehicle can be a challenge based on different vehicle weights and geometries. It is also not reasonable to consider only a singular scenario to be the worst case. For the upright analysis, a total of five (5) different load cases are established to identify the critical load case, which was been presented with detailed results. Finite element modeling also requires establishing the technique which includes -to represent the load case scenario. Few load cases consist of single point constraints (boundary conditions) and single point loads (forces and moments). Most load case scenarios need internal force calculations to model them as single point loads and constraints. Load cases when the vehicle is turning needs a prescribed displacement load in synchronization with the force and moment timelines.

Establishing load transfer and load response is a major aspect of loads analysis. If the upright was analyzed by itself i.e. without other components of the quarter-car, the dynamic load transfer (reaction forces and moments) from the tire contact patch would need to be calculated for accurate representation of upright loading. In such cases, the internal loads need to be translated from the wheel center force transducer. Multibody dynamics can also be employed to extract internal loads assuming a rigid member. Easier problems in multibody dynamics can also be solved by hand calculations. Borg [3] created a suspension member loads calculator and used the internal forces

and moments to model loads. Multibody dynamics enables quick calculations with its rigid body assumption. It gives an initial understanding of the problem. The simplicity of using multibody dynamics and solving dynamics problems by hand with the rigid body assumption makes it accessible. It also helps verify complex and intensive methodologies like finite element analysis. This research model started with the four bar mechanism because the problem is accessible and a strong foundation to start a building block.

A more precise and reliable method to extract loads would be to use test data from an accelerometer and correlate with FEA results. This method eliminates apprehensions about the loads and helps create a finite element model that is repeatable and extendable.

Another method to calculate elastodynamic loads would be to measure strains (axial, torsion and bending) on the suspension members using strain gauges. Correlating these member forces will also help validate finite element material and interactions model.

8.3. Discussion of Upright (Knuckle) Elastodynamic analysis procedure

8.3.1. Convergence

Building the upright model included running multiple simulations to tune various factors like mesh density, partitioning strategy, element types, convergence criteria as well as different representations of interactions. These finite element modeling (FEM) techniques help understand the behavioral response with the decreasing element stiffness until convergence of the entire model. To study convergence of the interference fit between the bearing and bearing housing, a separate convergence study was performed and documented. The convergence results are documented in Appendix C.

Another trial model was built with unstructured elements and there was visually significant variation in the displacement response to the load as well as how components articulate. Unlike conventional linear FEA where gradual increase in mesh density shows a convergence of results, a “Segmented Convergence Approach” was adopted. The components are separated and internal loads on critical sections are studied to assess different mesh densities for convergence. For the interference fit, the segmented approach was taken within the bearing housing.

The addition of partitioning and element sizing, for example, across the wall thickness of the bearing housing during interference fit simulations helped get results with minimal variations.

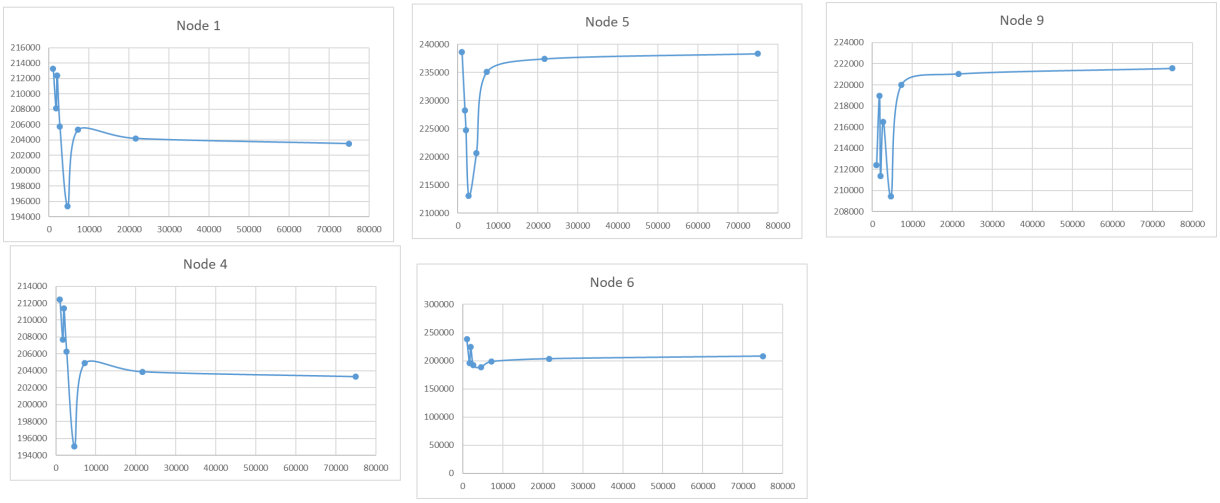

Figure 8.1: Convergence Results from Appendix C

The 3D simulations of the upright and overall quarter-car model immediately revealed the large computational power required and the need to use supercomputing resources provided by Advanced Research Computing at Virginia Tech.

8.3.2. Increment steps to build the model

The increment step of using four bar mechanisms helped learn the difference of results by using prescribed forces instead of prescribed displacement. Since a double A-arm suspension system is close to a four-bar mechanism, animating the mechanism helped understand the underlying modeling and physical dynamics which helped better understand the solver and modeling techniques.

- The type of element used had a major effect on the simulations. Examples are:
    1. Brick vs Shell elements for the Bearing Housing: Shell elements are more computationally efficient like effects of normalization (zero thickness elements- calculations involve material shell thickness in post processing) - Continuum shell elements are chosen over brick elements for meshing the bearing housing for their superior efficiency computationally.
    2. Truss vs Special Spring vs Connector elements for Shocks – The Special Spring element is used over the others for making quick iterations and directly specifying the stiffness and damping coefficient.

- The type of interaction representation used also had a similar effect on the simulations as well as model behavior. Examples are:
    1. Coupling constraints vs. Multi-point constraints vs. Connector elements – To represent spherical joints, bolted rose joints, U-joints and pull rod mounts. A combination of connector elements and coupling constraints are employed in the model. They can isolate the degrees of freedom that are unconstrained for a set of nodes and are easier to modify.
    2. Tie Constraints vs. Contact Interactions (Node to Surface or Surface to Surface) to represent Welded Joints. *TIE constraints are used for our purpose but surface-to-surface (S2S) with "Freeze" functionality would be more accurate as well as computationally expensive.
    3. Analytical Rigid Bolts + Connector Elements for Spherical Rod Ends for Suspension Members.
- The type of loading used – coupled reference points or analytical rigid bearings – is seen to have a large effect on load displacement data as we investigated the results from the interference fit model. The most physically accurate model would be a deformable elastic representation of the bearing with accurate material properties – linear elastic as well as elastic-plastic stress-strain data.
- The next parameter that was studied was the direction, timeline and load trends. Static and steady-state load calculations were established but cornering gains, braking force trends were implemented to observe the different dynamic scenarios and the response they excite from the model components. The load case chosen- cornering+braking is also a conservatively assumed abusive load, but it helps the designer make redesign decisions.
- The type of solver used – Implicit or Explicit – evokes different response behavior even though the range of results are within reasonable limits. The implicit solver is found to be suitable for the application of this thesis.

8.3.3. Loads Analysis – State of Stress and Strain, Compliance, Durability Modeling

The analysis using BEAM elements for suspension members does not ignore bending and buckling. The results help the suspension designer in assigning an appropriate factor of safety depending on the stress and strain trends. Adding an arbitrary factor of safety to bending and buckling loads without an analysis of the behavior of suspension does not show understanding to what loads and conditions the vehicle is subjected.

There is a large increase in member loads during cornering and the suspension parts must be designed to accommodate this. A dynamic implicit analysis helps the suspension designer with data that can be used to determine the static as well as dynamic stresses and stiffness of the suspension assembly. The finite element model discussed also investigates the joints and connections that need to resist the increased cornering loads. The bearings and bolts at each end of the suspension members (assumed to be rigid) will need to withstand the increased forces in cornering as well as resist fatigue that comes with varying (in magnitude and direction) cornering loads.

The tie rod must be displaced laterally to induce a steering angle on the upright assembly to model a properly articulated steering suspension. To find the travel distance, steering and suspension geometry calculations are carried out. This method is established by Borg [3]. This approach was extended to the Virginia Tech 2015 FSAE car suspension geometry and the tie rod travel is modeled as a prescribed displacement. Accounting for the varying cornering loads can give the car a performance advantage in the form of reduced compliance in common cornering conditions. It reveals that the loads are carried in different ways depending on the steering angle. The compliance is directly proportional to the internal member loads and reduction in compliance during cornering helps improve the tire attitude to the road surface. The racetracks designed for the FSAE competition are smaller and consist of sharp corners. The vehicle often spends a higher percentage of lap time in smaller corners compared to larger, faster corners or straights. The tracks also have a large percentage of larger corners where the vehicle cannot get to maximum speed that approaches handling limits. Moreover, this gives importance to maximizing tire grip or traction during cornering. Maximizing compliance resistance of suspension members will increase vehicle performance. Knowledge of the changes in member loads that occur with varying steer angles will improve the suspension design for all future teams.

Incremental changes to improving the realism of the model will bring durability to the design, which can be quantified. The effort to make changes to represent realism needs to be discussed and well thought out. This will also stretch the capabilities of the solver and computing resources but it will be interesting to learn ways to make the model computationally efficient.

8.4. Future Study- Experimental Validation

To understand modeling interactions and joints, multiple simpler FEA models were built and run to verify the characteristics and element response. While the inability to model all the details of the quarter-car suspension exists, how the upright and the suspension behaves/reacts to different loads (magnitude and direction) is understood.

Representing heim joints is one of the unique modeling techniques established in this research to represent spherical joints and a hard-stack bolted joint. Experimental verification is necessary to validate the representation. An approximate prediction about the stress concentration throughout the loading cycle can be made as well as an iterative design process can be initiated by extending this model. Accuracy in modeling will be achieved with incremental test data. A start to gathering test data would be running different quasi-static load cases with strain gauges and shock pots to validate the member loads. Experimental correlation helps establish the modeling technique and allows its use to further explore different aspects and problems of suspension analysis. In some cases, linearity can be established, and the test data can be interpolated or extrapolated with confidence.

Physical test data from accelerometers, shock pots and strain gauges will also help study deeper into the underlying formulation in Abaqus. Test data and proper post processing of that test data can shed light to inaccuracy as well as the reasons for inaccuracy. This methodology can then be used for much more complex systems. Correlation with the physical tests and accurate wheel loads would validate the model to accurately predict failure modes. Validation of the model with actual test data is the most immediate and high priority goal for future studies on this project.

Another important aspect of future work can be to establish more post processing methods and extract relevant information about the model using the same code, model and parameters. With the resources of Advanced Research Computing available, FSAE students or research students can build some sophisticated models with elastodynamics, for example, a simulation of the quarter-car on a racetrack with the full tire model characteristics. It would be an investment and a legacy for the future teams as well as other researchers at Virginia Tech.

8.5. Recommendations to extend the model

These recommendations are not a priority until the vehicle verification and validation methods are established to maintain the accuracy of simulations and animations.

8.5.1. Tire Model

Even though the model in this work makes use of wheel center loading, a tire model would contribute to the simulation in several different ways.

1. Stiffness parameters and response to bump and load transfer situations will be much more accurate.

2. Slip and lateral load parameters will help analyze cornering situations with test data and interpretations towards understeer and anti-roll.

3. Introduction of loading with static camber, camber gain dynamics, cornering in different tire compounds and combinations will extend the scope of research from a single quarter-car model.

4. Small details, like assuming the tire stiffness to be rigid, will be eliminated and the hyperelastic material model will reveal different responses as well as help correlate the test data.

However, modeling tire data will come with another set of challenges to model the rubber compounds, the treads variations, the accuracy of hyperelastic material modeling in Abaqus, as well as seeking the data either from manufacturers, testing firms (Calspan, Milliken, MTS, etc.) Another challenge would be to model the tire geometry and ground interaction properties. It is also challenging since ground interaction properties cannot be comprehensively tested or correlated to the model. Li [25] covers this topic with good correlation to the Virginia Tech FSAE vehicle.

8.5.2. Monocoque Chassis addition to the suspension model

The composite chassis modeling technique developed by Angelini [6] can be added to the quarter car suspension models for all four wheels to investigate the compliance, interactions, interfaces and joints (bolted heim joints at lock, spring compression, etc.) and overall behavior of the chassis to the wheel loads.

The chassis model will also show how isolated the chassis, body, driver, steering is to the wheel loads. Modeling the steering system could be a challenge but the different linkages of the steering system can be modeled with connector elements. Depending on the area of focus, the connector elements can be scaled to add more detail to study the joints and steering components or only focus on the chassis behavior.

8.5.3. Loading Scenarios Correlation

It is unlikely that the critical load scenarios will be tested and correlated during the design phase. Destructive testing with abusive loading will be expensive on students' effort, time, experience and money. Instead, the simulation can be tailored for moderate loading conditions, correlated and then simulated from the critical loads found from the same set of physical test data.

Correlated data will help faster design-analysis work to progress. The run time presented in this work is relatively small than what it will take for a fully simulated quarter-car on the test track. Enough number of load cases must be developed to run the entire test track simulation stitched together in time.

8.6. Fatigue life of welds and Verity

Fatigue life assessment is an important part of analyzing vehicle reliability and durability. Fatigue is a major failure mechanism in automobiles (including 2 and 3 wheelers). Welded joints are usually the weakest locations in a vehicle system and there has been interest and efforts to accurately and quickly run fatigue models to predict durability.

Different methods of fatigue life assessment of welded joints:

1. Stress- Life methods for high cycle fatigue
2. Strain- Life methods for low and high cycle fatigue
3. Fracture and crack propagation

Some of the above have been incorporated in commercial engineering codes. Structural stress methods based on internal loads is becoming popular for fatigue life assessment of welded joints. Verity is one of the popular methods in the automotive industry.

Verity can evaluate weld corners (usually stress concentrated in the weld) as well as single master S-N curve which is favorable for complex loading analysis. Also because of the deep connectivity of Verity within Abaqus' fe-safe module and Abaqus having a good educational framework in Virginia Tech, learning Verity would not only be beneficial in learning an additional skill for students, but also help them understand stress and fatigue analysis of welded joints by studying them closely. Fully understanding fatigue failures, crack propagation and overall deformation of welding joints would be invaluable for future designers and engineers.

The priority for future work should be Vehicle Verification and Testing (VV&T) before Verity model is implemented. Adding capabilities to the model without testing the representation should not be a priority.

9. References

[1] D. Schramm, M. Hiller and R. Bardini, Vehicle Dynamics: Modeling and Simulation, Springer, 2014.

[2] A. Jain, C. Kuo, P. Jayakumar and J. Cameron, "Constraint Embedding for Vehicle Suspension Dynamics," *Archive of Mechanical Engineering,* 2016.

[3] L. Borg, "An Approach to Using Finite Element Models to Predict Suspension Member Loads in a Formula SAE Vehicle," Blacksburg, 2009.

[4] A. Hellman, "Simulation of complete vehicle dynamics using FE code Abaqus," Luleå University of Technology, 2008.

[5] MSC Adams (R), "Adams," MSC Software Corporation, [Online]. Available: http://www.mscsoftware.com/product/adams.

[6] N. Angelini, "Simulating Dynamic Vehicle Maneuvers Using Finite Elements For Use In Design Of Integrated Composite Structure," Blacksburg, 2014.

[7] D. Palmer, "Ford saves $1.1 million on bracket re-design using FEA and optimisation," *Eureka,* p. 30, January 2005.

[8] M. Trapp and F. Chen, Automotive buzz, squeak and rattle: mechanisms, analysis, evaluation and prevention, 2012.

[9] R. D. Cook, D. S. Malkus, M. E. Plesha and R. J. Witt, Concepts and Applications of Finite Element Analysis, Wiley, 2002.

[10] H. Adams, Chassis Engineering, Penguin, 1993.

[11] J. Rauh, "Virtual Development of Ride and Handling Characteristics for Advanced Passenger Cars," *Vehicle System Dynamics,* vol. 40, pp. 135-145, 2003.

[12] D. Maher and P. Young, "An insight into linear quarter car model accuracy," *Vehicle System Dynamics,* vol. 49, 2011.

[13] P. Sathishkumar, J. Jancirani, D. John and S. Manikandan, "Mathematical modelling and simulation quarter car vehicle suspension," *International Journal of Innovative Research in Science, Engineering and Technology,* vol. 3, no. Special 1, 2014.

[14] M. Elmadany and Z. Abduljabbar, "Linear quadratic gaussian control of a quarter-car suspension," *Vehicle System Dynamics,* 1999.

[15] Abaqus Simulia 2016 Documentation, "Abaqus Analysis User's Guide," Dassault Systemes, 2016. [Online]. Available: http://docs.software.vt.edu:8080/abaqus/v2016.

[16] W. F. Milliken, D. L. Milliken and L. D. Metz, Race Car Vehicle Dynamics, SAE International, 1997.

[17] T. D. Gillespie, Fundamentals of Vehicle Dynamics, Society of Automotive Engineers, 1992.

[18] T. D. Gillespie, THE DYNAMIC BEHAVIOR OF NONUNIFORM TIRE/WHEEL ASSEMBLIES, 1983.

[19] C. Harris, "FSAE racecar suspension system design process using ADAMS/Car," 2006.

[20] "Full Vehicle Durability Using Abaqus/Standard to Abaqus/Explicit Co-simulation," *Abaqus Technology Brief,* November 2011.

[21] K. N. Richard Budynas, Shigley's Mechanical Design, McGraw Hill Education Material, 2015.

[22] V. Bhandari, Design of Machine Elements 3rd Edition, McGraw Hill Education India, 2010.

[23] H. NISHIMURA, S. ONO and E. TACHIBANA, "IDENTIFICATION OF FRICTIONAL COEFFICIENTS OF STAINLESS STEEL SLIDING BASE ISOLATORS," 13th World Conference on Earthquake Engineering, Vancouver, 2004.

[24] P. Clarke, "Pat’s Seven Deadly Sins of FS Design," Formula Student Germany, [Online]. Available: https://www.formulastudent.de/pr/news/details/article/pats-seven-deadly-sins-of-fs-design/.

[25] Y. Li, "Effective Simplified Finite Element Tire Models for Vehicle Dynamics Simulation," Virginia Polytechnic Institute and State University Library - ETD, 2017.

[26] P. F. Wasielewski, Speed as a measure of driver risk: observed speeds versus driver and vehicle characteristics, 1982.

[27] C. Smith, Racing Chassis and Suspension Design, Society of Automotive Engineers Inc., 2004.

[28] A. Smiley and S. Rochford, "Behavioural adaptation and anti-lock brake systems. Report for Transport Canada," 1991.

[29] F. Sagberg, S. Fosser and I.-A. F. Sætermo, "An investigation of behavioural adaptation to airbags and antilock brakes among taxi drivers," Institute of Transport Economics, Oslo, Norway, 1996.

[30] HLDI, "Collision and Property Damage Liability Losses of Passenger Cars With and Without Antilock Brakes," Highway Loss Data Institute, Arlington, Virginia 22201, 1994.

[31] C. M. Farmer, A. K. Lund, R. E. Trempel and E. R. Braver, "Fatal crashes of passenger vehicles before and after adding antilock braking systems," Elsevier, Arlington, VA , 1998.

[32] L. Evans, Traffic Safety and the Driver, 1991.

[33] L. Evans and P. Gerrish, "Antilock Brakes and Risk of Front and Rear Impact in Two vehicle crashes," 1995.

[34] L. Evans, "Antilock Brake Systes and Risk of Different Types of Crashes In Traffic," 1998.

[35] "PID Controller," Wikipedia, [Online]. Available: https://en.wikipedia.org/wiki/PID_controller.

[36] "National Crash Analysis Center (NCAC)," [Online]. Available: www.ncac.gwu.edu.

[37] "Automotive FEA examples," [Online].

[38] Abaqus Simulia 2016 Documentation, "Abaqus 6.16 Example Problems Documentation," Dassault Systemes Simulia, 2016. [Online]. Available: http://docs.software.vt.edu:8080/abaqus/v2016.

[39] W. Garrott and E. Mazzae, "An Overview of National Highway Traffic Safety Administration's Light Vehicle Antilock Brake Systems Research Program," *Society of Automotive Engineers,* 1999.

10. Appendices

A. Four Bar Mechanism Dynamic Analysis – Hand Calculations

The four mechanism is driven at O_2 at a constant angular velocity of 500 rad/s. From the data given, make a complete dynamic analysis including a kinematic analysis, inertia force determinations and a force analysis.

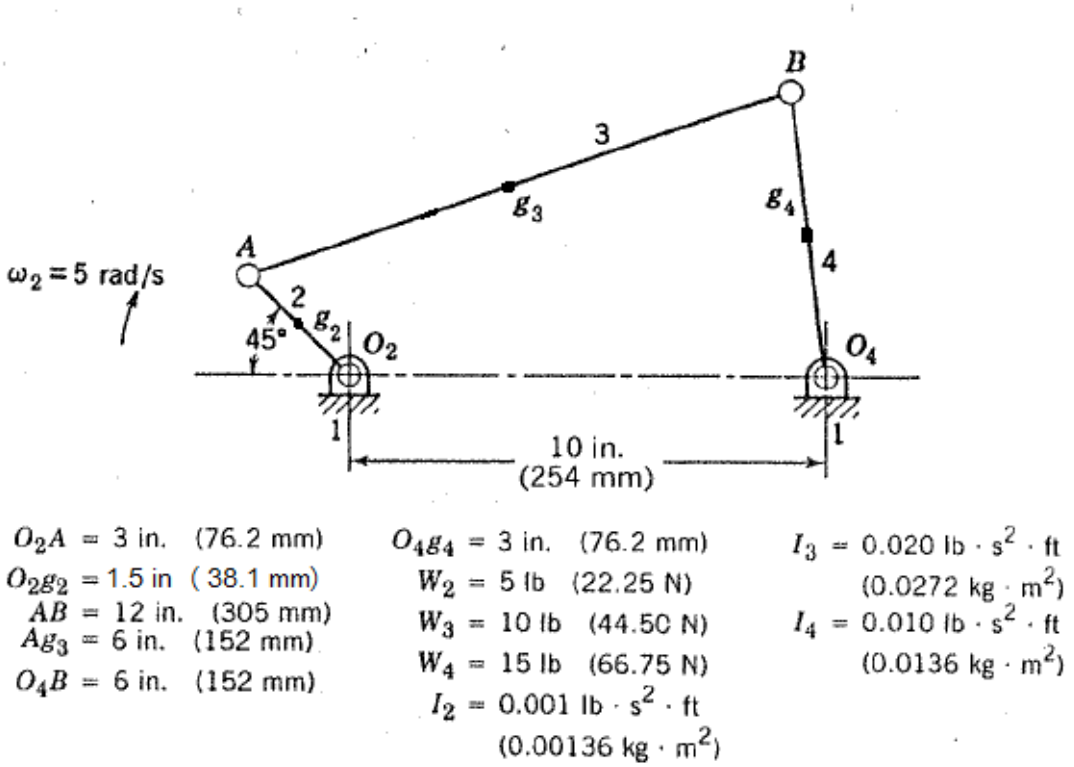

Figure 10.1: Four Bar Mechanism Example Problem.

We start with the kinematic analysis of the mechanism. We will use the global coordinate system for this solution.

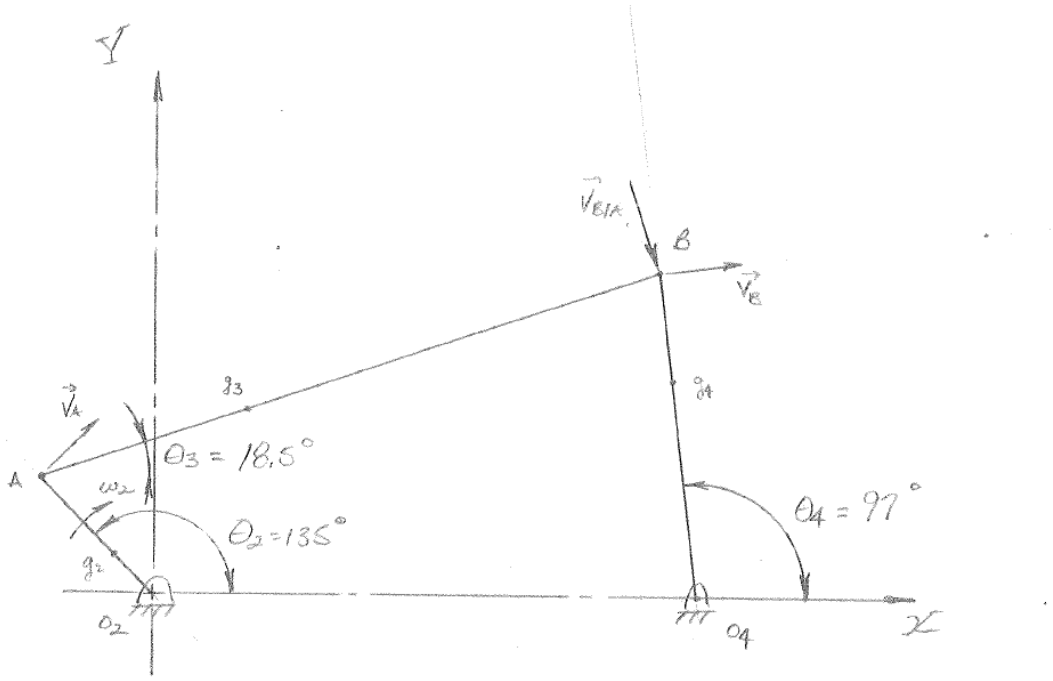

Figure 10.2: Four Bar Mechanism Geometry

$$\left|\overrightarrow{V_A}\right| = \omega_2 R_{O_2A} = 5 \times 3 = 15\frac{in}{s} = 1.25\frac{ft}{s}$$

Using the velocity polygon,

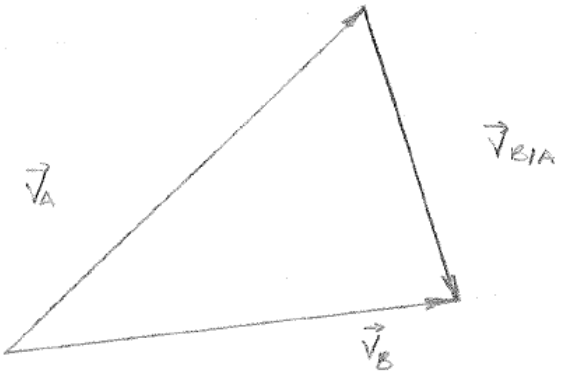

Figure 10.3: Velocity Polygon for link AB.

$$\left|\overrightarrow{V_B}\right| = \left|\overrightarrow{V_A}\right| \times \frac{\sin 63.5°}{\sin 78.5°}$$

$$\left|\overrightarrow{V_{B/A}}\right| = \left|\overrightarrow{V_A}\right| \times \frac{\sin 38°}{\sin 78.5°}$$

$$\therefore \left|\overrightarrow{V_B}\right| = 13.75\ \frac{in}{s}$$

$$\left|\overrightarrow{V_{B/A}}\right| = 9.25\ \frac{in}{s}$$

$$\omega_4 = \frac{\left|\overrightarrow{V_B}\right|}{R_{O_4B}} = \frac{13.75}{6} = 2.29\ \frac{rad}{s}\ CW$$

$$= -2.29\,\vec{k}$$

$$\omega_3 = \frac{\left|\overrightarrow{V_{B/A}}\right|}{R_{AB}} = \frac{9.25}{12} = 0.77\ \frac{rad}{s}\ CW = -0.77\,\vec{k}$$

Acceleration Analysis

$$We\ know\ A^n = \omega^2 R\ and\ A^t = \alpha \times R,$$

$$|A_A^n| = \omega_2^2 R_{O_2A} \searrow = 75\ in/s^2$$

$$|A_A^t| = 0 \because \omega_2 = constant$$

$$|A_B^n| = \omega_4^2 R_{O_4B} \searrow = 31.51\ in/s^2$$

$$|A_B^t| = \alpha_4 R_{O_4B}\ where\ we\ assume\ \nearrow direction$$

$$|A_{B/A}^n| = \omega_3^2 R_{AB} \swarrow = 7.13\ in/s^2$$

$$|A_{B/A}^t| = \alpha_3 R_{AB}\ where\ we\ assume\ \nwarrow direction$$

From Acceleration Polygon,

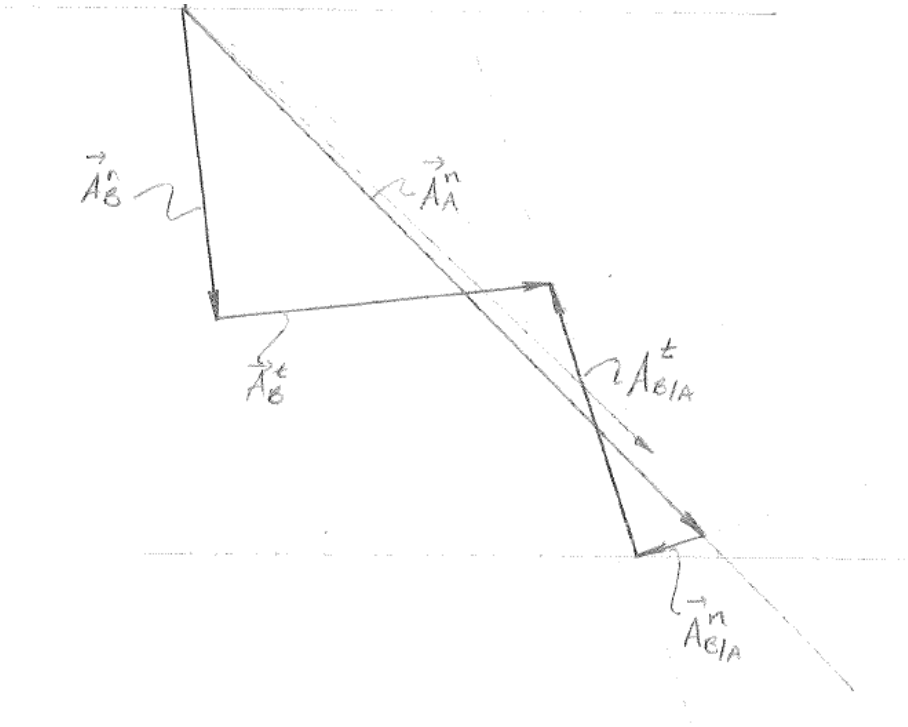

Figure 10.4: Acceleration Polygon for Link AB.

$$|A_B^t| = 34.25 \frac{in}{s^2}$$

$$|A_{B/A}^t| = 29 \frac{in}{s^2}$$

Since $\alpha = A^t/R$,

$$\alpha_4 = -5.71 \frac{rad}{s^2}\ \vec{k}$$

$$\alpha_3 = +2.42 \frac{rad}{s^2}\ \vec{k}$$

Now we determine the accelerations of C.G.'s

$$\overrightarrow{A_{g_2}} = \overrightarrow{A_{g_2}^n} + \cancel{\overrightarrow{A_{g_2}^t}} = -\omega_2^2 R_{O_2 g_2}(\cos\theta_2\,\vec{\imath} + \sin\theta_2\,\vec{\jmath}) = -37.5(\cos\theta_2\,\vec{\imath} + \sin\theta_2\,\vec{\jmath})$$

$$\overrightarrow{A_{g_4}} = \overrightarrow{A_{g_4}^n} + \overrightarrow{A_{g_4}^t}$$

$$\overrightarrow{A_{g_4}^t} = \overrightarrow{\alpha_4} \times \overrightarrow{R_{O_4 g_4}} = \alpha_4 \vec{k} \times R_{O_4 g_4}(\cos\theta_4\,\vec{\imath} + \sin\theta_4\,\vec{\jmath})$$

$$\therefore \overrightarrow{A_{g_4}^t} = \alpha_4 R_{O_4 g_4}(-\sin\theta_4\,\vec{\imath} + \cos\theta_4\,\vec{\jmath}) = -17.13(-\sin\theta_4\,\vec{\imath} + \cos\theta_4\,\vec{\jmath})\ \frac{in}{s^2}$$

$$\overrightarrow{A_{g_4}^n} = \overrightarrow{\omega_4} \times \overrightarrow{\omega_4} \times \overrightarrow{R_{O_4 g_4}} = -\left|A_{g_4}^n\right|(\cos\theta_4\,\vec{\imath} + \sin\theta_4\,\vec{\jmath})$$

$$\left|A_{g_4}^n\right| = \omega_4^2 R_{O_4 g_4} = 15.76\ \frac{in}{s^2}$$

$$\therefore \overrightarrow{A_{g_4}^n} = -15.76\ (\cos\theta_4\,\vec{\imath} + \sin\theta_4\,\vec{\jmath})$$

Since $\theta_2 = 135°\ and\ \theta_4 = 97°$, substitute and adding,

$$\therefore \overrightarrow{A_{g_4}} = 18.92\,\vec{\imath} - 13.55\,\vec{\jmath} = 23.27\,\frac{in}{s^2}\ @ -35.61°$$

$$\overrightarrow{A_{g_3}} = \overrightarrow{A_A} + \overrightarrow{\omega_3} \times \overrightarrow{\omega_3} \times \overrightarrow{R_{Ag_3}} + \overrightarrow{\alpha_3} \times \overrightarrow{R_{Ag_3}}$$

$$\overrightarrow{A_A} = \overrightarrow{A_A^n} = -\omega_2^2 R_{O_2 A}(\cos\theta_2\,\vec{\imath} + \sin\theta_2\,\vec{\jmath})$$

$$\therefore \quad \overrightarrow{A_A^n} = -75(\cos\theta_2\,\vec{\imath} + \sin\theta_2\,\vec{\jmath})$$

$$\therefore \overrightarrow{A_A} = 53.03\vec{\imath} - 53.03\vec{\jmath}$$

$$\overrightarrow{\omega_3} \times \overrightarrow{\omega_3} \times \overrightarrow{R_{Ag_3}} = -\omega_3^2 R_{Ag_3}(\cos\theta_3\,\vec{\imath} + \sin\theta_3\,\vec{\jmath})$$

$$= -35.65(\cos 18.5\,\vec{\imath} + \sin 18.5\,\vec{\jmath})$$

$$= -3.38\,\vec{\imath} - 1.13\,\vec{\jmath}$$

$$\overrightarrow{\alpha_3} \times \overrightarrow{R_{Ag_3}} = \alpha_3 R_{Ag_3}(-\sin\theta_3\,\vec{\imath} + \cos\theta_3\,\vec{\jmath})$$

$$= 14.5(-\sin 18.5\,\vec{\imath} + \cos 18.5\,\vec{\jmath})$$

$$= -4.6\vec{\imath} + 13.75\,\vec{\jmath} \quad in/s^2$$

$$\therefore \overrightarrow{A_{g_3}} = 45.05\,\vec{\imath} - 40.41\,\vec{\jmath} \quad in/s^2$$

$$\overrightarrow{A_{g_3}} = 60.52\,\frac{in}{s^2} \quad @ -41.89°$$

Now we consider separate links and apply D'Alembert's principle on each free body diagram,

Link 2:

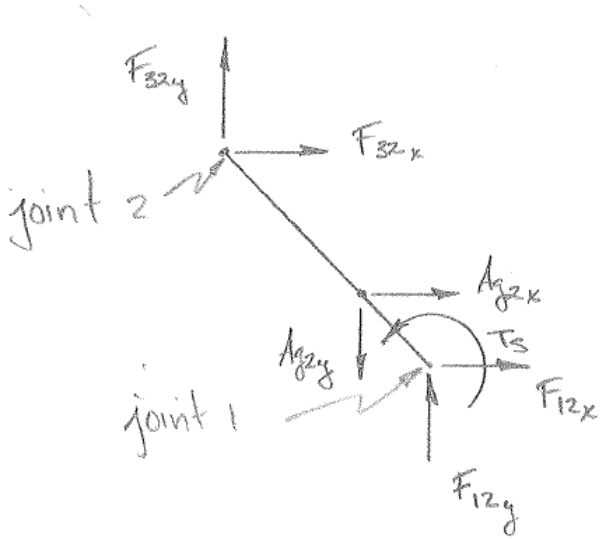

Figure 10.5: Free Body Diagram for Link O_2A.

$$\Sigma F_x = F_{32x} + F_{12x} = m_2 A_{g_2 x} \quad (1.)$$

$$\Sigma F_y = F_{32y} + F_{12y} = m_2 A_{g_2 y} \quad (2.)$$

$$\Sigma M_{g_2} = \overrightarrow{r_{21}} \times \overrightarrow{F_{12}} + \overrightarrow{r_{22}} \times \overrightarrow{F_{32}} + \overrightarrow{T_s} = I_2 \overrightarrow{\alpha_2}$$

$$\because \vec{r} \times \vec{F} = r_x F_y - r_y F_x$$

$$\Sigma M_{g_2} = r_{21x} F_{12y} - r_{21y} F_{12x} + r_{22x} F_{32y} - r_{22y} F_{32x} + T_S = I_2 \cancel{\alpha_2} = 0 \quad (3.)$$

$$\text{where } \overrightarrow{r_{21}} = -1.5(\cos\theta_2\, \vec{\imath} + \sin\theta_2\, \vec{\jmath}); \theta_2 = 135$$

$$r_{21x} = +1.061;\ r_{21y} = -1.061$$

$$\text{where } \overrightarrow{r_{22}} = 1.5(\cos\theta_2\, \vec{\imath} + \sin\theta_2\, \vec{\jmath}); \theta_2 = 135$$

$$r_{22x} = -1.061;\ r_{22y} = +1.061$$

$$\Sigma F_x = F_{32x} + F_{12x} = m_2 A_{g_2 x}$$

$$\Sigma F_y = F_{32y} + F_{12y} = m_2 A_{g_2 y}$$

$$\Sigma M_{g_2} = \overrightarrow{r_{21}} \times \overrightarrow{F_{12}} + \overrightarrow{r_{22}} \times \overrightarrow{F_{32}} + \overrightarrow{T_s} = I_2 \overrightarrow{\alpha_2}$$

$$\because \vec{r} \times \vec{F} = r_x F_y - r_y F_x$$

Link 3:

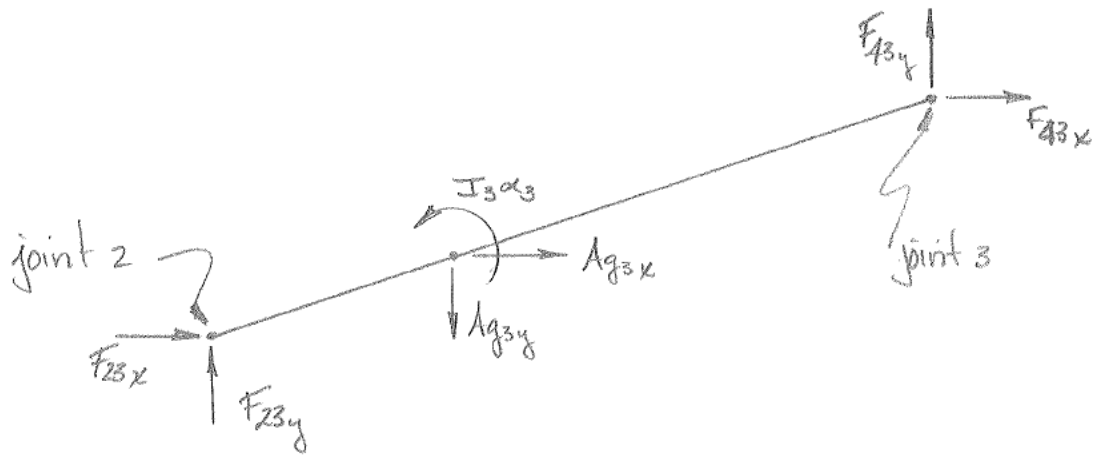

Figure 10.6: Free Body Diagram for Link AB.

$$\Sigma F_x = F_{23x} + F_{43x} = m_3 A_{g_3 x}$$

But $\overrightarrow{F_{23}} = -\overrightarrow{F_{32}}$ $$\therefore \Sigma F_x = -F_{32x} + F_{43x} = m_3 A_{g_3 x}$$ 4.

$$\Sigma F_y = -F_{32y} + F_{43y} = m_3 A_{g_3 y}$$ 5.

$$\Sigma M_{g_3} = \overrightarrow{r_{32}} \times -\overrightarrow{F_{32}} + \overrightarrow{r_{33}} \times \overrightarrow{F_{43}} = I_3 \overrightarrow{\alpha_3}$$

$$\overrightarrow{r_{32}} = -6(\cos\theta_3 \vec{\imath} + \sin\theta_3 \vec{\jmath}); \theta_3 = 18.5°$$

$$r_{32x} = -5.69;\ r_{32y} = -1.9$$

$$\overrightarrow{r_{33}} = 6(\cos\theta_3\,\vec{i} + \sin\theta_3\,\vec{j});\ \theta_3 = 18.5°$$

$$r_{33x} = 5.69;\ r_{33y} = 1.9$$

$$\Sigma M_{g_2} = r_{32x}(-F_{32y}) - r_{32y}(-F_{32x}) + r_{33x}F_{43y} - r_{33y}F_{43x} = I_3\alpha_3 \qquad 6.$$

Link 4:

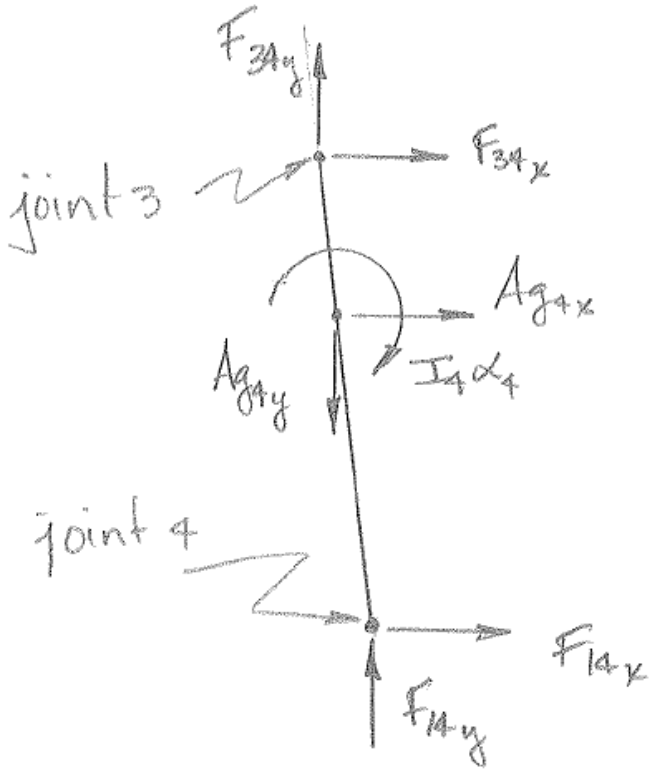

Figure 10.7: Free Body Diagram for Link O_4B.

$$\Sigma F_x = F_{34x} + F_{14x} = m_4 A_{g_4 x}$$

But $\overrightarrow{F_{34}} = -\overrightarrow{F_{43}}$ $$\therefore \Sigma F_x = -F_{43x} + F_{14x} = m_4 A_{g_4 x} \qquad 7.$$

$$\Sigma F_y = -F_{43y} + F_{14y} = m_4 A_{g_4 y} \qquad 8.$$

$$\Sigma M_{g_4} = \overrightarrow{r_{43}} \times -\overrightarrow{F_{34}} + \overrightarrow{r_{44}} \times \overrightarrow{F_{14}} = I_4\overrightarrow{\alpha_4}$$

$$\overrightarrow{r_{43}} = 3(\cos\theta_4\,\vec{i} + \sin\theta_4\,\vec{j});\ \theta_4 = 97°$$

$$r_{43x} = -0.37;\ r_{43y} = 2.98$$

$$\overrightarrow{r_{44}} = -3(\cos\theta_4\,\vec{\imath} + \sin\theta_4\,\vec{\jmath});\ \theta_4 = 97°$$

$$r_{44x} = +0.37;\ r_{44y} = -2.98$$

$$\Sigma M_{g_2} = r_{43x}(-F_{43y}) - r_{43y}(-F_{43x}) + r_{44x}F_{14y} - r_{44y}F_{14x} = I_4\alpha_4 \qquad 9.$$

Well now we have 9 equations and 9 unknowns. Hence we can solve it using the form

$$[A]\{X\} = \{B\}$$

Resulting Matrix Form,

$$\begin{bmatrix} 1 & 0 & 1 & 0 & 0 & 0 & 0 & 0 & 0 \\ 0 & 1 & 0 & 1 & 0 & 0 & 0 & 0 & 0 \\ +1.06 & +1.06 & -1.06 & -1.06 & 0 & 0 & 0 & 0 & +1 \\ 0 & 0 & -1 & 0 & +1 & 0 & 0 & 0 & 0 \\ 0 & 0 & 0 & -1 & 0 & +1 & 0 & 0 & 0 \\ 0 & 0 & -1.9 & +5.69 & -1.9 & +5.69 & 0 & 0 & 0 \\ 0 & 0 & 0 & 0 & -1 & 0 & +1 & 0 & 0 \\ 0 & 0 & 0 & 0 & 0 & -1 & 0 & +1 & 0 \\ 0 & 0 & 0 & 0 & +2.98 & +0.37 & +2.98 & +0.37 & 0 \end{bmatrix} \begin{Bmatrix} F_{12x} \\ F_{12y} \\ F_{32x} \\ F_{32y} \\ F_{43x} \\ F_{43y} \\ F_{14x} \\ F_{14y} \\ T_S \end{Bmatrix} = \begin{Bmatrix} m_2A_{g_2x} \\ m_2A_{g_2y} \\ 0 \\ m_3A_{g_3x} \\ m_3A_{g_3y} \\ I_3\alpha_3 \\ m_4A_{g_4x} \\ m_4A_{g_4y} \\ I_4\alpha_4 \end{Bmatrix}$$

Evaluating {B}:

$$\begin{Bmatrix} m_2A_{g_2x} \\ m_2A_{g_2y} \\ 0 \\ m_3A_{g_3x} \\ m_3A_{g_3y} \\ I_3\alpha_3 \\ m_4A_{g_4x} \\ m_4A_{g_4y} \\ I_4\alpha_4 \end{Bmatrix} = \begin{Bmatrix} (5/386.4)(26.51) \\ (5/386.4)(-26.51) \\ 0 \\ (10/386.4)(45.05) \\ (10/386.4)(-40.41) \\ (0.02)(12)(2.42) \\ (15/386.4)(18.92) \\ (15/386.4)(-13.55) \\ (0.01)(12)(-5.71) \end{Bmatrix} = \begin{Bmatrix} 0.343 \\ -0.343 \\ 0 \\ 1.166 \\ -1.046 \\ 0.581 \\ 0.734 \\ -0.526 \\ -0.685 \end{Bmatrix}$$

Using Matlab to compute {X}

$$\begin{Bmatrix} F_{12x} \\ F_{12y} \\ F_{32x} \\ F_{32y} \\ F_{43x} \\ F_{43y} \\ F_{14x} \\ F_{14y} \\ T_S \end{Bmatrix} = \begin{Bmatrix} 1.8609 \\ -0.6049 \\ -1.5179 \\ 0.2619 \\ -0.3519 \\ -0.7841 \\ 0.3821 \\ -1.3101 \\ -2.6628 \end{Bmatrix} (lbf\ or\ lbf - in)$$

Hence we establish a simple method to compute the dynamics problem of a four bar mechanism using the Matrix method.

The Microsoft Excel calculator spreadsheet does not employ the Matrix Method. Instead it follows the Superposition Method to formulate a solution for a dynamics analysis. The EXCEL calculator was created to solve for different iterations and different configurations of the mechanism as well as different instances of the same problem. The EXCEL calculator also uses SI units instead of English units.

Following are the input parameters:

4 bar linkage dynamics problem			
O_2A	76.2	mm	
O_2g_2	38.1	mm	
AB	305	mm	
O_4B	152	mm	
O_4g_4	76.2	mm	
Ag_3	152	mm	
Density of O2A	95809	Ns^2/m^4	
Density of AB	47341	Ns^2/m^4	
Density of O4B	142024	Ns^2/m^4	
Radius of O2A	10	mm	
Radius of AB	10	mm	
Radius of O4B	10	mm	
θ_2	135	deg	
θ_3	18.5	deg	
θ_4	97	deg	
Driving			
ω_2	5	rad/s	
Lumped Weights			
W_2	22.25	N	
W_3	44.5	N	
W_4	66.75	N	
Inertia Definitions			
O_2A:	I_{11}	0.00E+00	kgm^2
	I_{22}	1.10E-03	kgm^2
	I_{33}	1.10E-03	kgm^2
AB:	I_{11}	0.00E+00	kgm^2
	I_{22}	3.51E-02	kgm^2
	I_{33}	3.51E-02	kgm^2
O_4B	I_{11}	0.00E+00	kgm^2
	I_{22}	1.32E-02	kgm^2
	I_{33}	1.32E-02	kgm^2

Figure 10.8: Input Parameters for four bar mechanism - Set up in Excel.

Outputs												
Kinematics:												
$\overrightarrow{V_A}$	381	mm/s										
$\overrightarrow{V_B}$	347.9552971	mm/s		... Velocity Triangle								
$\overrightarrow{V_{B/A}}$	239.3724957	mm/s		... Velocity Triangle								
ω_3	0.784827855	rad/s										
ω_4	2.289179586	rad/s										
A_A^n	1905	mm/s^2										
A_A^t	0	mm/s^2		... Constant angular velocity								
A_B^n	796.5321632	mm/s^2										
A_B^t	869.9900035	mm/s^2		... Accelaration triangle					α_4	5.72362	rad/s^2	
$A_{B/A}^n$	187.8662022	mm/s^2										
$A_{B/A}^t$	736.6000087	mm/s^2		... Accelaration Triangle					α_3	2.41508	rad/s^2	
A_{g_2}	-952.5	$\cos\theta_2$ i +	$\sin\theta_2$ j	673.5192091	i	-673.519209	j				... Only Normal Component	
$A_{g_4}^t$	-436.1397254	$-\sin\theta_4$ i +	$\cos\theta_4$ j	432.8888061	i	53.152062	j					
$A_{g_4}^n$	-399.3141502	$\cos\theta_4$ i +	$\sin\theta_4$ j	48.6641533	i	-396.337723	j					
A_{g_4}				481.5529594	i	-343.185661	j					
A_{g_4}				591.3287163	mm/s^2	-35.4761202	degrees					
A_A	-1905	$\cos\theta_2$ i +	$\sin\theta_2$ j	1347.038418	i	-1347.03842	j					
$A_{g_3}^t$	367.0924633	$-\sin\theta_3$ i +	$\cos\theta_3$ j	-116.480148	i	348.122467	j					
$A_{g_3}^n$	-93.62512373	$\cos\theta_3$ i +	$\sin\theta_3$ j	-88.78691955	i	-29.7076877	j					
A_{g_3}				1141.771351	i	-1028.62364	j					
A_{g_3}				1536.785089	mm/s^2	-42.01574	degrees					

Figure 10.9: Output Variables for four bar mechanism kinematics problem - Set up in Excel.

Dynamics:

F_{O_2}	-2.160359327	N	45	degrees		$F = ma$	where m is the lumped mass and a is the accelaration at the prescribed CG
T_{O_2}	0				because	$I\alpha = 0$	
F_{O_3}	6.971145407	N	137.984	degrees			
T_{O_3}	0.08	Nm					
F_{O_4}	4.023566953	N	144.524	degrees			
T_{O_4}	0.08	Nm					
$\theta_{F_{O_4}}$	47.52387978	degrees				$F_{34}^4 = \frac{(T_{O_4} + F_{O_4} r_{O_{g4}} sin\theta_{F_{O_4}})}{r_{O_4} cos\theta_{F_{34}^4}}$	
$\theta_{F_{34}^4}$	11.5	degrees					
F_{34}^4	2.023888478	N					
F_{14X}^4	1.357320499	N				$F_{14X}^4 = -(F_{O_4} \cos\left(180 - \left\lvert\theta_{A_{g_4}}\right\rvert\right)) - F_{34}^4 \cos(\theta_3)$	
F_{14Y}^4	-2.97732103	N				$F_{14Y}^4 = -(F_{O_4} \sin\left(180 - \left\lvert\theta_{A_{g_4}}\right\rvert\right)) - F_{34}^4 \sin(\theta_3)$	
F_{14}^4	3.272118496	N	-65.4924	degrees			
F_{43}^4	-2.023888478	N					
F_{23}^4	2.023888478	N	18.5	degrees			
F_{32}^4	-2.023888478	N	198.5	degrees			
F_{12X}^4	-1.919301319	N				$F_{12X}^4 = F_{32}^4 \cos(\theta_3)$	
F_{12Y}^4	0.642189238	N					
F_{12}^4	2.023888478	N	18.5	degrees			
T_s^4	-0.138017048	Nm	CW				
F_{43}^3	-2.80	N				$F_{43}^3 = \frac{(T_{O_3} - F_{O_3} r_{Ag_3} cos\theta_{F_{O_3}})}{r_{AB} cos\theta_{F_{43}^3}}$	
$\theta_{F_{O_4}}$	29.48425996	degrees					
$\theta_{F_{43}^3}$	11.5	degrees					
F_{23X}^3	5.520822966	N					
F_{23Y}^3	-1.884458836	N					
F_{23}^3	5.833581346	N	-18.8467	degrees			
F_{14}^3	2.80	N	-83	degrees			
F_{12}^3	5.833581346	N	-18.8467	degrees			
T_s^3	-0.174894179	Nm	CW				
Total T_s	0.312911226	Nm	CCW				

Figure 10.10: Output Variables for four bar mechanism dynamics problem - Set up in Excel.

B. Interference Fit – Hand Calculations – Shigley's Mechanical Engineering Design [21]

Thick-wall cylindrical pressure vessel theory relating to stresses developed from interference fits

Stresses develop between cylinders due to the contact pressure generated by an interference fit. We achieve interference fit by pressing a larger inside member into the smaller opening of an outside member. Interference fit is the diametrical difference between the shaft OD and the ID of the hub hole.

- The radial deformation required by the interference fit causes an interfacial pressure, p, to develop at the nominal radius, at $r = R$. Consequently, radial and tangential stresses, σ_r and σ_t , are produced.
- We assume uncapped ends ($\sigma_l = 0$) a biaxial state of stress exists for which two non-zero principal stresses are considered.
- From the cylindrical pressure vessel theory, the radial and tangential stresses represent principal stresses.
- We assume the length of the outer member to be equal to the length of the inner member.

The geometric features of the cylindrical parts are:

r_i = the inside radius of the inner cylinder
R = nominal radius of internal outside radius and external inside radius after assembly
r_o = outside radius of the outer cylinder
δ = radial interference

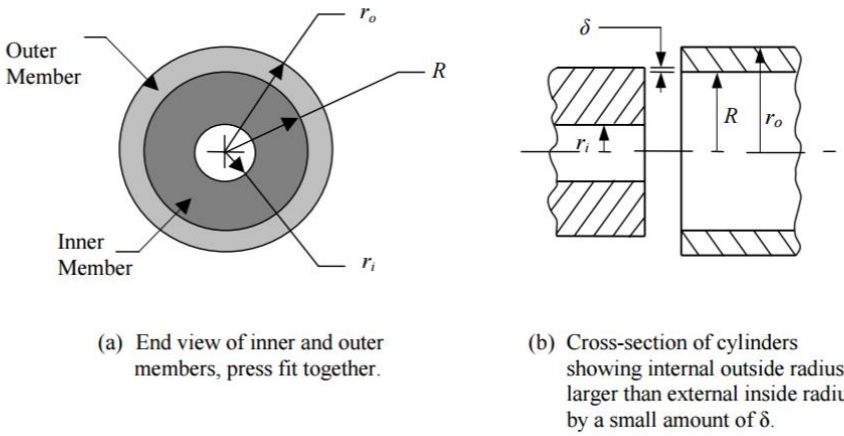

(a) End view of inner and outer members, press fit together.

(b) Cross-section of cylinders showing internal outside radius larger than external inside radius by a small amount of δ.

Figure 10.11: Interference fit of two cylinders of finite and equal length. Image taken from and reprinted Shigley's Mechanical Design. Permission document attached in Appendix E

Inside Cylinder

- Inner member experiences an external pressure, $p_o = p$, resulting in compressive tangential and radial stresses.
- Thick-Wall Theory may be applied with $r_o = R$:

$$(\sigma_t)_i|_{r=R} = -p_o\left(\frac{R^2 + r_i^2}{R^2 - r_i^2}\right) = -pC_{it} \tag{17}$$

$$(\sigma_r)_i|_{r=R} = -p_o = -p \tag{18}$$

Outside Cylinder

- Outer member only experiences internal pressure, $p_i = p$, resulting in tensile tangential stress and compressive radial stress.
- Thick-Wall Theory is, as always, applied with $r_i = R$:

$$(\sigma_t)_o|_{r=R} = -p_o\left(\frac{r_o^2 + R^2}{r_o^2 - R^2}\right) = -pC_{ot} \tag{19}$$

$$(\sigma_r)_o|_{r=R} = -p_i = -p \tag{20}$$

Definition of Interfacial Pressure

We presently have two equations and three unknowns for both the inside and outside cylinder analyses. A third equation which relates the contact pressure and the interference can be derived by examining the deformation of the members.

Deflection Equation

The total *radial* interference may be defined as:

$$\delta_{total} = \delta_i + \delta_o \tag{21}$$

where,

$\delta_i =$ decrease in radius of inner cylinder
$\delta_0 =$ decrease in radius of hole

The deformation may also be expressed as:

$$\delta_{total} = pRK_i + pRK_o \tag{22}$$

where the outside member constant K_o, is defined as

$$K_o = \frac{1}{E_0}\left[\left(\frac{R^2 + r_i^2}{R^2 - r_i^2}\right) - v_i\right] = \frac{1}{E_0}[C_i - v_i] \tag{23}$$

with $\zeta_i = \frac{R}{r_i}$, C_i is defined as

$$C_i = \frac{\zeta_i^2 + 1}{\zeta_i^2 - 1} \tag{24}$$

For the case of a solid shaft, $r_i = 0, \zeta_i = R/r_i = \infty$ and $C_i = 1$

We can now solve for the deformation for a given class of interference fits,

$$\delta_{total} = [K_o + K_i]pR \tag{25}$$

Or rearranging, the contact pressure p may be expressed as a function of interference without assumptions regarding material property values:

$$p = \frac{\left[\frac{1}{K_o + K_i}\right]\delta_{total}}{R} \tag{26}$$

C. Interference Fit Model – Convergence Study

The results of the interference fit model as described in Section 0 are given below. The Nodes mentioned are the display group set nodes which are probed at the end of the shrink fit simulation. Select nodes chosen at the midpoint of the width of bearing races are considered to perform a convergence study on the bearing housing. The number of elements selected for the model to be converged is used for further building the upright model and compatibility regarding mesh density with other connecting components is maintained.

The convergence study results are recorded and the convergence graphs are created on Microsoft Excel. The results are presented in the following page.

Following is a chart showing stress trends (y-axis) on different locations along the width (x-axis) of the bearing housing. The plot includes the stress values for different number of elements.

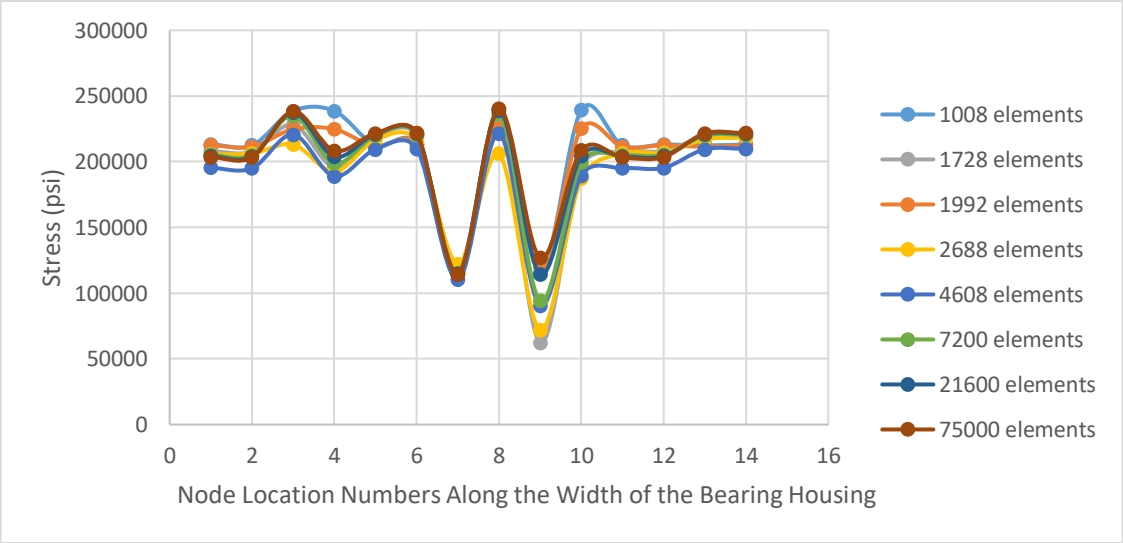

Figure 10.12: Stress vs. Width (cylinder height) of Bearing Housing.

Following is a spreadsheet study for convergence in the interference fir problem. These results justify the use of large element numbers and a denser mesh for the upright assembly components

Convergence study for Bearing+Bearing Housing Only

Bearing Housing Mesh

				Stress Mises (psi)															
CircMeshEdge	RadMeshEdge	ZMeshEdge	No. of elements	Node 1	Node 4	Node 5	Node 6	Node 9	Node 10	Node 20	Node 21	Node 23	Node 24	Node 34	Node 35	Node 37	Node 38		
7	1	6	1008	213301	212424	238598	238598	212424	213301	115933	239254	115933	239254	212424	213142	212424	213142		
6	2	6	1728	208150	207666	228298	195823	218976	219625	116516	228871	62337.8	196157	207664	208088	218975	219512		
21	1	8	1992	212420	211383	224750	224750	211383	212420	120064	225073	120064	225073	211381	212460	211381	212460		
7	2	7	2688	205736	206253	213050	192310	216517	215571	122086	206141	71966.4	187127	206230	206901	217029	218289		
8	3	8	4608	195381	195032	220653	188938	209456	209913	110201	221526	90616.1	189366	195032	195338	209455	209823		
10	3	10	7200	205302	204886	235082	198870	219996	220515	115434	236252	94163	199386	204885	205244	219995	220416		
15	4	15	21600	204198	203889	237422	203772	221040	221373	114674	239103	114332	204334	203888	204146	221039	221311		
25	5	25	75000	203515	203302	238336	208357	221553	221804	114281	240231	126875	208596	203301	203525	221550	221777		
			Convergence %	0.9913	0.9923	0.9863	0.9545	0.993	0.99419	0.99001	0.98344	0.742171	0.955848	0.992269	0.991625	0.99298	0.99386	Avg %	0.968125

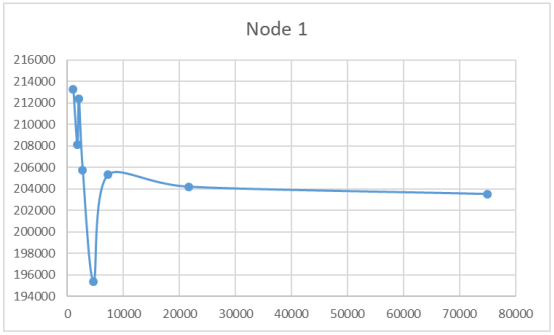

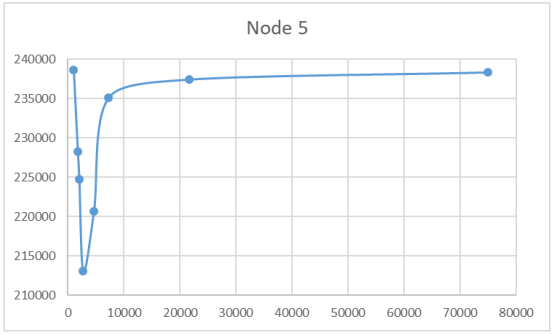

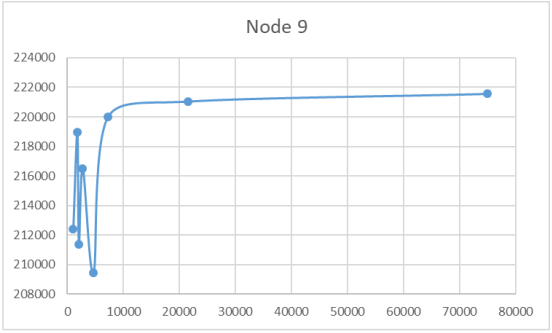

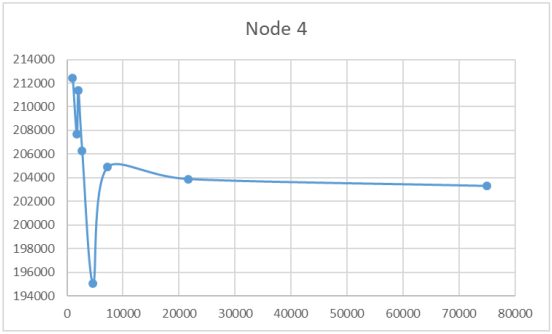

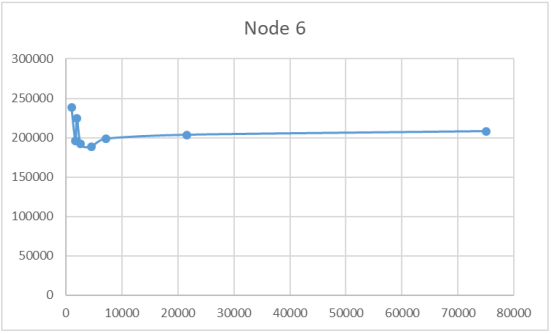

Figure 10.13: Convergence Study - Data recording and Chart creation done with MS-Excel.

D. Energy Trends for Cornering + Braking Model

While working on either debugging or building the model with simple steps along the way, it was understood that energy studies and the data extracted can often point the engineer in the right direction. In case one is looking for why the solver reacted in a certain way at a certain problem, energy studies can help understand the underlying physics and dynamics. It is also a way to verify what the user assumes in their understanding of the solver and the model. Energy studies can also be used to check for energy balance in some problems like statics or heat transfer.

For a dynamics problem like the upright cornering+braking model, external energy is constant supplied with loads and prescribed displacement. It is still relevant to investigate the energy trends and based on the different events of loading and interference fit, this data helps the modeler with a sanity check along the journey.

1. External Work

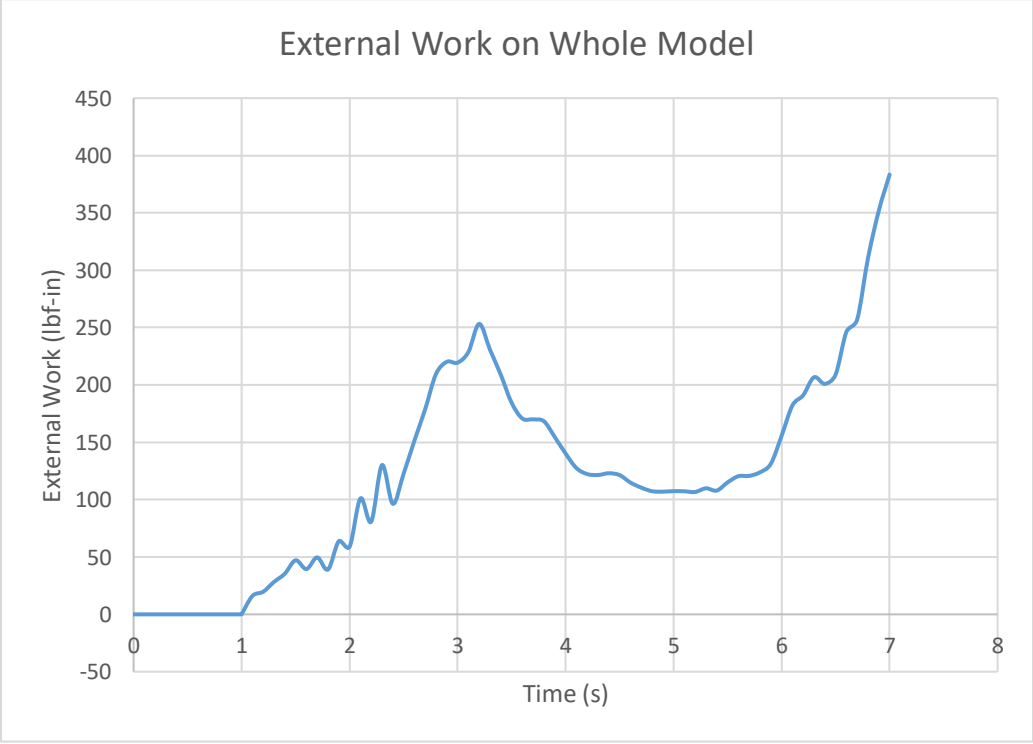

Figure 10.14: External Work response of model to cornering+braking loads.

2. Frictional Dissipation

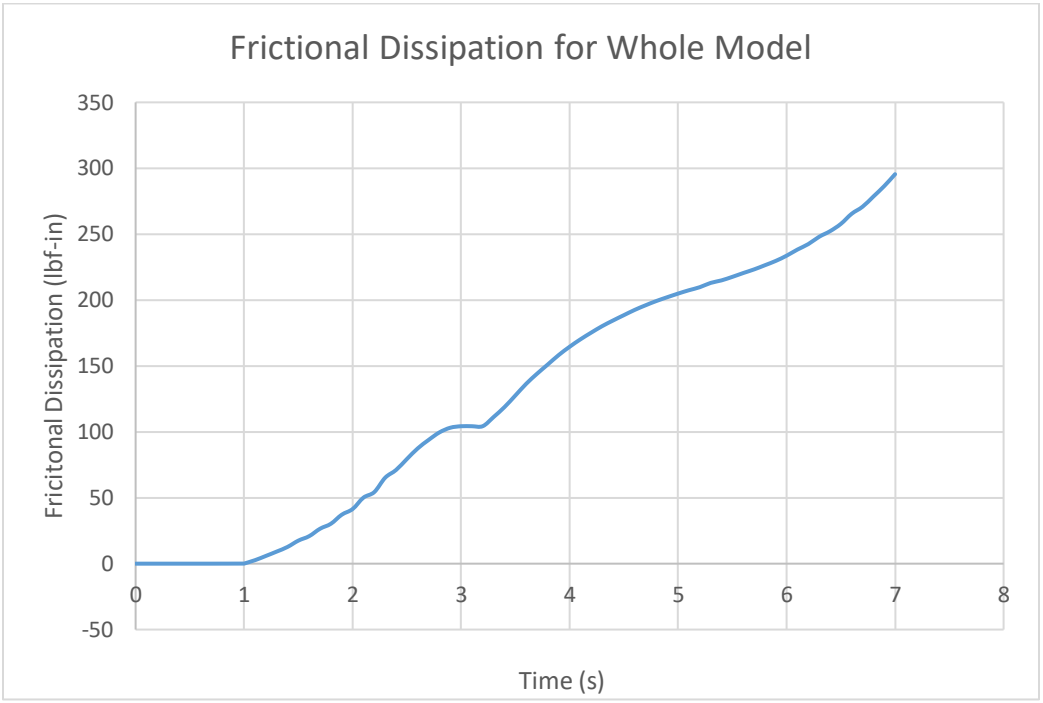

Figure 10.15: Frictional Dissipation response of model to cornering+braking loads.

3. Viscous Dissipation

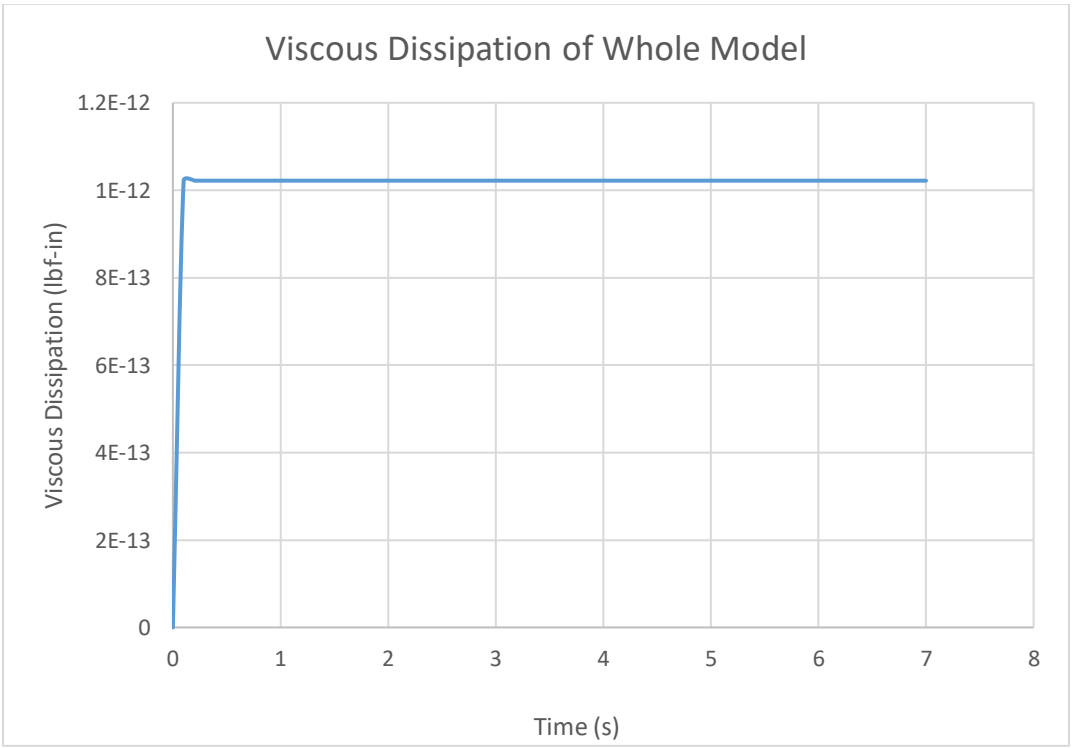

Figure 10.16: Viscous Dissipation response of model to cornering+braking loads.

4. Internal Energy

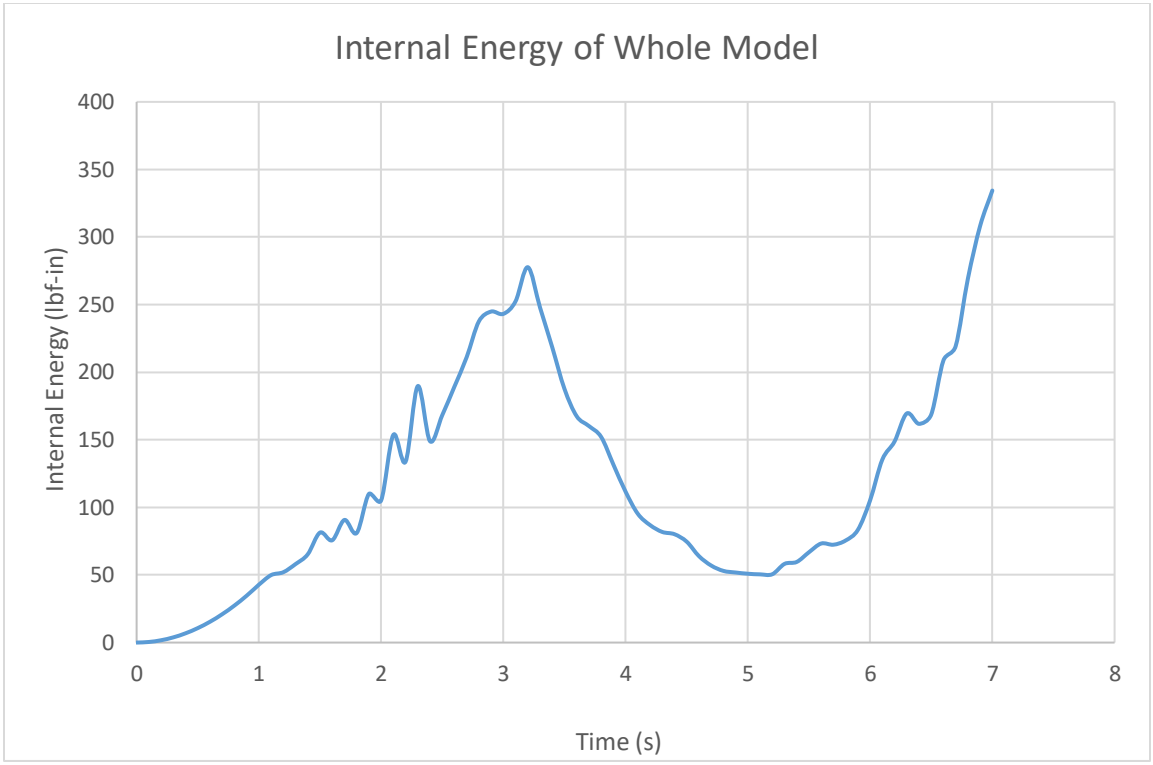

Figure 10.17: Internal Energy response of model to cornering+braking loads.

5. Kinetic Energy

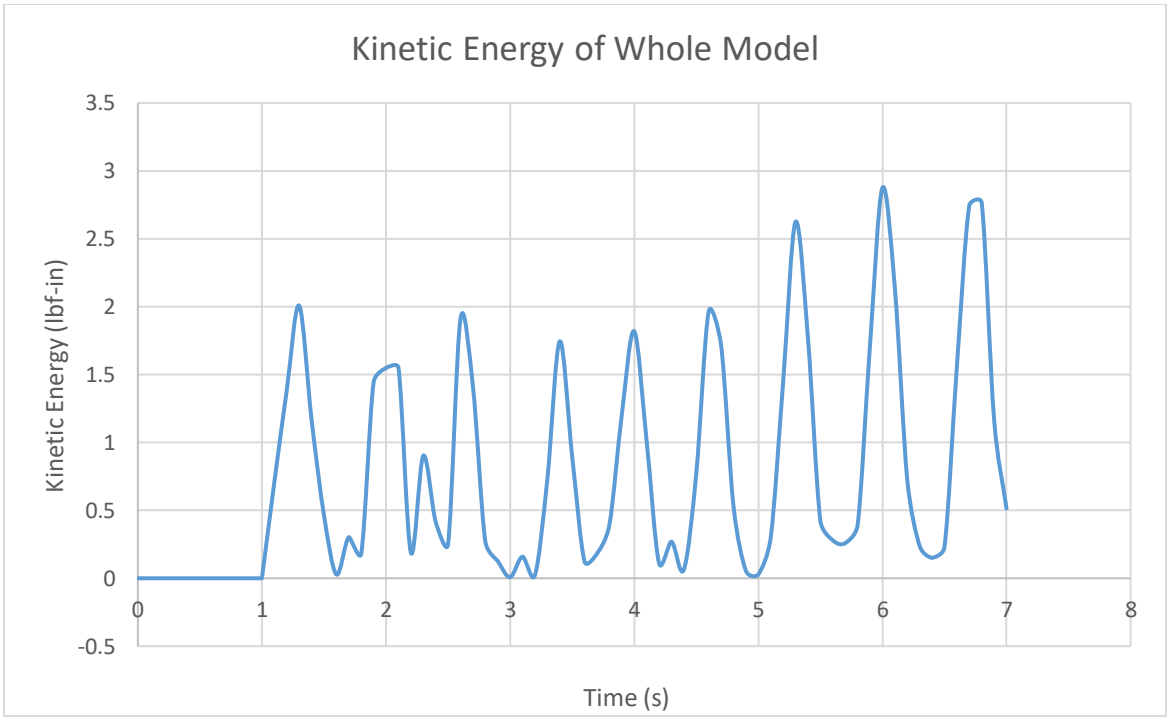

Figure 10.18: Kinetic Energy response of model to cornering+braking loads.

6. Total Energy

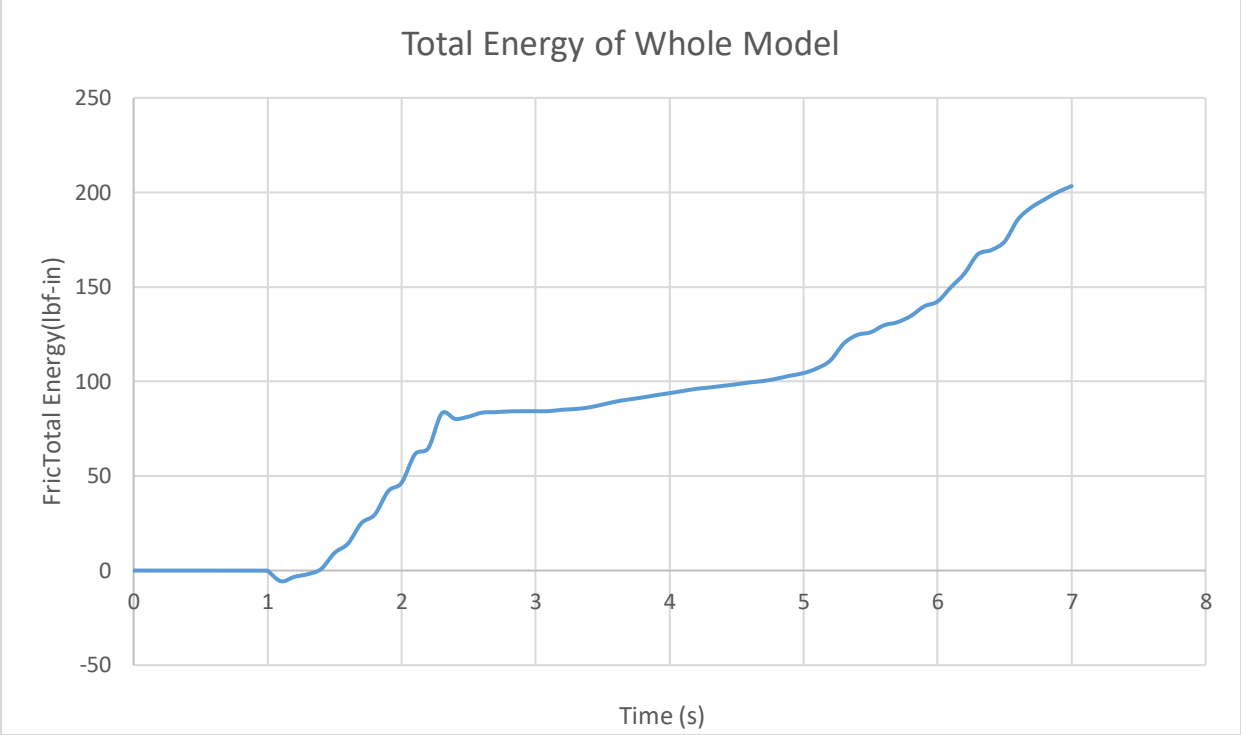

Figure 10.19: Total Energy response of model to cornering+braking loads.

E. Figure/ Table Permissions

1. Concepts and Applications of Finite Element Analysis by Malkus, Plesha, Cook and Witt

JOHN WILEY AND SONS LICENSE TERMS AND CONDITIONS

Mar 14, 2018

This Agreement between Virginia Tech -- Harsh Mehta ("You") and John Wiley and Sons ("John Wiley and Sons") consists of your license details and the terms and conditions provided by John Wiley and Sons and Copyright Clearance Center.

License Number	4307851509493
License date	Mar 14, 2018
Licensed Content Publisher	John Wiley and Sons
Licensed Content Publication	Wiley Books
Licensed Content Title	Concepts and Applications of Finite Element Analysis, 4th Edition
Licensed Content Author	David S. Malkus Michael E. Plesha Robert D. Cook Robert J. Witt
Licensed Content Date	Oct 1, 2001
Licensed Content Pages	1
Type of use	Dissertation/Thesis
Requestor type	University/Academic
Format	Electronic
Portion	Figure/table
Number of figures/tables	
Original Wiley figure/table number(s)	11.4.3
Will you be translating?	No
Title of your thesis / dissertation	Elastodynamic Analysis of Vehicle Uprights
Expected completion date	May 2018
Expected size (number of pages)	150
Requestor Location	Virginia Tech 467 Goodwin Hall, 635 Prices Fork Road BLACKSBURG, VA 24061 United States Attn: Harsh Mehta/ Bob West
Publisher Tax ID	EU826007151
Total	0.00 USD
Terms and Conditions	

TERMS AND CONDITIONS

This copyrighted material is owned by or exclusively licensed to John Wiley & Sons, Inc. or one of its group companies (each a"Wiley Company") or handled on behalf of a society with which a Wiley Company has exclusive publishing rights in relation to a particular work (collectively "WILEY"). By clicking "accept" in connection with completing this licensing

2. Shigley's Mechanical Design by Richard Budynas and Keith Nisbett

PERMISSION LICENSE: EDUCATIONAL ELECTRONIC USE

Request ID/Invoice Number: HAR552273212-1

Date: March 21, 2018

To: Harsh Mehta
Virginia Tech
1050 Ferry Street
Apartment 402A
Eugene
OR
97401
United States
"Licensee"

McGraw-Hill Education Material

Author: Budynas, Richard and Nisbett, Keith
Title: Shigley's Mechanical Engineering Design
ISBN: 9780073398204
Edition: 10
Copyright: 2015
Description of material: Page 130 (including Figure 3-33)

Fee: "Waived"

Purpose of Reproduction

School: Virginia Tech
Semester: 2017/2018 Academic Year
Format: Electronic (Internet) - To be used on an access restricted website/platform only
Distribution: One-time educational use in a thesis titled 'Elastodynamic Analysis of Vehicle Suspension Uprights'